INFORMATION TO USERS

This manuscript has been reproduced from the microfilm master. UMI films the text directly from the original or copy submitted. Thus, some thesis and dissertation copies are in typewriter face, while others may be from any type of computer printer.

The quality of this reproduction is dependent upon the quality of the copy submitted. Broken or indistinct print, colored or poor quality illustrations and photographs, print bleedthrough, substandard margins, and improper alignment can adversely affect reproduction.

In the unlikely event that the author did not send UMI a complete manuscript and there are missing pages, these will be noted. Also, if unauthorized copyright material had to be removed, a note will indicate the deletion.

Oversize materials (e.g., maps, drawings, charts) are reproduced by sectioning the original, beginning at the upper left-hand corner and continuing from left to right in equal sections with small overlaps. Each original is also photographed in one exposure and is included in reduced form at the back of the book.

Photographs included in the original manuscript have been reproduced xerographically in this copy. Higher quality 6" x 9" black and white photographic prints are available for any photographs or illustrations appearing in this copy for an additional charge. Contact UMI directly to order.

UMI®

Bell & Howell Information and Learning
300 North Zeeb Road, Ann Arbor, MI 48106-1346 USA
800-521-0600

WIND PRESSURE COEFFICIENTS FOR GABLE ROOFS OF INTERMEDIATE SLOPES

KAI WANG

A Thesis

at

the School for Building

Presented in Partial Fulfillment of the Requirements

for the Degree of Master of Applied Science

at

Concordia University

Montreal, Quebec, Canada

October 1998

ABSTRACT

WIND PRESSURE COEFFICIENTS FOR GABLE ROOFS OF INTERMEDIATE SLOPES

Kai Wang

The present study examines the suitability of the current wind provisions of the National Building Code of Canada for design wind loads on gable roofs of intermediate roof angles (10°-30°). The study is initiated by the discrepancies found in recent research projects against the current design wind loading provisions for such roofs.

Five building models with roof angles of 10° 15°, 20°, 25° and 30° equipped with an interchangeable roof slope panel have been tested in a typical open country exposure in the boundary layer wind tunnel of the Centre for Building Studies at Concordia University. The experimental settings satisfy the corresponding wind tunnel simulation criteria specified in the wind load test standards of American Society of Civil Engineers.

Local and area-averaged roof pressure coefficients have been obtained from the wind tunnel measurements. Extreme value analysis has been performed to establish the peak pressure coefficient values. This thesis presents a comparative study based on the experimental data, which consists of two parts. The first part includes the comparisons of

the measured results with those from other researches. The comparisons show that the present experimental results are appropriate and suitable for application to codification. The second part of the study examines the suitability of the current wind provisions by comparing the present results with those specified in the provisions. It appears that there is underestimation of the extreme suctions in the current wind provisions, particularly those on the ridge and edge regions of the roofs with intermediate slopes.

As a result of the present study, an alternative zoning and loading definition is attempted, accompanied by a set of new curves. At the same time, the codal roof categories are re-arranged. The proposed design roof wind pressure coefficients are somewhat higher than the current design values.

ACKNOWLEDGEMENTS

The author wishes to express his sincere gratitude to his supervisors Drs. T. Stathopoulos and H. Wu for their excellent guidance and support during this study. The author is most grateful to Dr. P. J. Saathoff for his suggestions and timely assistance in experiments and thesis writing.

Special thanks are due to Mr. S. Bélanger for his computer expertise, Dr. Suresh Kumar for his constructive suggestions, and the China-Quebec Education Exchange Program for the International Tuition Fee Exemption.

Special appreciation is felt for my family, particularly for my wife Hui and my sister Yi, for the love and encouragement during the study.

TABLE OF CONTENTS

LIST OF FIGURES

LIST OF TABLES

LIST OF SYMBOLS

B	gable wall length [L]
C_g	geostrophic drag coefficient; gust effect factor
C_p	pressure coefficient
C_{pmean}	mean pressure coefficient
C_{pmin}	minimum pressure coefficient
C_{pmax}	maximum pressure coefficient
C_{prms}	root-mean-square pressure coefficient
F_i	geometric weighting factor
H	mid-roof height [L]
h	eaves height [L]
L	long wall length [L]
${}^xL_v$	longitudinal integral scale of turbulence [L]
n	frequency [T^{-1}]
P	probability
P_i	pressure [FL^{-2}]
P_{mean}	mean pressure [FL^{-2}]
P_{min}	minimum pressure [FL^{-2}]
P_{max}	maximum pressure [FL^{-2}]
S_v	spectral density function of velocity [L^2T^{-1}]
V	mean wind velocity at gradient height [LT^{-1}]
V_g	mean wind velocity [LT^{-1}]

V_{rms}	rms wind velocity [LT^{-1}]
Z	height above the ground-level [L]
Z_g	gradient height [L]
α	wind incidence angle
θ	roof angle
σ	standard deviation

CHAPTER 1

INTRODUCTION

1.1 GENERAL

Low building gable roofs are heavily loaded during strong winds. Severe wind damage on the roofs has often been reported. In order to minimize the wind damage, the National Building Code of Canada (NBCC, 1995) and the American Wind Standard (ASCE-7, 1995), as well as many other national and international wind standards and codes of practice, have specified detailed provisions for these low building roofs. However, with the increasing use of fast-assembled and light-weighted structural members and components in roof design and construction, better performance of roofs has necessitated the continuous updating process of the wind standards and codes of practice, after research findings from wind tunnel experimentation and full-scale investigation.

In addition to the valuable full-scale investigation, wind tunnel experimentation plays an important role in the evaluation of design roof wind loads. However, an accurate wind tunnel simulation for low building roofs remains hard to achieve because lots of factors

are involved in wind tunnel simulation. The variation in approach flow properties such as the velocity profile, turbulence intensity and length scale, the variation in building size and roof geometry, and the variation in terrain condition, building grouping etc. have great influences on the roof wind loads (Stathopoulos, 1984a). It has been reported that using different wind tunnel experimental simulations to measure wind loading on an identical model might obtain different pressure coefficients sometimes over 40 percent (Sill et al, 1992). The difficulty in accurate wind tunnel simulations was regarded as a trademark for the low building wind loading tests and prevented most previous wind tunnel experiments from codification usage.

Up-to-date achievement in accurate wind tunnel simulation comes out as the ASCE wind-tunnel load-test standard (ASCE Draft, 1997), after research findings for more than two decades. This standard sets criteria to regulate the wind tunnel experimental studies that aim to be used for codification purposes.

The present study is to examine the suitability of the current wind provisions for gable roofs of intermediate slopes of the National Building Code of Canada (NBCC, 1995). This study consists of a comparative research based on experimental measurements carried out in a wind tunnel. These experiments have been elaborately simulated, following the ASCE wind loading test standard (ASCE Draft, 1997). This research is justified by the discrepancies found in previous research findings against the current wind provisions, which is focusing on the roofs in the intermediate roof range (10°-30°).

1.2 SCOPE AND OBJECTIVES

Wind standards and codes of practice have specified detailed provisions for gable roofs of pitched slopes. However, recent research results have shown discrepancies from the codal specifications for roofs of intermediate slopes. Therefore, there is a need to carry out a detailed research study to examine the validity of the current wind provisions. Generally speaking, the scope of the present study is to examine the suitability of the current wind provisions of the National Building Code of Canada (NBCC, 1995), specified for gable roofs of intermediate slopes ($10^{\circ}<\theta\leq30^{\circ}$).

As defined in the current wind provisions, a given gabled roof may fall into one out of three roof ranges depending on its roof angle (θ), namely quasi-flat roof ($0^{\circ}<\theta\leq10^{\circ}$), intermediate roof ($10^{\circ}<\theta\leq30^{\circ}$), and high-pitched roof ($30^{\circ}<\theta\leq45^{\circ}$). In fact, the intermediate slope is a common roof style for low-rise buildings. Primary reasons to choose this roof style include prevention of rain and snow accumulation. Steeper roofs are less prevalent, but they are constructed to achieve aesthetic appeal or also functional use in extreme snowfall environments. The examination of the codal definition of the roof angle range is one of the objectives of the present study.

In addition to roof slope categorization, the current wind provisions are also specified in terms of pressure coefficients appropriate to provide design wind loads for roof elements and components in various locations. A roof surface is made up of different roof regions (eaves and ridge corners; eaves, apex and gable edges; ridge; and interior). These regions,

which may be different for each roof angle range, can be grouped into a set of pressure zones, provided that the appropriate regions are governed by similar design pressure coefficients. For these appropriate pressure zones, a set of design pressure coefficient curves is provided. The assessment of suitability of pressure zones is another objective of the present study.

In order to attain these objectives, a series of wind tunnel experiments have been conducted in the present study. Five gable roof models of intermediate roof slopes (10°, 15°, 20°, 25° and 30°) have been tested in a simulated open country exposure in the Building Aerodynamic Laboratory of the Centre for Building Studies at Concordia University. The experiments rigidly followed the American Society of Civil Engineers (ASCE) wind loading test standard (ASCE Draft, 1997). Detailed measurements have been carried out in order to produce the required local and area-averaged wind pressure coefficients.

The approach followed in the present research work consists of validating the experimental results through comparisons with previous research findings; comparing measured data with the current wind provisions; examining the appropriateness of roof regions, pressure zoning and loading, as presently described in the Code. Finally, a new set of provisions will be proposed, and its feasibility will be discussed. This will be particularly important if design wind pressure coefficients are increased, since this will have inference on the cost of roof and its construction.

1.3 THESIS ORGANIZATION

The next chapter discusses the previous work in this area. The justification of the need of the present study is also elaborated.

Chapter 3 presents the atmospheric boundary layer wind tunnel experimental techniques and describes the aerodynamic characteristics of the simulated upstream flow. Details of the instrumentation, model configuration, and data acquisition and processing are described. The current experimental settings are also compared with the respective criteria specified in the ASCE standard (ASCE Draft, 1997). The comparison shows that the present wind tunnel experiments satisfy the standard in terms of accurate simulation and the present experimental results obtained could be suitable for codification purposes.

Chapter 4 presents the experimental results in terms of their variations with roof angle and wind azimuth, compared with those from previous studies. The latter is for validation purposes. The discussions provide global pictures on the local and area-averaged pressure coefficients with their regional distributions. After that, these pressure coefficients are formed into the codal format used by the current wind provisions for further codification usage.

In Chapter 5, the examination of the suitability of the current wind provisions for the intermediate roof range is conducted. Through detailed comparison of the present results

with the current wind provisions, it is found that there is underestimation of the peak suctions in the current wind provisions, particularly for the corner and edge regions. Modifications also seem necessary for the codal zoning and slope definition. Consequently, new provisions are attempted and discussed from the feasibility point of view.

Finally, conclusions and suggestions for further research on this topic are provided in Chapter 6.

CHAPTER 2

LITERATURE REVIEW

2.1 DESCRIPTION OF PREVIOUS WORK

Wind tunnel studies on low building roof wind loading began in the mid-1960s, accompanied with researches for improving techniques of accurate wind tunnel simulation. Previous work has provided considerable insights into the turbulent action of roof wind loads, and also provided reliable wind tunnel simulation techniques.

The wind tunnel work of Barnaud et al (1974), as reviewed by Stathopoulos (1984a), examined mean and root-mean-square (rms) pressures of three different roof angles, namely 0°, 22.5°, 45°. It was observed that high suctions appeared on the edges and corners of flat roofs, decreased on 22.5° roof and disappeared on 45° roof. This work described the roof loads as a function of roof angle and discussed the regional characteristics of roof wind loads.

Vickery (1976), as reviewed by Stathopoulos (1984a), examined four gable roof buildings with roof angles of 0°, 6°, 12° and 22°, the latter two of which fell into the intermediate roof range. Roof pressure distributions were found essentially continuous across the ridge in the cases of the 0°- and 6°-roofs. When approaching the 12°-roof, there was a separation of the flow at the ridge accompanied by a remarkable change of the wind loading magnitude. The pressure coefficient immediately behind the ridgeline was similar to that at the leading edge but fell away rapidly towards the trailing edge. In the case of the 22°-roof, the flow pattern and the load distribution are not far from those for the 12°-roof except that pressure coefficients on the leeward roof slope were roughly constant.

In this study, Vickery (1976) indicated that the pressure variation as a function of roof slope was associated with the flow separation. On nearly flat roofs, the flow separated at the leading edge, then reattached and remained attached over the ridgeline and through to the trailing edge. When the roof angle approached 12°, the flow reattached on the windward slope and then re-separated at the ridgeline before reattaching on the leeward slope. When approaching 22°, the flow did not reattach after separation at the ridgeline and the leeward roof was in a region of constant suction. Furthermore, this work implied that the wind loads distributed on different roof areas could show similar pressure coefficients, which is important for codification purposes.

Stathopoulos (1979) carried out a series of experimental studies on low-rise buildings with gable roofs. Four slopes of flat (0°), 1:12 (4.8°), 4:12 (18.4°) and 12:12 (45°) were

selected for tests. This work systematically described the loads on low-rise buildings. Based on the experimental results, the subsequent codification was made by Stathopoulos, Surry and Davenport (1985). This work has become the theoretical and experimental basis of the current wind provisions of NBCC and ASCE-7.

Holmes (1981) conducted experiments with a set of gable buildings with overhangs. The roof angles were 10°, 15°, 20° and 30°. This work provided valuable experimental data that are used in the present study. Holmes (1983) also described the variation of the flow separation associated with the flow turbulence as illustrated in Figure 2.1. It was indicated that the turbulence characteristics inherent in the flow have strong influence on the roof wind loads.

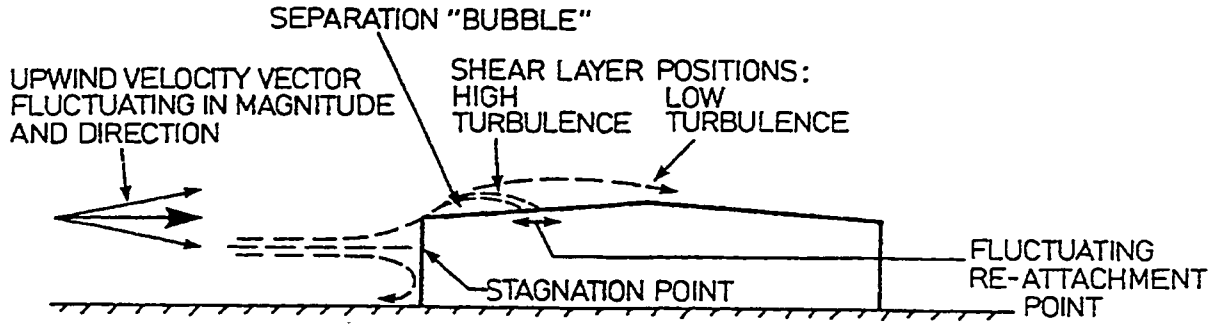

Figure 2.1 Flow around a low-rise building – after Holmes (1983)

To provide information for design loads for agricultural and horticultural buildings in the United Kingdom, Hoxey and Moran (1983) carried out a full-scale experimental program to study the effects of low building geometries on wind loads. As part of the program, a set of gable buildings with intermediate roof slopes (11°, 15°, 22° and 26°) were selected

for studying the wind loading effect of roof angle. Although the geometry of the model buildings was not in consistent style, Hoxey and Moran (1983) concluded that there was certain inadequacy of many national standards with respect to the prediction of wind loads on low-rise buildings.

Saathoff and Melbourne (1989) studied the peak roof loading generation mechanism by investigating the occurrence of the large pressures and the accompanying vortex generation. The intermittent peaks were observed when the separated wind flow rolled up to form a large vortex near the surface. The increase of wind flow turbulence reduced the size of flow separation bubble. The magnitude of the peak was found to be strongly dependent on the inherent turbulence intensity and turbulence length scale. This work is important for accurate wind tunnel simulation for roof loading measurement, since this study indicated that different simulations of wind turbulence in wind tunnel can bring variation in roof pressure coefficient to certain extent.

Richardson, Robertson, Hoxey and Surry (1990) carried out a collaborative research program called Silsoe Structure Building Project. The initial purpose of this project was to improve the wind tunnel measurement techniques by comparison of the wind tunnel data with full-scale data. The field test data were collected in England while the wind tunnel results were measured on the scaled models in Canada. The roof angles of the model buildings were 10° and 15°. The 10°-building had curved eaves that could be modified into regular sharp ones. In these experiments, only the loads along the roof central line across the ridgeline were measured. Richardson et al (1990), as well as

Savory, Dalley and Toy (1992), reported that the wind tunnel underestimated the peak suctions while it overestimated rms pressures in comparison with the full-scale measurements. However, the reason behind the discrepancies was not clearly explained by the authors.

Stathopoulos and Saathoff (1991), Meecham, Surry and Davenport (1991) worked separately on the wind loading distributions on gable models with identical roof slope, which is 4:12 (18.4° roof angle). Some of their results were compared with the current wind provisions specified for gable roofs of intermediate slopes.

The results of Stathopoulos and Saathoff (1991) indicated that for some cases the measured peak negative coefficient was approximately 20 percent higher than that indicated in the current wind provisions. For instance, a peak suction coefficient of -5.0 at the region of ridge corner was derived from their experimental results, while the design pressure coefficient is -4.1 as indicated in the current wind provisions.

Most critical local pressure coefficients measured by Meecham et al (1991) are shown on the upper part of Figure 2.2. The bottom part of Figure 2.2 shows data extracted from the current wind provisions by multiplying by 1.25 to eliminate the directionality factor, which will be discussed in Chapter 4. Although the trend of the experimental result of Meecham et al (1991) is similar with that of the current wind provisions, their experimental results are indeed higher in many roof locations than those indicated in the current wind provisions.

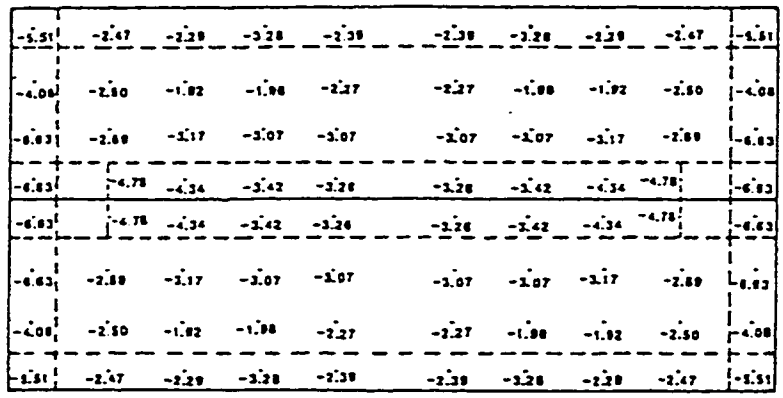

Enveloped Experimental Peak Negative CpCg's

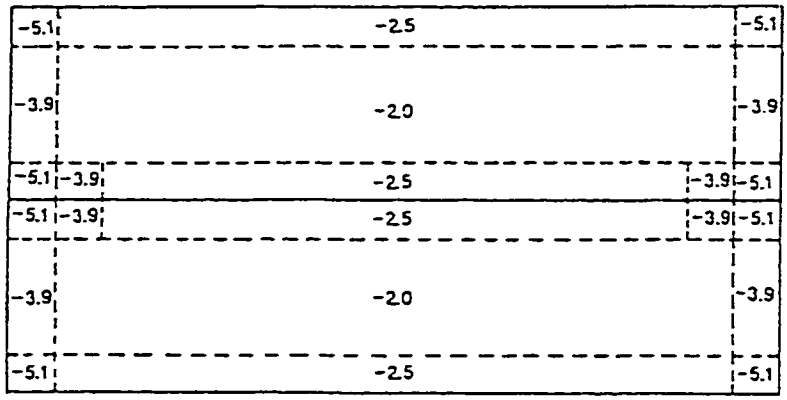

Enveloped Experimental Peak Negative (Unfactored) CpCg's

Figure 2.2 Comparison of the experimental and NBCC local pressure coefficients (multiplied by 1.25) on a gable roof of 18.4°, after Meecham et al (1991)

Sill, Cook, and Fang (1992) reviewed the studies on the Aylesbury Comparative Experiment. The Aylesbury Comparative Experiment project formulated an experimental wind tunnel program with the objective of estimating tunnel-to-tunnel differences in the pressure measurements in order to improve the current wind tunnel simulation techniques. The experiment was based on the Building Research Establishment full-scale experimental building, a low-rise building with gable roof at Aylesbury, England. Wind tunnel results had been reported from seventeen wind tunnels world wide that were carried out on the identical models at 1:100 scale. In general, the results indicated that the lab-to-lab variation in mean pressure coefficients was above 40 percent. However, the valuable databases obtained were very helpful to improve wind tunnel simulation techniques.

Ginger and Letchford (1992) investigated the flow separation and vortex formation mechanism on a set of canopy roofs with roof angles of 0°, 5°, 10°, 15°, 22.5° and 30°. A flow visualization test was carried out using oil flow on the 22.5° roof. The results agreed well with those of Saathoff and Melbourne (1989), demonstrating that the flow separation, particularly the vortex formation, was the cause of the large peak roof loads. Furthermore, it was reported that the peak loads on roof corners were accompanied by a stable conical vortex for the whole set of the slopes tested under oblique wind attacks.

Mean and rms pressure coefficients at corner and edge regions of a flat rectangular roof were measured by Tieleman, Surry and Lin (1994) under different wind profiles. The measured results were compared with the field data obtained at Texas Tech University. It

was emphasized that better simulation of the turbulence scale could reduce the inaccuracies of the wind tunnel results. Furthermore, this work and Surry and Lin (1995) stated that minor modification of roof geometry could affect roof loads to a large extent.

Separately, Tieleman, Surry and Lin (1994) and Kawai and Nishimura (1996) introduced hypotheses of physical interpretation of the correlation of the flow characteristics in the corner conical vortex with the roof surface pressure distribution directly beneath the vortex. These studies also provided suggestions on how to improve the wind tunnel measurement techniques.

In order to provide an empirical formula for estimating the design pressure coefficients on gable roofs by using peak factor approach, Uematsu and Isyumov (1996) measured the wind pressure coefficients on the leading edge and corner regions of a set of gabled-roof buildings with the slope of 4:12 (18.4°). The time-space correlation of the pressure distribution was investigated, based on the cross-spectra of the pressure fluctuations. Effects of the spatial and time averages on the peak pressures were discussed. The work was expected to contribute to the update of the Japanese wind standards.

2.2 JUSTIFICATION OF THE PRESENT STUDY

Previous studies have used three kinds of approaches to evaluate low-building roof loads, namely wind tunnel experimentation, full-scale investigation and theoretical simulation.

It can be found that the state of the art wind tunnel experimentation remains as the practical approach in evaluation of roof wind loads, though the valuable theoretical simulation and full-scale investigation have experienced developments recently, as described in Hoxey and Moran (1983), Tieleman et al (1994) and Kawai and Nishimura (1996). However, despite the reliability of wind tunnel experimentation, accurate wind tunnel simulation appears difficult for the current wind tunnel measurement techniques, as indicated by Richardson et al (1990) and Cook et al (1992). Errors in wind tunnel experimental results should be seriously concerned.

Regardless of difficulty in accurate wind tunnel simulation, significant achievements in determination of low-building design wind loads have been made (Stathopoulos et al, 1985), leading to the development of the current format of wind provisions for low-building roofs adopted by NBCC and ASCE-7. A key component in this development was the extensive experimental program carried out by Stathopoulos (1979) in which a variety of low-rise buildings with different sizes, heights, roof slopes and upstream exposures were examined.

Controversies have been presented in recent studies against the current wind provisions of NBCC, with respect to the gable roofs of intermediate slopes. Examples include those presented by Hoxey and Moran (1983), Meecham, Surry and Davenport (1991) and Stathopoulos and Saathoff (1991). However, there exist two reasons preventing those research results from further codification usage. The first is that only few roof angles were incorporated into these studies for the wind loading effect of roof angle, whose

effect on roof wind loads is so strong as shown in the preceding literature review. In fact, most experiments of these studies were carried out on various models but with the identical roof slope of 4:12. A single roof angle might not be sufficient to represent the total intermediate slope range. Another reason was that there were inconsistencies in experimental wind tunnel simulation, which will be fully discussed in Chapter 4

In summary, the literature review shows that it is necessary to carry out a comparative study to examine the suitability of the current wind provisions. The study should be built on wind tunnel experimental results based on commonly recognized experimental criteria in order to ensure consistency with full-scale data. Moreover, the tests should be able to represent the intermediate slope as a whole range. Generally speaking, the present study has incorporated these features so that it could be applied to the update of the current wind provisions.

As a matter of fact, the present study follows the criteria of the ASCE wind loading test standard (1997). A set of five models with roof angles of 10°, 15°, 20°, 25° and 30° have been constructed in order to represent the intermediate roof range; and wind loading information has been intensively measured. Two types of comparison have been made: first, the present results are compared with previous data; second, the present results are compared with the current wind provisions. The first type is for validation purposes, and the second is to examine the suitability of the current wind provisions.

CHAPTER 3

EXPERIMENTAL METHODOLOGY

3.1 WIND TUNNEL AND ATMOSPHERIC BOUNDARY LAYER WIND SIMULATION

The experiments have been carried out in the boundary layer wind tunnel of the Centre for Building Studies at Concordia University. The working section of the wind tunnel is 12.2m long and 1.8m wide. It has an adjustable roof height around 1.8m to provide negligible pressure gradient in the test section. More details about this wind tunnel are given by Stathopoulos (1984b) and further information on wind tunnel can be obtained Simiu and Scanlan (1986).

The boundary layer wind flow was simulated using triangular boards, a steel plate and carpet roughness. Four boards of the same triangular shape were erected side by side on the screen of the tunnel entrance and bound to the screen. The base and the height of each of the boards are 190mm and 1200mm, respectively. The distance between the centre of one of the two end boards to the tunnel wall is 350mm and the distance between the

boards themselves is 365mm centre to centre. The steel plate of 150mm height was placed on the floor at a distance of 750mm parallel to the screen. Carpet roughness was placed on the tunnel floor. These settings are used to generate an appropriate wind profile matching that in typical open country exposure.

For the experimental program, scaling factors of time, velocity and length were determined at first. The length scale depended on the ratio of the thickness of the simulated boundary layer to that in the real condition. The gradient height of 650mm developed over the wind tunnel floor could approximately match 260m boundary layer thickness in full-scale given the length scale as 1:400. The free-stream wind speed in the wind tunnel was set at 12.5m/s given the assumption of the velocity scale as 1:4, to simulate the full-scale velocity of 50m/s at the atmospheric boundary layer height. Corresponding to the length scale of 1:400 and the velocity scale of 1:4, the time scale was determined as 1:100. In this scale system, a 6-second sampling period matched an equivalent 10-minute full-scale sampling period.

Figure 3.1 shows the longitudinal mean-velocity profile (V/V_g) and turbulence-intensity-profile (V_{rms}/V), which were measured by a hot wire. In this figure, Z is a variable height over the tunnel floor and Z_g is the gradient height over the floor; V represents the wind speed and V_g is the tunnel wind speed at the gradient height, which was set at 12.5m/s. Also in this figure, the theoretical simulation of the experimental mean-velocity profile indicates that a power law simulation with an exponent of 0.14 is appropriate for the wind tunnel simulation.

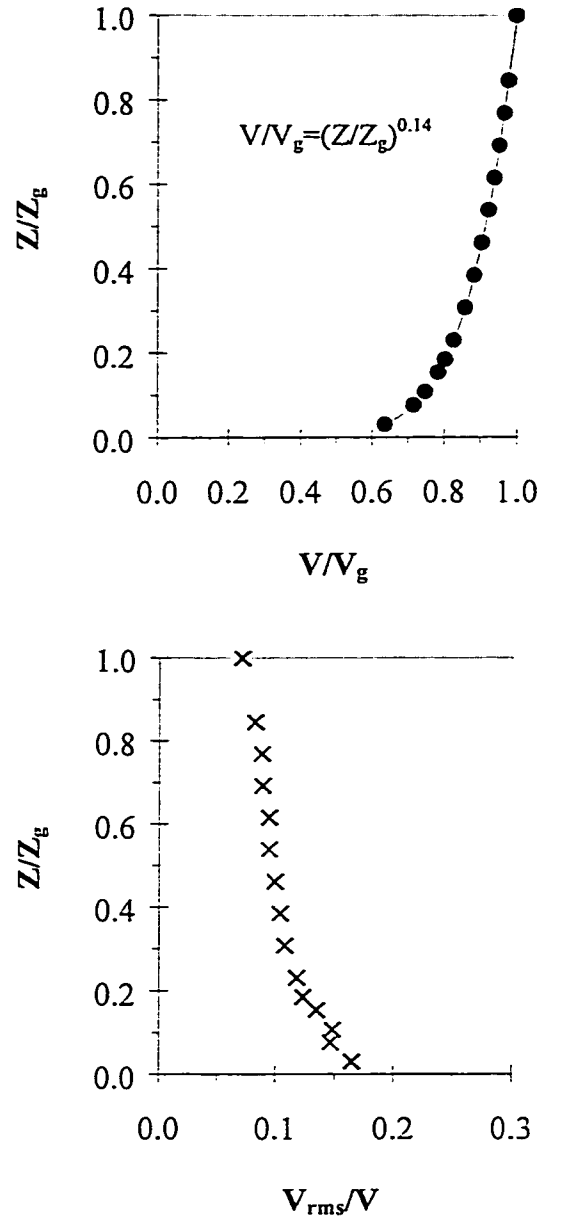

Figure 3.1 Profiles of mean velocity and turbulence intensity

Figure 3.2 shows the experimental and theoretical longitudinal power spectral densities of the approaching flow at 25mm height over the tunnel floor (10m height above ground in full-scale). The spectrum S_v is calculated from the experimental wind velocity, in the wind tunnel. The scattered points presented in this figure come from the experimental power spectral density and the smooth curve represents the spectral simulation using the Von Karman equation, i.e.

$$\frac{nS_v(Z,n)}{\sigma^2} = \frac{4n\ {}^{x}L_v/V}{\left[1+70.8\left(n\ {}^{x}L_v/V\right)\right]^{5/6}} \tag{3.1}$$

where the longitudinal integral scale ${}^{x}L_v$ is 280mm as simulated from the experimental data, which is equivalent to 112m in full-scale given the length scale as 1:400.

The properties of the simulated atmospheric boundary layer are summarized in Table 3.1, accompanied by the criteria of the ASCE wind loading test standards (ASCE Draft, 1997). The experimental roughness length Z_o is fitted by using the logarithmic law equation in the form:

$$\frac{V}{V_g} = 0.4C_g \ln\left(\frac{Z}{Z_o}\right) \tag{3.2}$$

where C_g is regarded as a property of the terrain roughness.

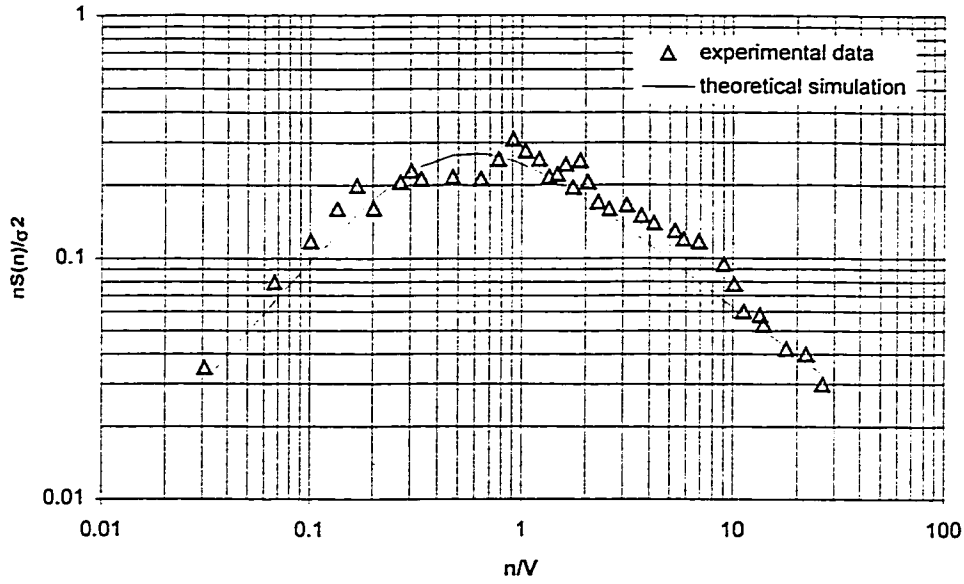

Figure 3.2 Comparison of experimental and theoretical velocity spectra

Table 3.1 Comparison of the experimental setting with the corresponding criteria of the ASCE Standard for wind loading tests (ASCE Draft, 1997) - the current geometrical scale is 1:400

		Standard open country exposure	Wind tunnel simulation	Equivalent full-scale values
Terrain Description		Open flat terrain; grass; few isolated obstacles	Carpet roughness	-
Roughness length z_o		0.03 m	0.07 mm	0.028m
Gradient height Z_g		274m	650mm	260m
Mean velocity power-law exponent α		0.14	0.14	0.14
Longitudinal turbulence-intensity at z = 10m in full-scale		17.2 %	17.1 %	17.1%
Integral length scale of Turbulence ^xL_v(m)	Z = 10 m	110m	280mm	112m
	Z = 200m	510m	-	-

Table 3.1 shows that the parameters of the present wind tunnel simulation generally satisfy the criteria (ASCE Draft, 1997), which indicates that the results obtained from the present wind tunnel experiments could be appropriate and suitable for codification usage as far as accurate simulation is concerned.

3.2 MODEL CONFIGURATIONS

Five gable roof models with an interchangeable roof panel have been used for the wind tunnel experiments. Figure 3.3 shows the original models in the wind tunnel. These models had a set of roof angles of 10°, 15°, 20°, 25° and 30°, which were used to represent the intermediate slope range. The dimensions of the models are shown in Figure 3.4. The interchangeable panel had an area of 150×52 mm^2, which was equivalent to 60×20.8m^2 in full-scale. The five models had the same eaves height (h) of 27.5mm (11m in full-scale) and the same long wall length (L) of 150 mm (60m in full-scale), but varied mid-roof heights and varied building spans (B). Thus there is a variation of the ratio of long wall length to building span (L/B). However, the difference of this ratio is not considered significant in the present study.

The perspective view of these models is shown in Figure 3.5. It is indicated in this figure that the wind azimuth (α) started at 0° when the wind was normal to the ridgeline. It increased in counter-clockwise direction.

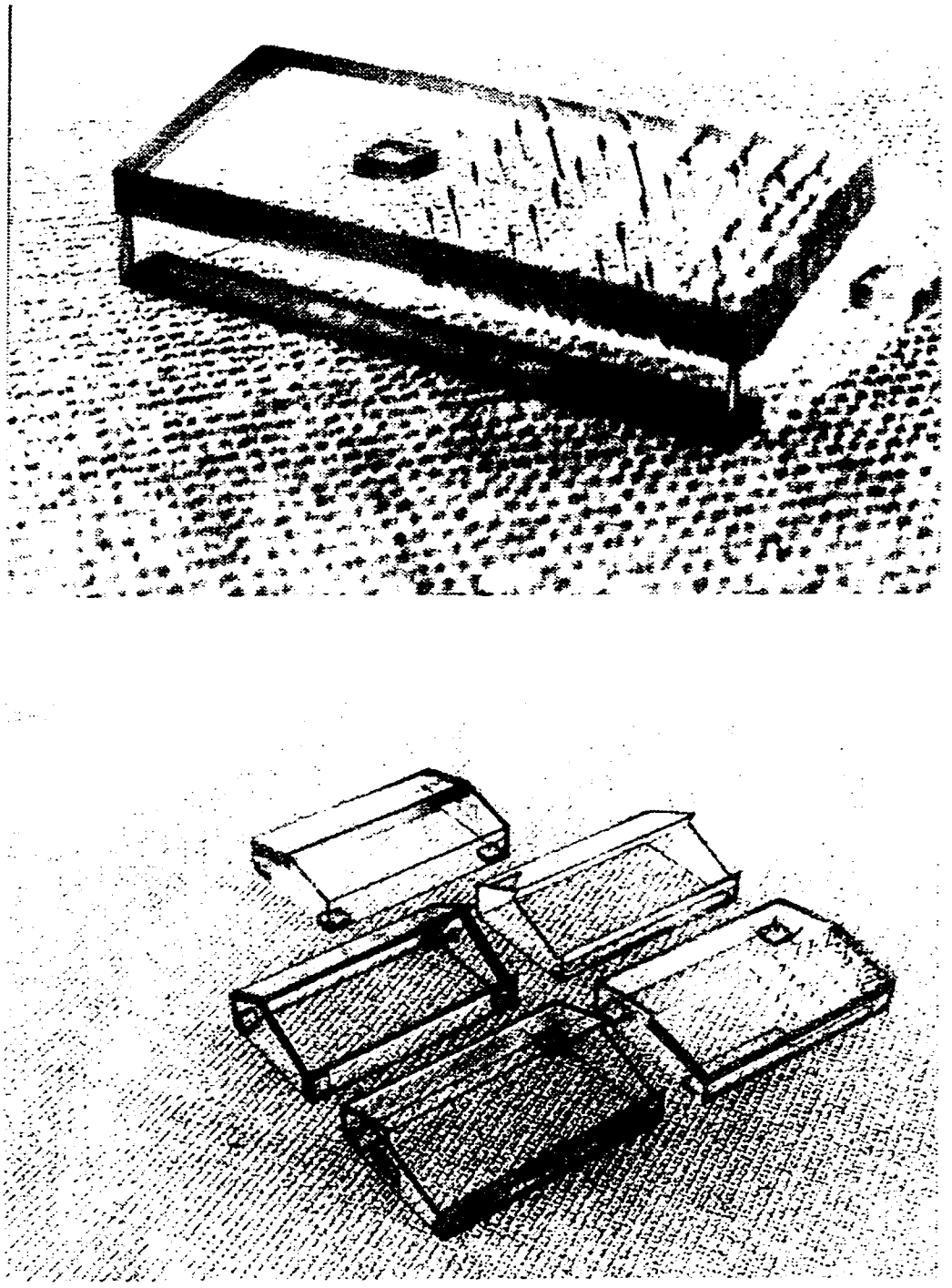

Figure 3.3 A typical and a set of building models with the interchangeable roof panel

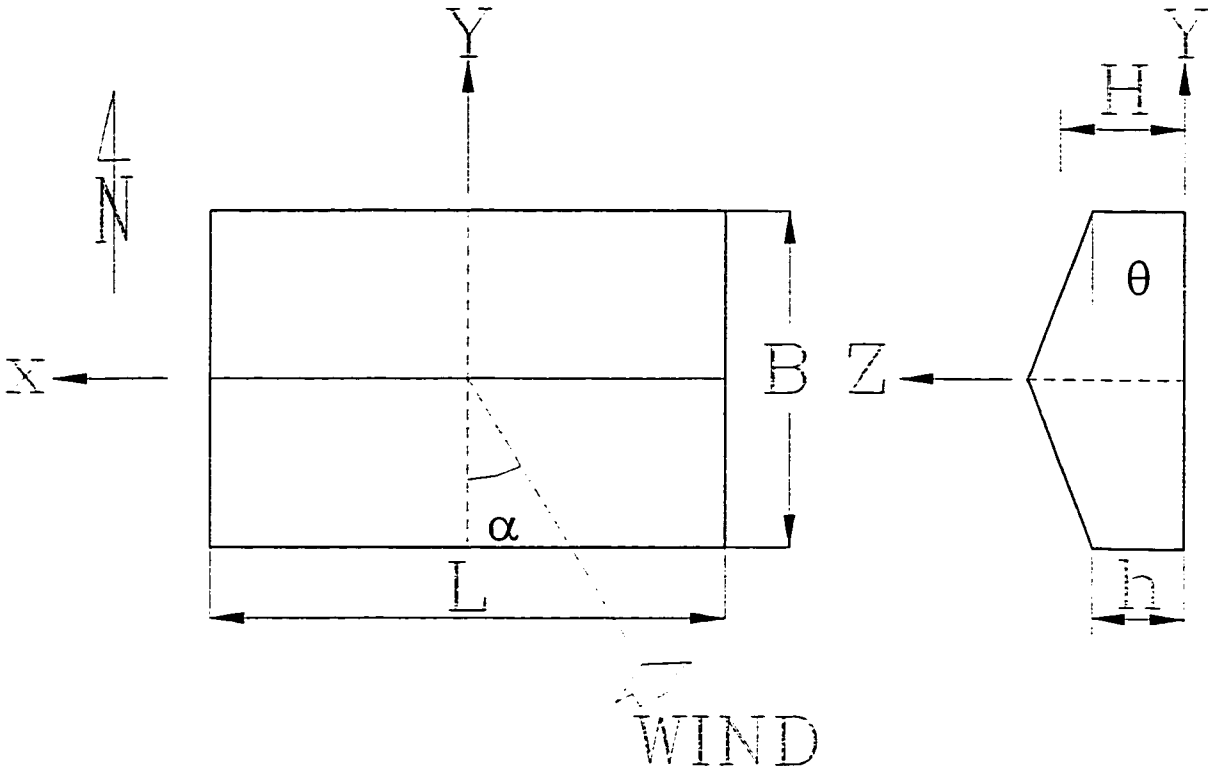

θ	L (m)	B (m)	h (m)	H (m)
10°	60	40.8	11	12.8
15°	60	40.2	11	13.7
20°	60	39.1	11	14.6
25°	60	37.7	11	15.4
30°	60	36.0	11	16.2

Figure 3.4 Schematic illustration of the model buildings in full-scale

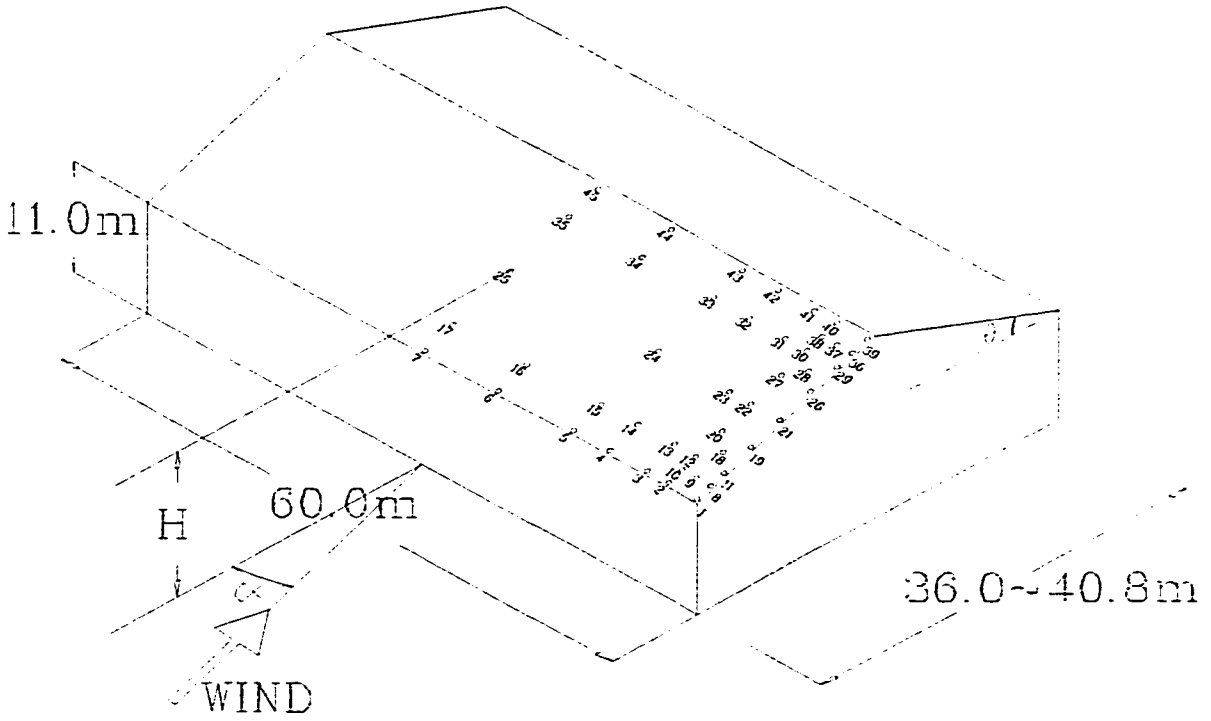

Figure 3.5 Illustration of the model buildings in full-scale

Forty-five pressure tappings were mounted on a half of the interchangeable roof panel. Most of the pressure tappings were located on the corner and edge regions. By virtue of symmetry, the 45 pressure tappings on a quartering part of a roof are effective as 180 tappings for the entire roof surface.

Figure 3.6 shows details of the pressure tappings on the interchangeable roof panel. The pressure tappings were numbered as Tap 1 through Tap 45, beginning at the right bottom corner and increasing leftwards and then upwards. The taps were mounted as close as possible to the roof edges and ridge. The distance from each of the dashed lines to the corresponding edge and ridge was 10 percent of the building width (B) of the 20° model, equivalent to 3.9m approximately in full-scale, delimiting the seven code-defined regions. It followed the current codal definition on roof region. This distance was assumed as a constant for convenience purposes in the present study, though it varied from 36.0m to 40.8m in full scale due to the variation of building width (B). The seven roof regions are named in the present study as follows:

-Region A (Eaves corner)

-Region B (Ridge corner)

-Region C (Apex ridge)

-Region D (Eaves edge)

-Region E (Gable edge)

-Region F (Ridge)

-Region G (Interior)

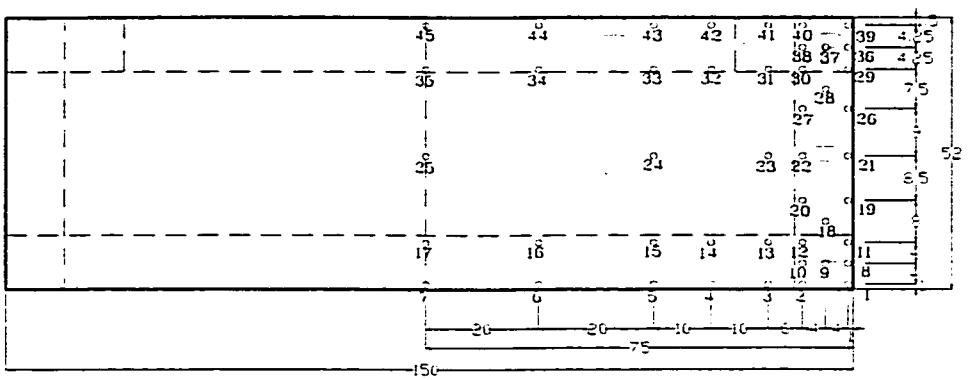

Figure 3.6 Schematic illustration of the tappings and the regions on the interchangeable roof panel (unit: mm)

Table 3.2 Tapping combinations used in area-averaged pressure calculations

Area code	Tapping	Full-scale area(m^2)	Area code	Tapping	Full-scale area(m^2)
A-0	The worst local	≤0.1	E-0	The worst local	≤0.1
A-1	1,8	1.9	E-1	18,19	7.7
A-2	1,2	3.2	E-2	19,21	2.4
A-3	8,11	2.2	E-3	18,19,20	6.4
A-4	1,8,11	3.3	E-4	18,19,20,21,22	27.5
A-5	1,8,9	5.8	E-5	18,19,20,21,22 26,27,28	51.9
A-6	1,8,9,11	9.6			
A-7	1,2,8,9,10	9.6	F-0	The worst local	≤0.1
A-8	1,2,8,9,10,11,12	17.3	F-1	42,43	5.8
B-0	The worst local	≤0.1	F-2	32,42	8.6
B-1	36,39	2.3	F-3	32,33,42,43	36.8
B-2	36,37	4.1	F-4	32,33,34,42,43,44	73.6
B-3	39,40	4.8	F-5	32,33,34,35 42,43,44,45	99.8
B-4	36,37,39	6.9			
B-5	36,37,38,39,40	11.6	G-0	The worst local	≤0.1
C-0	The worst local	≤0.1	G-1	23,24	11.5
C-1	31,41	17.3	G-2	23,24,25	61.4
D-0	The worst local	≤0.1			
D-1	3,13	10.0			
D-2	3,4	5.1			
D-3	3,4,13,14	26.6			
D-4	3,4,5,13,14,15	43.3			

Table 3.2 presents the combinations of those pressure tappings for the calculations of the most critical area-averaged pressure coefficients, accompanied by their corresponding full-scale areas. These tapping combinations were presumed to expose to the most critical area-averaged wind loads since the area-averaged loads here were merely the electrical averages of the local loads that have been found to be the largest ones.

3.3 DATA ACQUISITION AND PROCESSING

3.3.1 Data Acquisition System and Measurement Program Setting

Pressure tappings consisting of 10mm length steel tubes of 0.8 mm inside diameter were mounted on the model roof panel, with flexible tubes 610mm length and 1.6mm interior-diameter leading them to the pressure transducer. Restrictors were inserted within the tubes at halfway of tube length, to provide a flat frequency response above 100 Hz. Frequencies of pressure fluctuations at the tappings are expected to be well below this value (Saathoff and Stathopoulos, 1992).

The 45 tubes were divided into 3 groups, 15 tubes each group. These 15 tubes of each group could be in turn connected with the Scanivalve ZOC-14 electronic pressure transducer that has altogether 16 pressure channels. Consequently, the 15 pressure tappings of each group were connected to the 15 pressure channels on the pressure transducer, while one pressure channel remained was left to be used by the pitot tube in order to measure the reference free-stream velocity pressure.

A Scanivalve HyScan-1000 system was used for the data acquisition. A 60-MHz 80486-based PC-AT computer was utilized to host the HyScan-1000 system and to control the data acquisition. The pressure scanning system was programmed to record the pressure signals through an analog/digit converter with the frequency of 256Hz. The data were streamed directly into the hard drive as time series. During the pressure acquisition runs, the HyScan-1000 system provided the function of real-time visualization of the magnitudes of the roof pressures. It is noteworthy that the measuring frequency response of 256Hz is adequate in reducing the attenuation of wind peaks in wind tunnel measurement (Holmes, 1984).

During the pressure signal acquisitions, every pressure tapping in each of the three tapping groups was measured with six segments of pressure data in a given experimental setting. Each data segment had a 6-second sampling time and in 256Hz sampling frequency. Taking into account the time scale, the sampling time and frequency of each segment were equivalent to approximate 10 minutes and 3Hz in full-scale, respectively.

The five models were investigated for all azimuths by virtue of the real-time visualization function of the HyScan-1000 system, which could provide clear pictures of roof pressure variations during data sampling. Thus some pressures in some wind azimuths which did not appear critical were not saved into the hard disk space. Although the data samples have been reduced in this way, 250MB hard disk space has been consumed at the final. The detailed measurements were performed for the following eighteen wind azimuths: 0° (wind direction normal to the ridgeline), 15°, 30°, 45 °, 55°, 60°, 65°, 70°, 90 ° (wind

direction normal to the gable wall), 120°, 130°, 135°, 140°, 150°, 180°, 225°, 270° and 315°. These wind azimuths appear either as critical azimuths or characteristic ones.

3.3.2 Data Processing System

Roof pressure signals have been collected in form of time series. Typical time series obtained are illustrated in Figure 3.7. Data processing programs were developed by using the FORTRAN77 programming language to calculate the local and area-averaged pressure coefficients including their peaks.

Equations for the evaluation of the mean, minimum, maximum, and rms pressure coefficients are presented as follows:

Mean pressure coefficient: $$C_{pmean} = \frac{P_{mean}}{\frac{1}{2}\rho V_H^2} \quad (3.3)$$

Minimum pressure coefficient: $$C_{p\min} = \frac{P_{\min}}{\frac{1}{2}\rho V_H^2} \quad (3.4)$$

Maximum pressure coefficient: $$C_{p\max} = \frac{P_{\max}}{\frac{1}{2}\rho V_H^2} \quad (3.5)$$

Rms. pressure coefficient: $$C_{prms} = \frac{\sqrt{\sum_{i=1}^{n}(P_i - P_{mean})^2 / n}}{\frac{1}{2}\rho V_H^2} \quad (3.6)$$

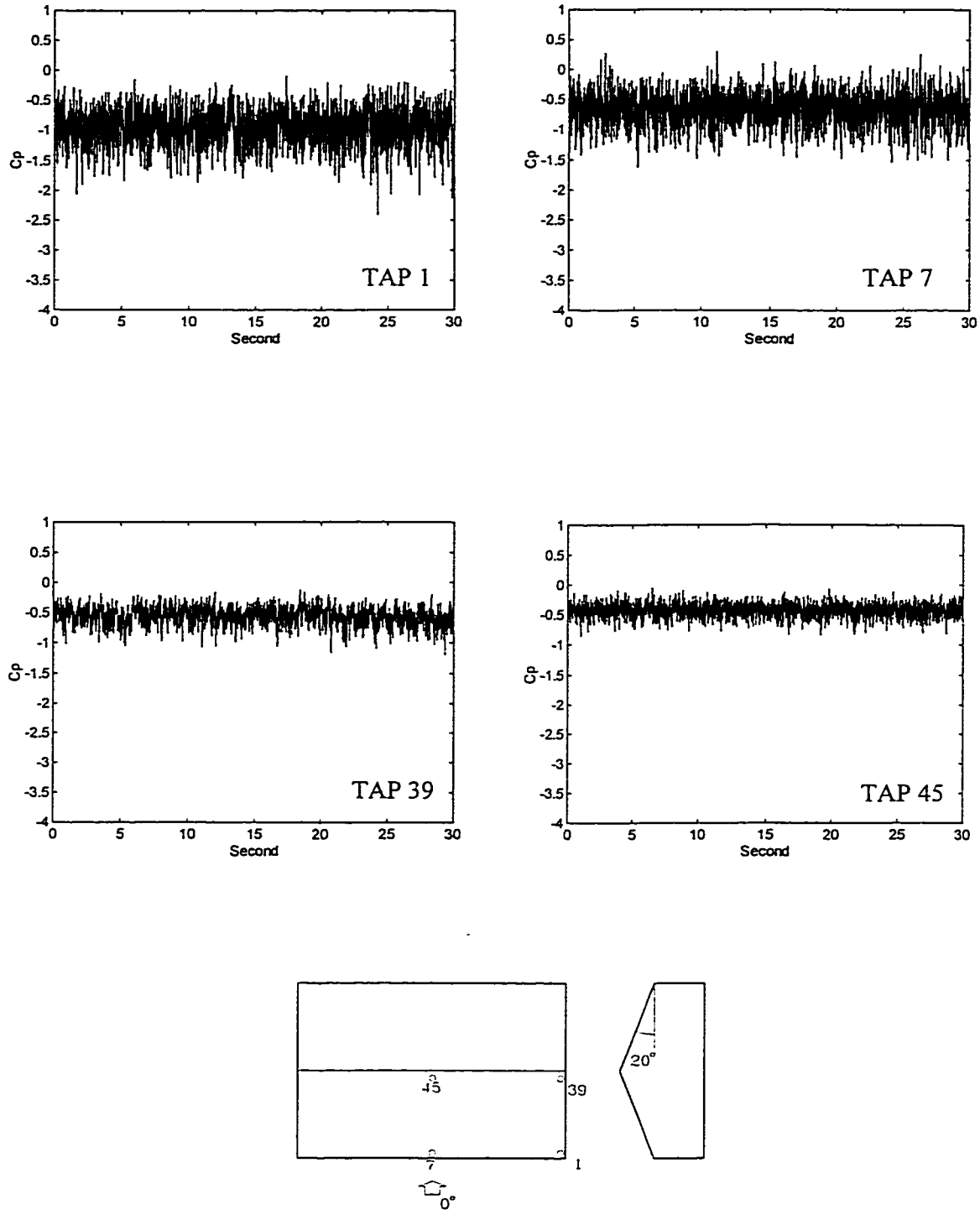

Figure 3.7 Typical time series for $\theta = 20°$ and $\alpha = 0°$

where V_H is the reference wind velocity measured at the mid-roof height in accordance with the codal definition; ρ is the air density. In order to obtain their peaks, the Type-I extreme value analysis approach is used, which is described in detail in the next sections.

Extreme values of times series are important in determining the design wind loads. Generally, the Type-I extreme value analysis approach is regarded suitable as far as low-building roof loading predictions are concerned (Mayne and Cook, 1980); and the working approach (Gumbel, 1958) is briefly introduced as follows.

Let X_m be the random variable associated with the extreme value of the initial variable X. The cumulative distribution function of the Type-I asymptotic form for the distribution of X_m is as follows:

$$P(X_m < x) = \exp(-\exp(-(x-u)/s)) \tag{3.7}$$

where u corresponds to a characteristic largest value of the initial variable X (mode) and s corresponds to a measure of dispersion of X_m. The extremal parameters s and u can be estimated by using Gumbel's plot by taking twice the logarithm on both sides of Equation 3.7, which becomes:

$$\ln[-\ln(P)] = -\frac{(x-u)}{s} \tag{3.8}$$

The probability term P can be determined as follows: the observed extreme values, in present case is 18 extreme values, evenly extracted from the 6×6-second pressure record

time series (the 3 highest peaks from each segment), are sorted into ascending order of magnitude, after which each is assigned a rank, r, where r = 1 for the smallest and r = Q for the largest of Q values. An estimate of P corresponding to each extreme value can be calculated from their ranks using the following equation:

$$P = \frac{r}{Q+1} \tag{3.9}$$

The mode (u) and dispersion (s) can be determined from plotting Equation 3.8. Mode corresponds to the x value when

$$y=-\ln[-\ln(P)] \tag{3.10}$$

is zero and the dispersion is the slope of the line fitting the data.

The scheme for generating the area-averaged pressure coefficients has been presented in Table 3.2. It is noteworthy that the electric averaging approach utilized for the present study to measure the instantaneous spatially averaged pressure acting over a rectangular area is different from the pneumatic averaging technique developed by Surry and Stathopoulos (1978).

3.4 REPEATABILITY OF MEASUREMENT RESULTS

Figure 3.8 shows the repeatability of the wind tunnel results. Two sets of C_{pmean} data have been measured in the same experimental setting on two occasions, 30 days apart, on Taps 1 to 45 on the 15°-roof under 60° wind azimuth. Such an agreement is typical for other cases tested and it is quite encouraging for further application of the present experimental results.

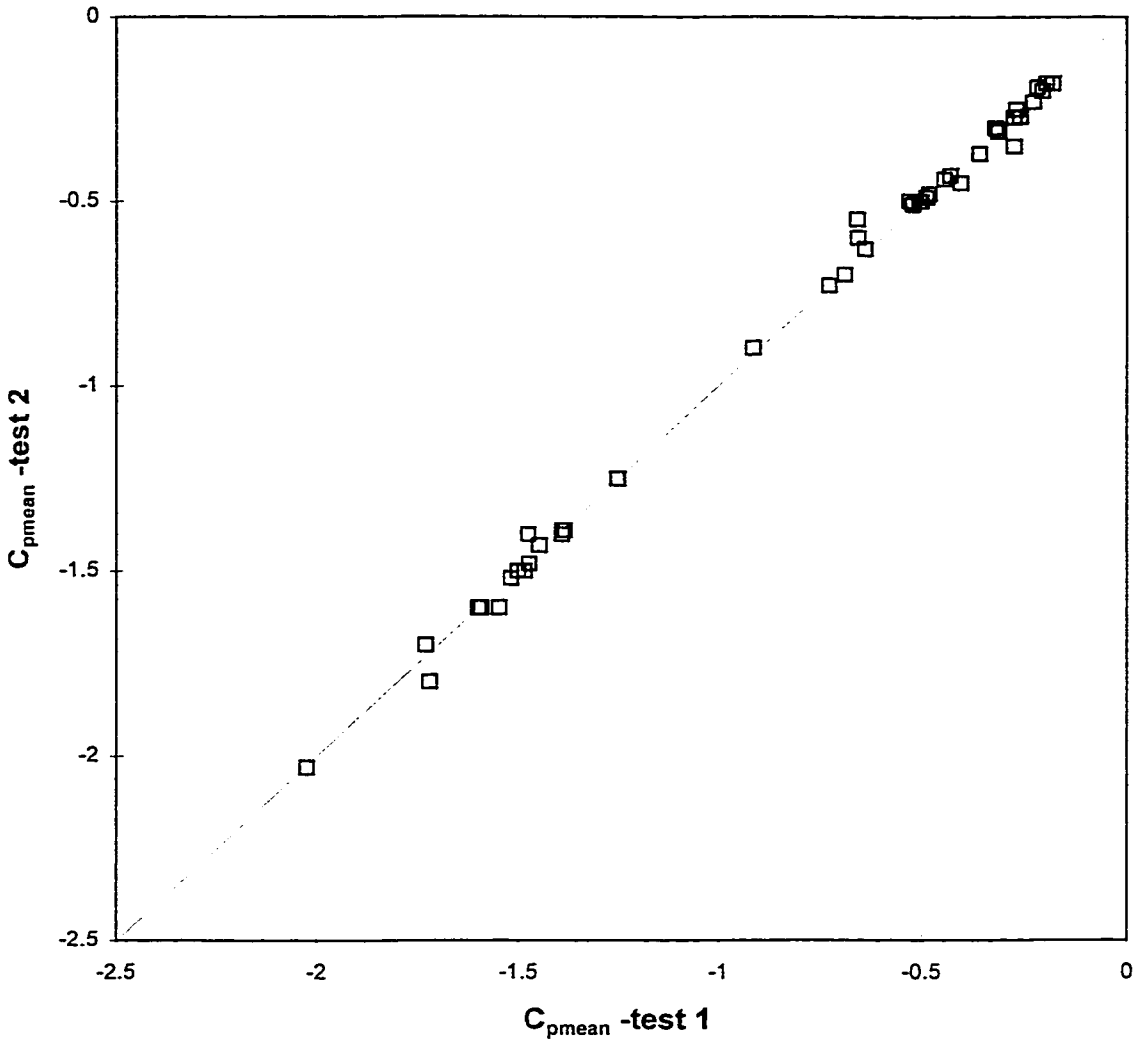

Figure 3.8 Repeatability of typical measured mean pressure coefficients

CHAPTER 4

RESULTS AND DISCUSSION

4.1 GENERAL DESCRIPTIONS

The current wind provisions classify the low-building gable roofs into three categories in terms of roof slope. The provisions also separate the roof into seven roof regions, based on distributions of most critical local pressure coefficients on these roof regions. This is shown in Figure 4.1, which will be intensively used in this and the following chapters. Furthermore, the wind pressure coefficient specifications provide pressure zoning and loading definitions for the roofs based on the similarities of their regional most-critical pressure coefficients. These roof regions can be grouped into pressure zones, provided that the regions grouped together have similarity in terms of their most critical regional pressure coefficients. For the intermediate roofs, the pressure zones can be called as Zone 1 (Eaves and Ridge Corners), which includes Regions A and B, Zone 2 (Edges near Apex), which includes Regions C and E, Zone 3 (Edge and Ridge), which includes Region D and F, and Zone 4 (Interior), which includes Region G.

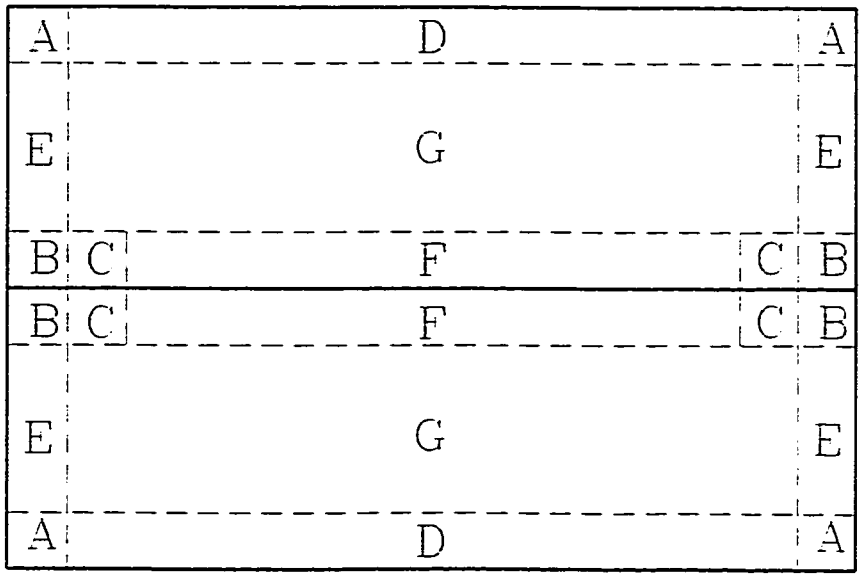

Region A: Eaves corner

Region B: Ridge corner

Region C: Apex edge

Region D: Eaves edge

Region E Gable edge

Region F: Ridge

Region G: Interior

Figure 4.1 Illustration of the seven code-defined roof regions

In this chapter, the discussion on the present results is carried out with respect to roof region, pressure zoning and loading and slope range, which are the major concerns of the current wind provisions. The findings in this discussion will provide solid information for the codification process carried out in the next chapter. Prior to the discussion, the comparisons of the present results with those from previous studies are conducted at first for the purpose of validating the present experimental results.

4.2 PREVIOUS DATA AND PRESENT RESULTS

In this section, the present wind pressure coefficients obtained from four wind azimuths of 0° 60°, 90° and 135° are compared with the previous research findings. The zero wind direction is a characteristic wind direction and the slope effect on flow separation and attachment has been mostly investigated by previous studies in this wind direction. At the same time, it has been found that most critical pressure coefficients are generally induced by around 60°, 90° and 135° wind azimuths.

Figure 4.2 compares the experimental pressure coefficients measured at 0° wind azimuth along the central lines of the roofs across ridge with those from previous studies. These diagrams describe the relationship between the roof pressure distribution and the flow separation, besides the validation of the results of the present study.

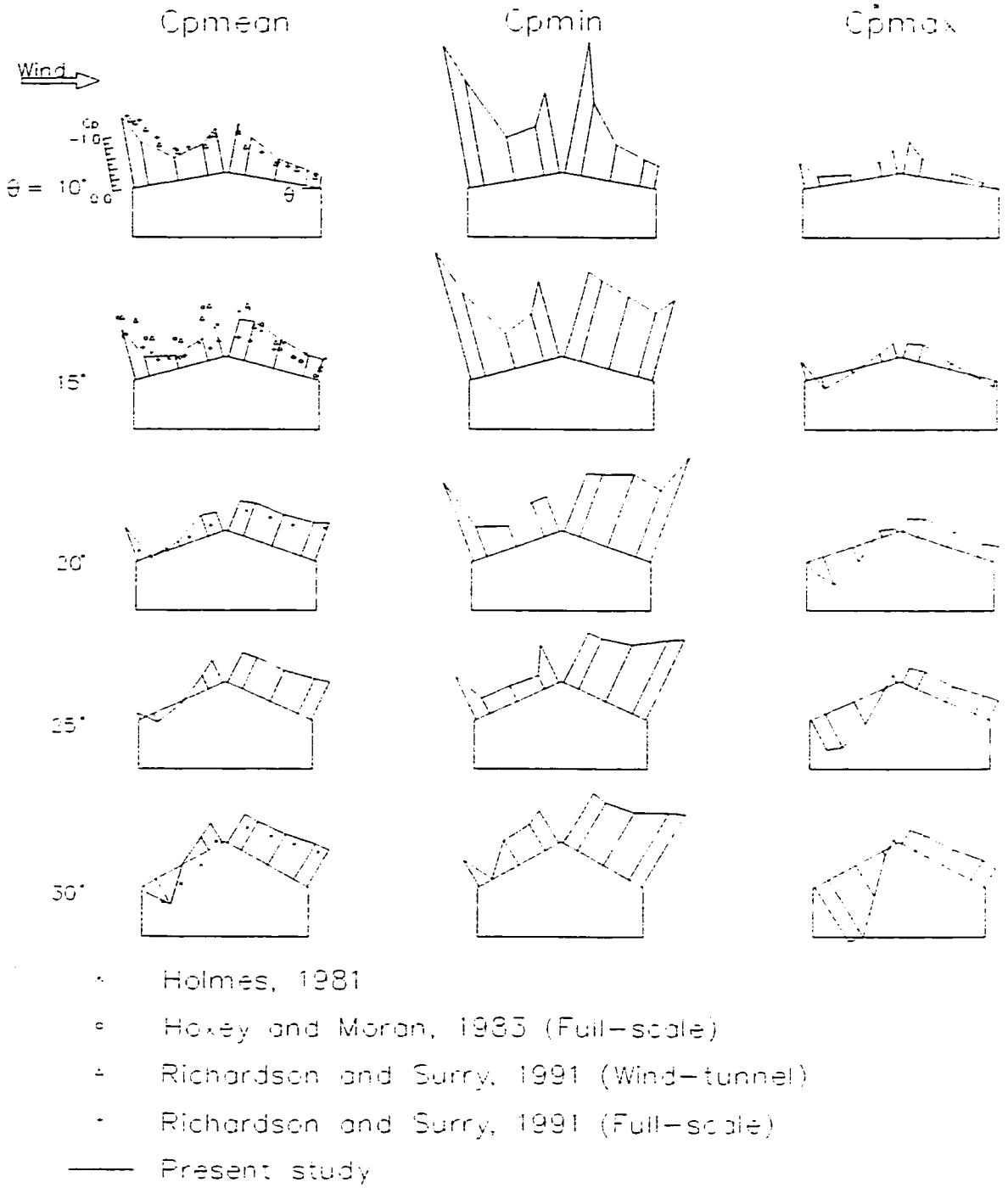

Figure 4.2 Pressure coefficient profiles along the central lines across the roofs, α=0°

The data incorporated in Figure 4.2 come from the previous wind tunnel and full-scale research studies for comparison purposes, which include Holmes (1981), Hoxey and Moran (1983) and Richardson and Surry (1991). It is noted that all of these previous data available are mean pressure coefficients.

While a strong wind flow separation occurs at the leading edge when θ =10° and 15°, high suctions are induced near the eaves and the ridge. When θ =30°, a different flow pattern is created with flow attaching onto the leading edge (positive mean) and accelerating or even separating half way (negative mean) over the windward slope. In the latter case, the maximum pressure coefficients over the windward slope exceed, in magnitude, the minimum pressure coefficients. Furthermore, the other two circumstances (θ =20° and 25°) represent the transition of flow pattern, which is quite complex as indicated by the variations in mean and fluctuating pressure coefficients. Except for the 10°-roof, the leeward slopes are exposed to similar negative pressures somewhat independent of the roof angle due to the second separation from the ridgeline.

For the 10°-roof, both the wind tunnel and full-scale data measured by Richardson and Surry (1991) agree well with the present results. For the 15°-roof, the full-scale data from Hoxey and Moran (1983) agree well with the wind-tunnel data from Richardson and Surry (1991) but they have higher values than those measured in the present study. Agreement is better among the results of Holmes (1981), the full-scale data of Richardson and Surry (1991) and those of the present study. For the 20°- and 30°-roofs, only the

pressure coefficients measured by Holmes (1981) are available, whose values are comparably lower than those of the present study.

Generally speaking, in spite of some differences in terms of building dimension and flow characteristics, these wind tunnel results appear to be in reasonable agreement. Some of the differences in the pressure coefficients could be also due to differences in the experimental settings. More details about the experimental settings used in the previous studies, when available, are presented in the following comparisons.

Figure 4.3 presents mean pressure coefficient contours for the normal wind direction, measured on the roofs of 15°, 20° and 30° by Holmes (1994) and by the present study. The agreement between these two studies is generally satisfactory, though the present data measured for the corner regions are comparably larger than those of Holmes (1994). The difference shown in the comparison may be attributed to the difference in the geometrical ratio of eaves height to the long wall length (h/L), which is 0.2 for the present study while that of Holmes (1994) is 0.4. Furthermore, it is noted that the eaves had overhangs in the study of Holmes (1994).

In Figure 4.4a, the present data measured for the 20° roof are compared with those measured by Meecham et al (1991) on a 18.4° roof (slope: 4:12). Both studies are carried out on wind-tunnel open country exposures; however, the power-law exponent was equal

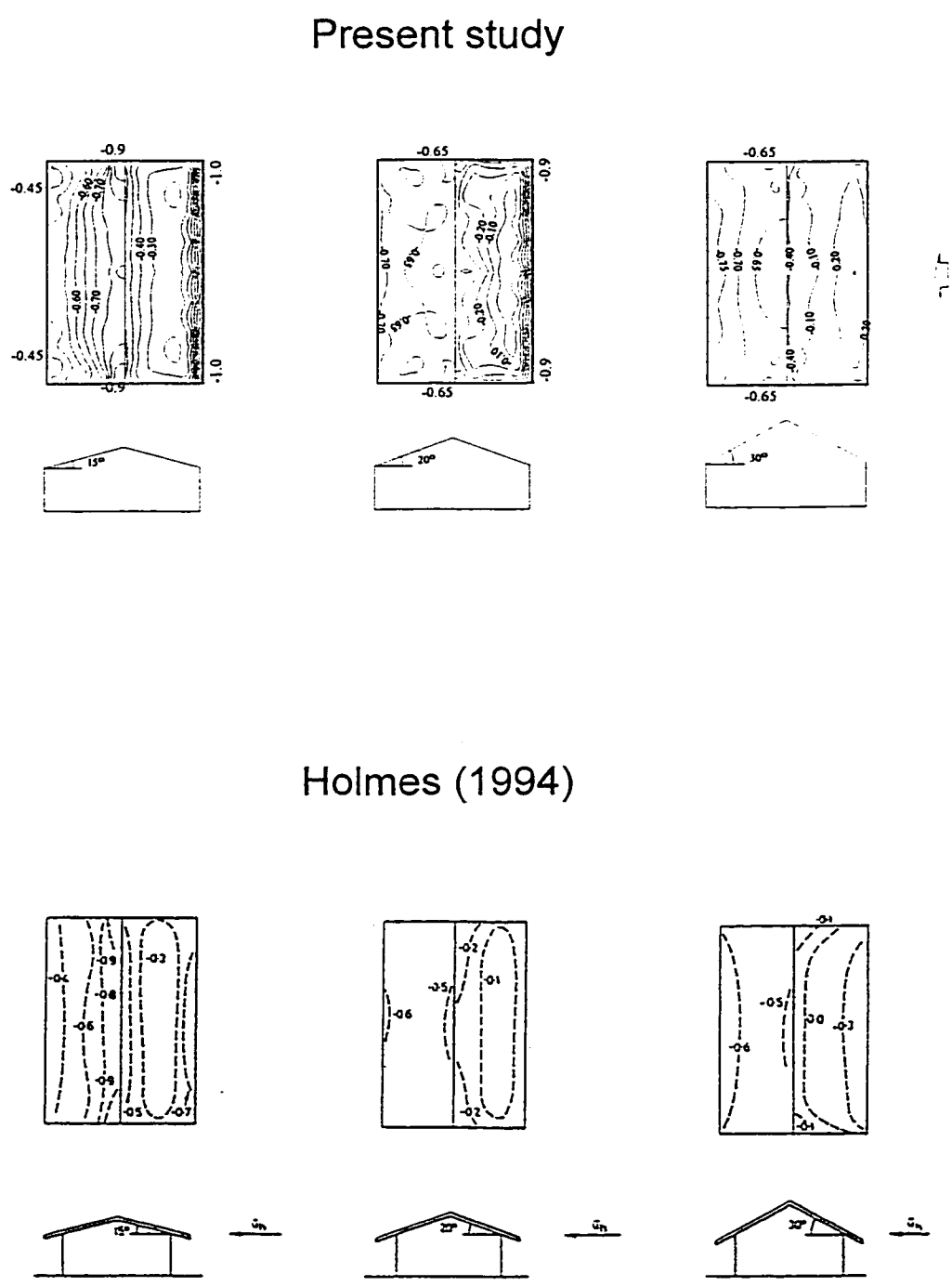

Figure 4.3 Mean pressure coefficients measured in this study and those presented by Holmes (1994) for three roof slopes at 0° wind azimuth

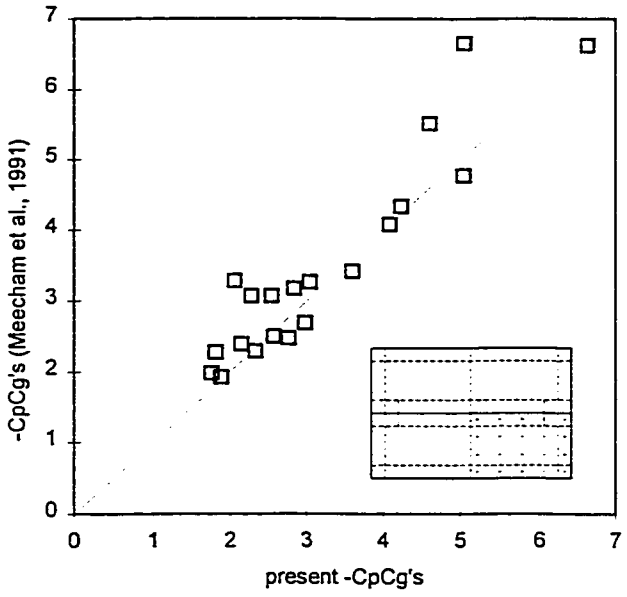

Figure 4.4a) Comparison of the most critical local pressure coefficients measured for the present study with those measured by Meecham et al (1991) for 20 tappings

Meecham et al (1991)
(θ = 18.4°)

Present study
(θ = 20°)

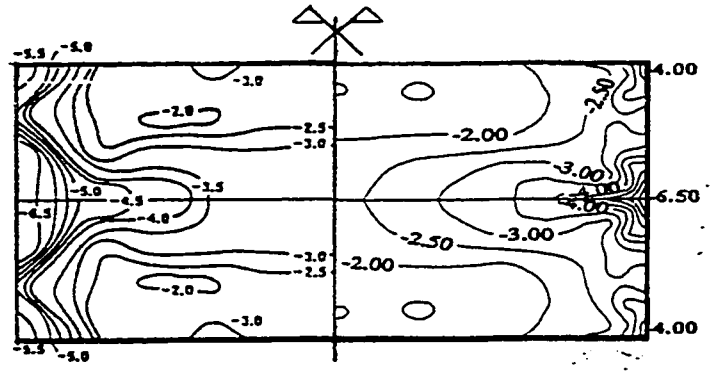

Figure 4.4 b) Comparison of the most critical local pressure coefficients measured for present study with those measured by Meecham et al (1991) in contour format

to 0.14 in the present study as opposed to 0.19 in the research of Meecham et al (1991). The comparison is in terms of most critical local pressure coefficients, with the present results interpolated into the corresponding locations of those tested by Meecham et al (1991). Figure 4.4b compares the same data in pressure coefficient contour form. The data of Meecham et al (1991) seem to be somewhat higher than those of the present study, particularly for those on the region of Eaves corner.

The discrepancies are likely due to the differences between the two studies in wind simulation and model configuration. Since the terrain exposure of Meecham et al (1991) is rougher than that of the present study and rougher terrain could induce higher peak pressure coefficients (Holmes, 1983), the differences in the pressure coefficients are reasonable. The difference could also be attributed to the difference in the roof slopes that may strongly affect the roof wind loads as discussed before.

Figures 4.5 through 4.7 show the pressure coefficient contours from Uematsu and Iysumov (1996) and the present study, both of which are based on the experimental mean and minimum values. The magnitudes of the pressure coefficients of Uematsu and Iysumov (1996) are higher than those of the present study. This is not surprising since the terrain exposure simulated by Uematsu and Isyumov (1996) was rougher as indicated by its power law exponent of 0.17. The roof angle tested by Uematsu and Isyumov (1996) is the same as that of Meecham et al (1991) of 18.4° (slope: 4:12), which is also different from the present 20°-roof taken into the comparisons.

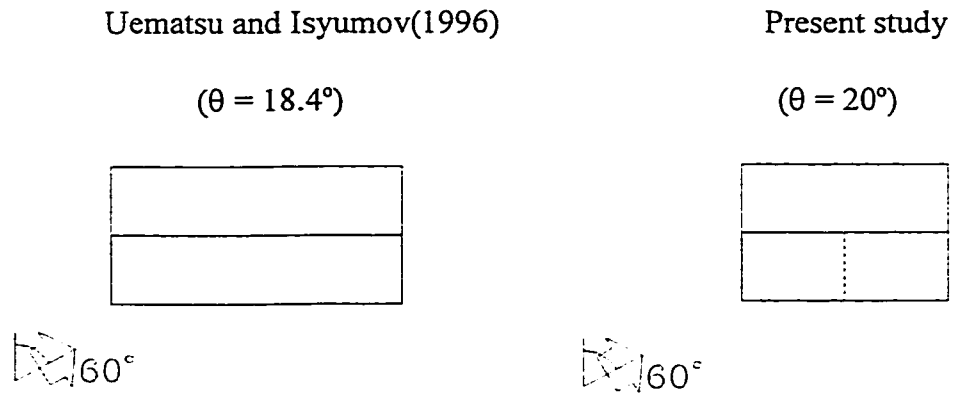

Figure 4.5 Comparison of the mean and minimum pressure coefficients measured for the present study with those from Uematsu and Isyumov (1996)

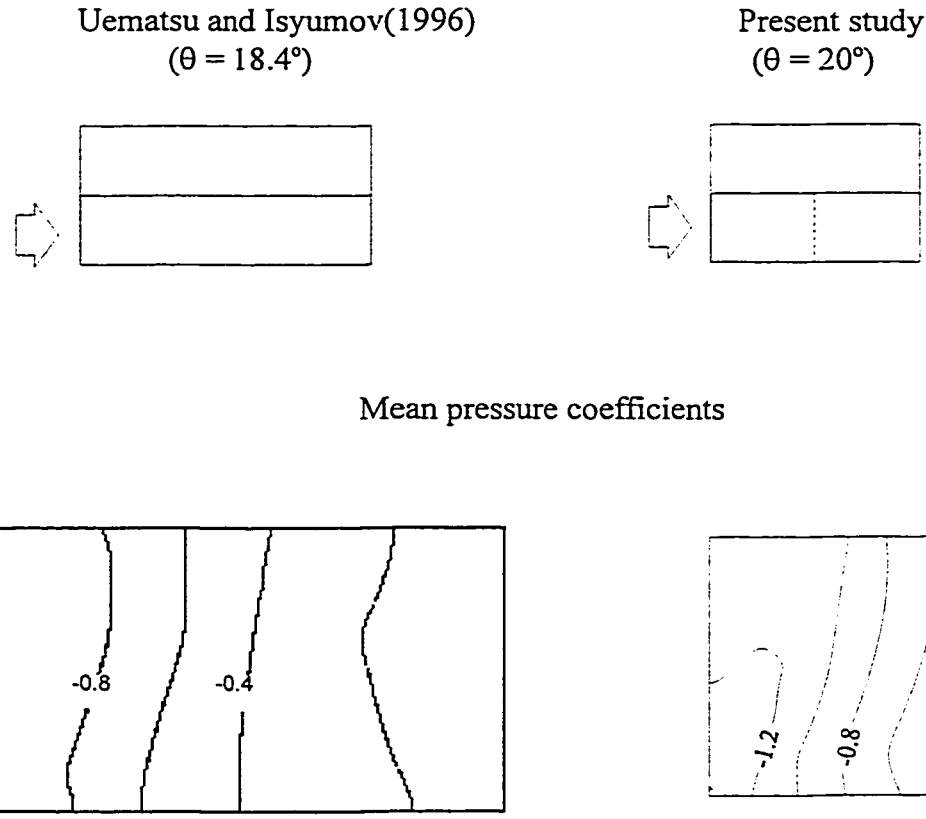

Figure 4.6 Comparison of the mean and minimum pressure coefficients measured for the present study with those from Uematsu and Isyumov (1996)

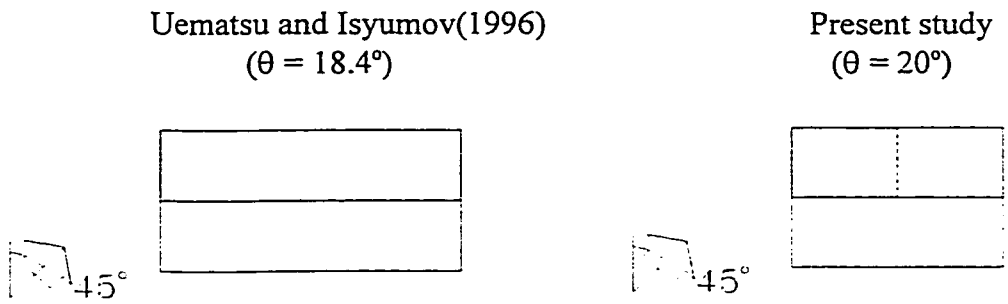

Mean pressure coefficients

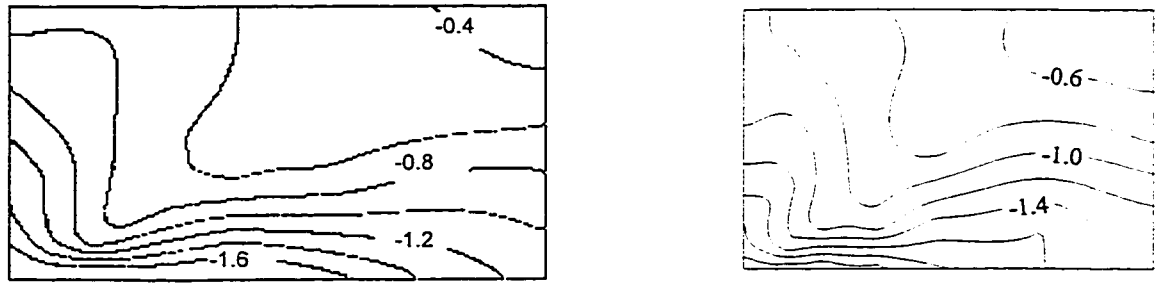

Minimum pressure coefficients

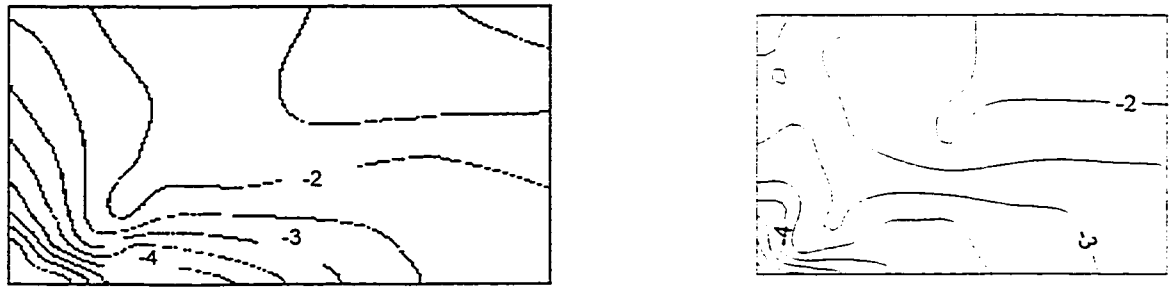

Figure 4.7 Comparison of the mean and minimum pressure coefficients measured for the present study with those from Uematsu and Isyumov (1996)

The present results so far have been compared with data from previous wind tunnel and full-scale studies in terms of mean and minimum pressure coefficients. Although some differences have been found through the comparisons, the agreement is generally reasonable.

It is also to be noted that all of those experimental data from different studies are not far from each other in terms of pressure magnitude. However, data from Meecham et al (1991) and Uematsu and Isyumov (1996) are generally higher than the present results, while the wind tunnel data of Holmes (1994) and the full-scale data from Richardson and Surry (1991) are generally lower than the present ones. Moreover, the data from Holmes (1981) agree well with the present results, for the particular configuration of 15° roof angle.

Therefore, the present experimental results appear consistent with those of previous studies for similar configurations. This validation process, along with the appropriate wind tunnel simulation (see Table 3.1), shows that the results of the present study are suitable for codification purposes.

4.3 LOCAL PRESSURE COEFFICIENTS

Roof structural components, such as bolts, fasteners and secondary structural members, are directly exposed to local wind forces. Local suction seems to play a more important

role for gable roofs of intermediate slopes. For simplicity, the term pressure used in this thesis could be applied to both positive pressure and negative pressure (suction), depending on the magnitudes of the respective pressure coefficients. The most critical local pressure coefficients and their distributions are important for the codal definitions on roof region and pressure zoning and loading. In this section, research findings on the behaviour of the local pressure coefficients will be presented at first, followed with the regional most critical local pressure coefficients and the conditions for their occurrences. At the same time, the respective parts of the current wind provisions will be discussed.

The distributions of the most critical mean, minimum, maximum and rms local pressure coefficients measured from all pressure tappings are presented in pressure contour forms in Figures 4.8 through 4.12, and the distributions of those local pressures coefficients under the wind azimuths of 60°, 90°, 135° are presented in Figures A-1.1 through A-1.20 in Appendix-1. These pressure contours provide global pictures for the local pressure distributions. It is to be noted that all these pressure contours have taken advantage of the symmetries of the roof models, thus the contours on a quartering part of a roof can reflect those for the entire roof. In these figures, the dashed lines superimposed on these pressure contours delimit the boundaries of the code-defined roof regions, which has been shown in Figure 3.6.

It is found in these pressure contours that the regional characteristics of these local pressure coefficients are distinctive, and the current codal definition on roof region seems

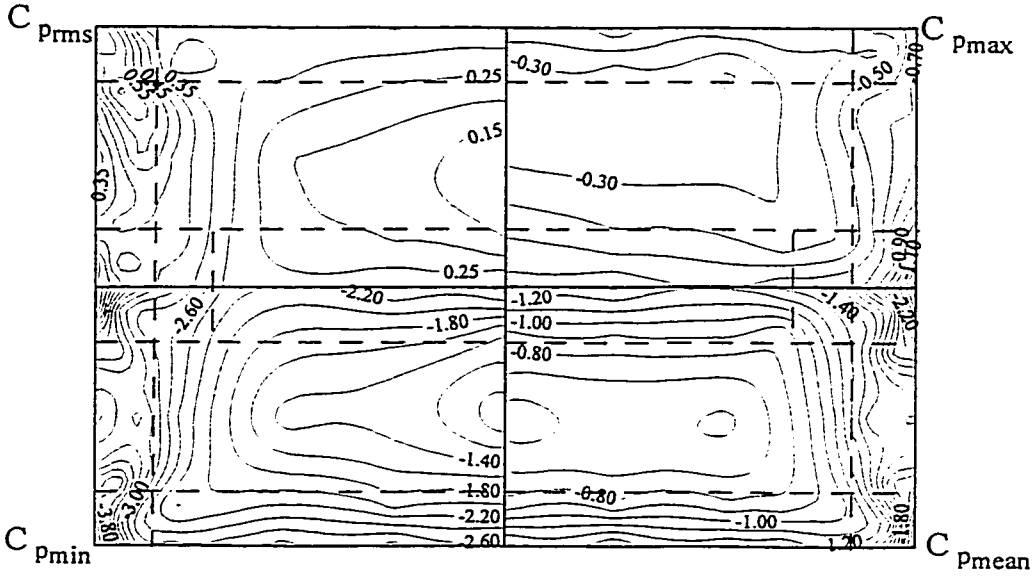

Figure 4.8 Most critical local pressure coefficients for the 10°-roof

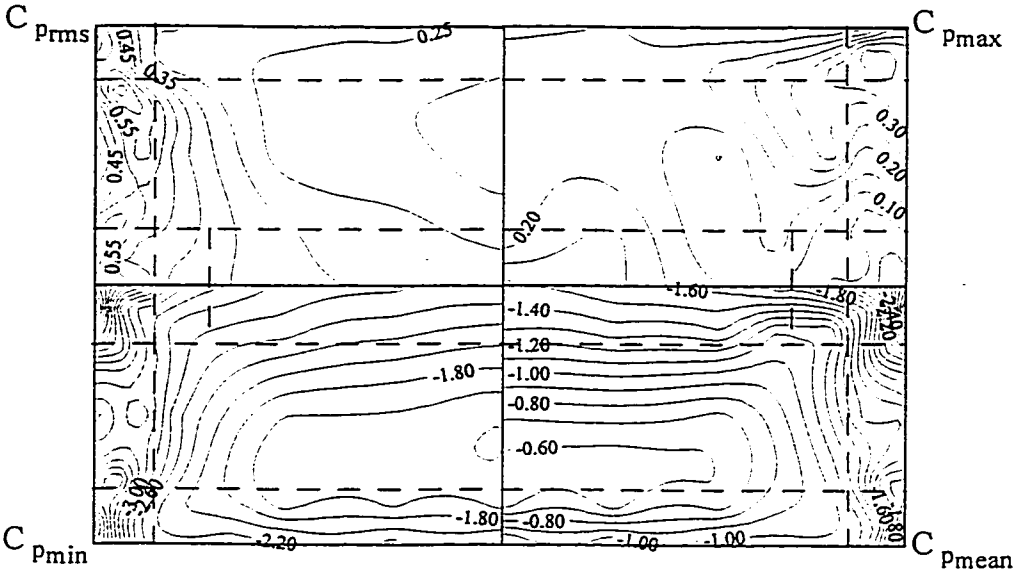

Figure 4.9 Most critical local pressure coefficients for the 15°-roof

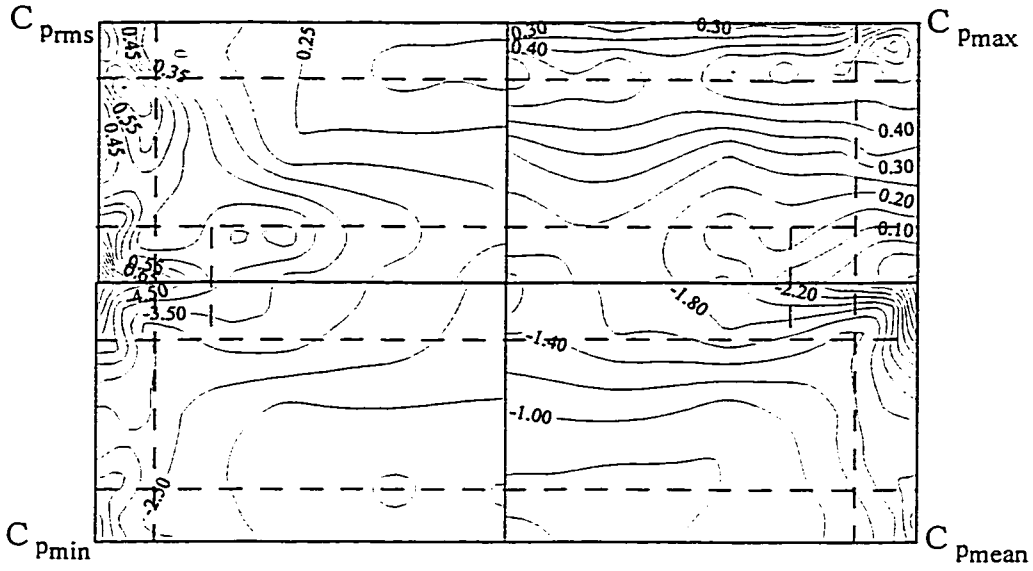

Figure 4.10 Most critical local pressure coefficients for the 20°-roof

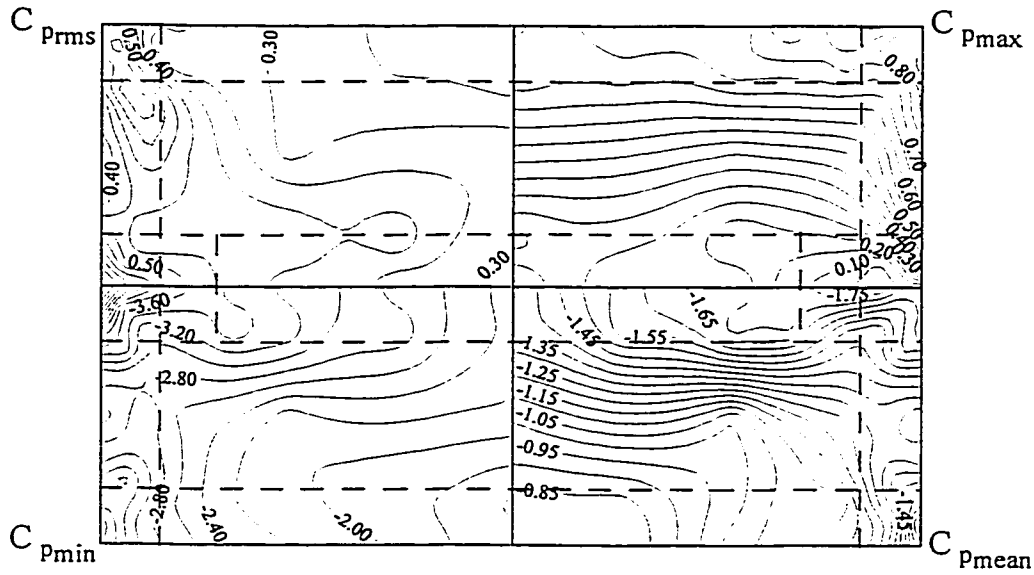

Figure 4.11 Most critical local pressure coefficients for the 25°-roof

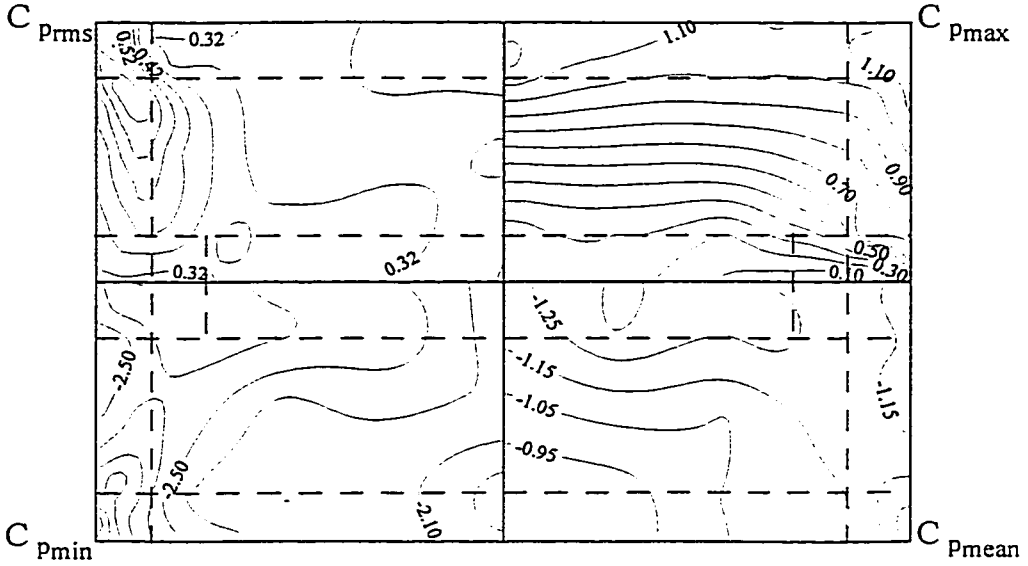

Figure 4.12 Most critical local pressure coefficients for the 30°-roof

appropriate. The most critical local pressure coefficients on most parts of the roof regions near gable ends and ridgeline are very high, particularly for Ridge corner. These large pressure coefficients are accompanied by the conical vortices just behind the ridge (Kanda and Maruta, 1993). On the other hand, the most critical local pressure coefficients on Eaves edge are relatively low. It shows that the wind loading effect of the first separation of flow occurring at the leading edges is not so strong as that at ridge and gable ends. Furthermore, the local most critical pressure coefficient distributions on Apex edge (Region C) do not show distinctive characteristics by comparison with those pressure coefficients on their neighbourhood.

Figure 4.13 shows the minimum local pressure coefficients measured at Taps 29, 36, 39, 40 and 41 that are located near Ridge corner. When the wind azimuth (α) is around 135°, the peak suction appears with a coefficient of -5.1 on the 10°-roof, and of -6.6 on the 20°-roof. Such peak suction decreases when the roof angle reaches 25°, and almost disappears on the 30°-roof. The coefficient of –6.6 measured on the 20°-roof is the largest value of the pressure coefficients measured in the whole experimental program. It is also found that these local pressure coefficients are relatively low for most of the wind azimuths, which shows that the directionality factor has to be considered in evaluation of the roof wind loads. Furthermore, the local pressure coefficients measured on the 20°-roof are generally higher than those measured on the other roofs for almost all these local tappings, while the local pressure coefficients of the 30°-roof have considerable smaller values.

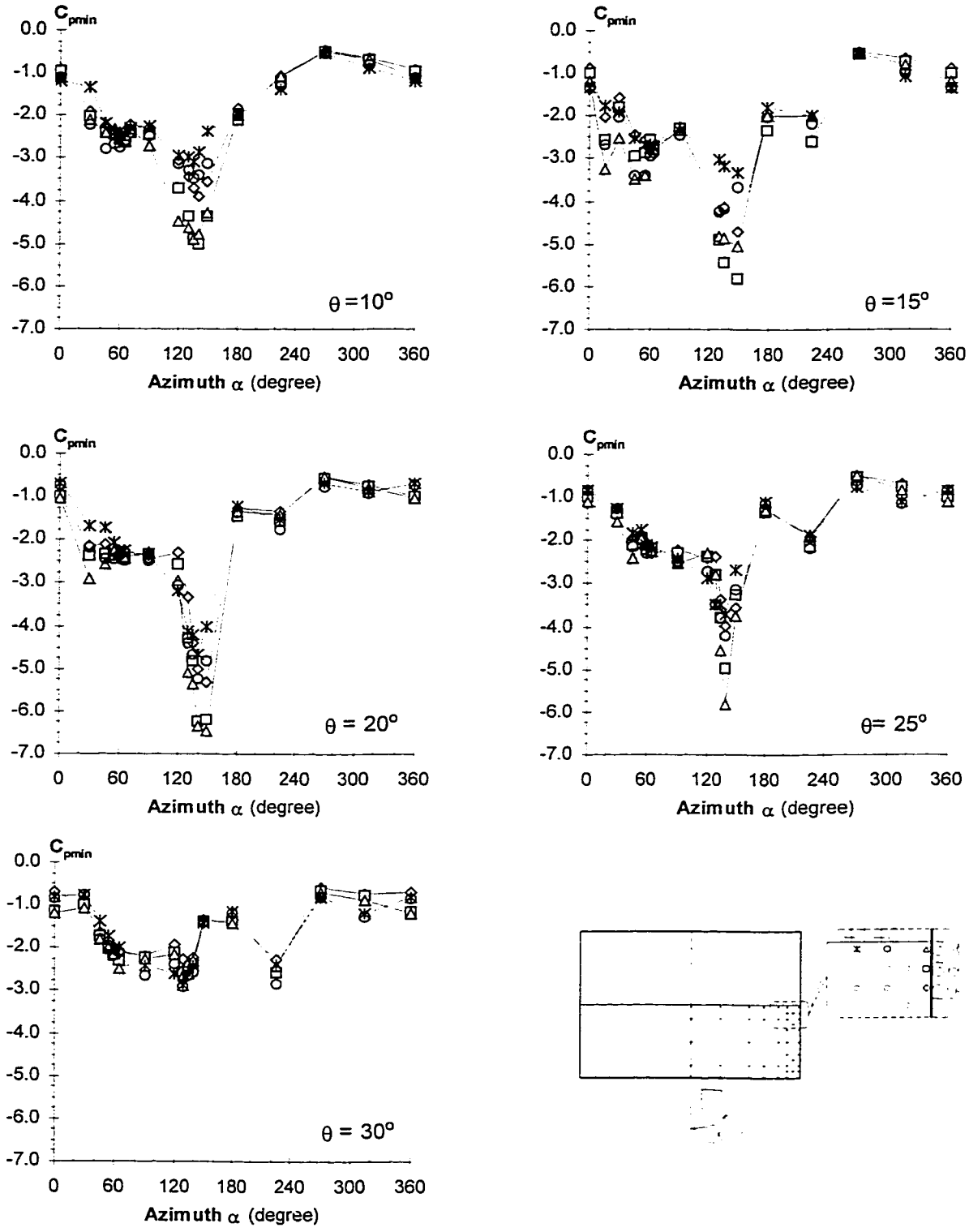

Figure 4.13 Minimum local pressure coefficients at taps near Ridge corner

Variations of the mean, minimum, maximum and rms local pressure coefficients on Taps 1, 2, 3, 8, 11, 29, 36, 39, 40 and 41 are presented as functions of wind azimuth in Figures A-2.1 through A-2.10 in Appendix-2. Note that these pressure tappings are distributed along the boundaries of the corner and edge regions-see Figure 3.5. Local pressure coefficients on these pressure tappings were found generally higher than those on the other tappings.

It is found Figures A-2.1 through A2.10 that the wind directions around 60°, 90° and 135° induce very high local wind loads; however, they do not appear coherent. In other words, their spatial correlation is not strong. It confirms that the directionality factor has to be considered into roof design. It is also found that local pressure coefficients measured around Ridge corner appear generally higher than those around Eaves corner for these angles and this confirms the importance of the very large loads on Ridge corner in roof design. Furthermore, it appears that local pressure coefficients on Gable edge are generally higher than those on Eaves edge, but appear similar to those along the ridgeline.

Figure 4.14a displays the most critical local pressure coefficients as functions of roof angle (θ) for four gable end tappings. As discussed previously, the most critical local pressure coefficients on the gable-end regions have been found to be higher than those on the other roof regions. The tapping line consists of Taps 1, 19, 26 and 39 with the ratio x/h of 0.036, where x is the distance between the tapping line and gable wall, and h is the eaves height. However, this value is not so satisfactory as compared with that of Surry and Lin (1995) which has taken the advantage of larger model scale.

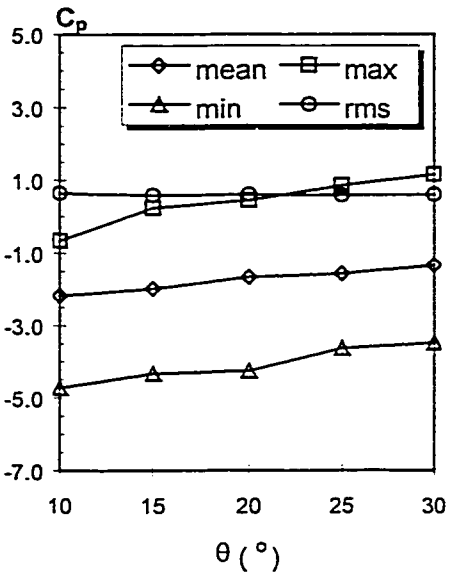

Tap 1

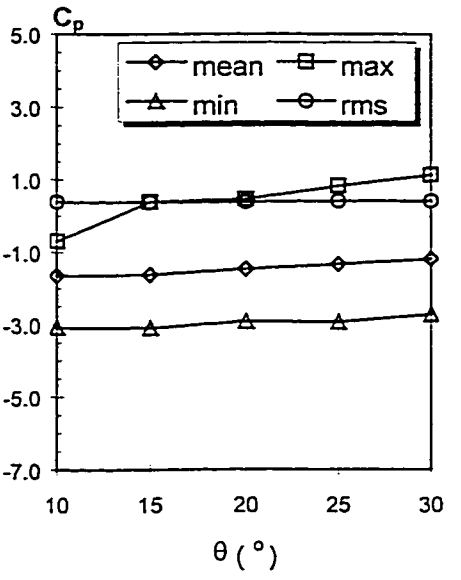

Tap 19

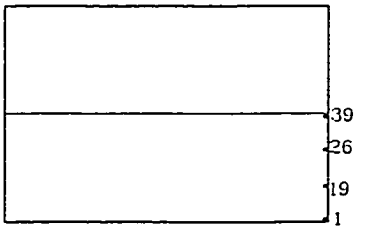

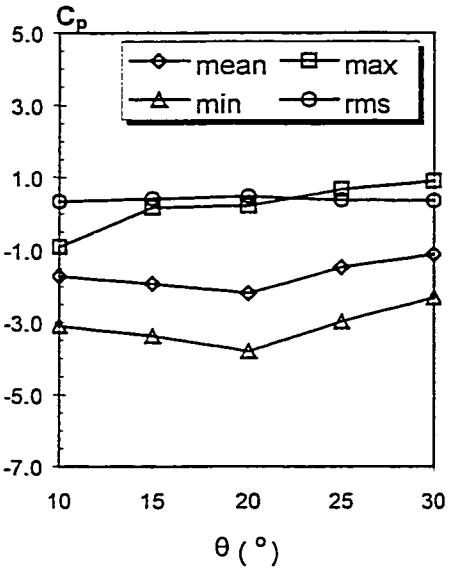

Tap 26

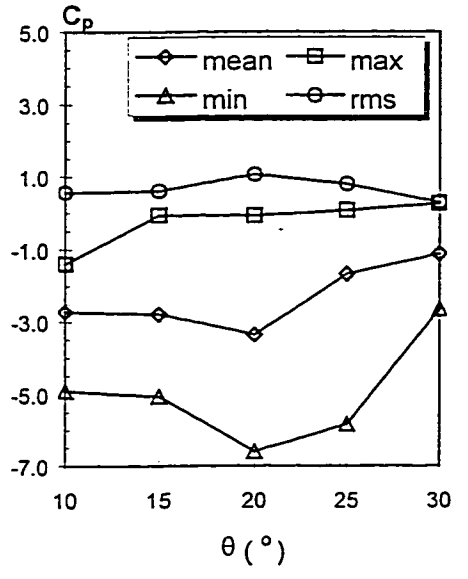

Tap 39

Figure 4.14a) Most critical local pressure coefficients along the roof gable end as functions of roof angle (θ)

The tapping line consisting of Taps 9, 18, 28 and 37 is the second closest tapping line to the gable wall with the ratio x/h as 0.072. Figure 4.14b shows that the slope effect on the most critical local pressure coefficients is less pronounced in some cases. Therefore, it appears difficult to break down the intermediate slope range into more subsets in terms of the most critical local pressure coefficients. However, the other cases show that the behaviours of the most critical local pressure coefficients are not monotonic, which appear to increase gradually from both ends of the roof slope range (10° and 30°), and reach their peaks at the 20°. Therefore, for the intermediate slope range which is difficult to separate, these peaks have to be considered as their representative values in codification process.

The examination of the measured local pressure coefficient trends shows that severe wind loads cover most part of the gable end and ridge regions; most critical wind pressure coefficients on Ridge corner are high, but those on the regions of Eaves edge and Interior are comparably low. These trends are common for three models of 15°, 20° and 25° roof angles. For both ends of the intermediate slope range (10° and 30°), there are exceptions. For instance, the pressure gradient is relatively small across the ridge for the 10°-roof, as has also been illustrated in the mean pressure variation shown in Figure 4.1, where the pressure coefficient magnitude immediately downstream the ridgeline is approximately equal to the pressure coefficient upstream the ridgeline. The characteristic of continuous flow for quasi-flat roofs has been discussed in Chapter 2. Another exception is that the most critical pressure coefficients for Ridge corner of the 30°-roof are small, which has also been presented in Figure 4.13.

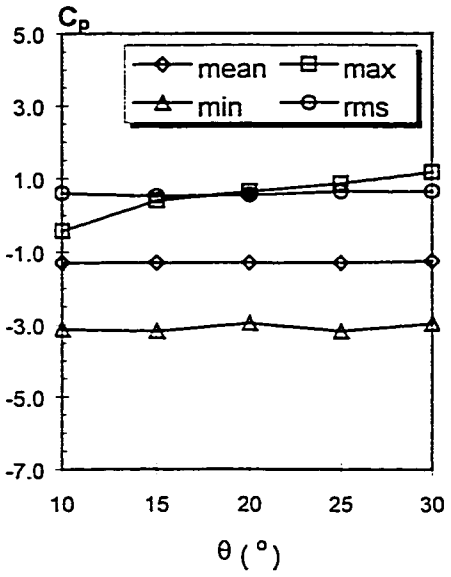

Tap 9

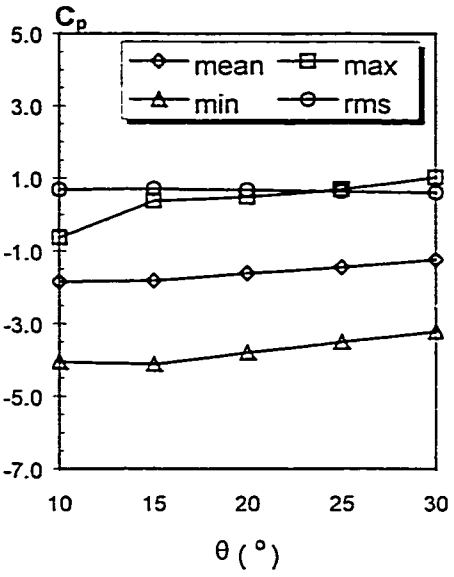

Tap 18

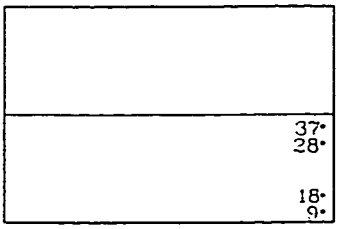

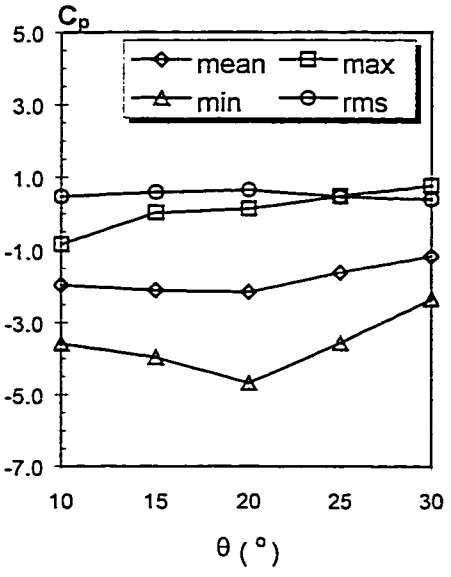

Tap 28

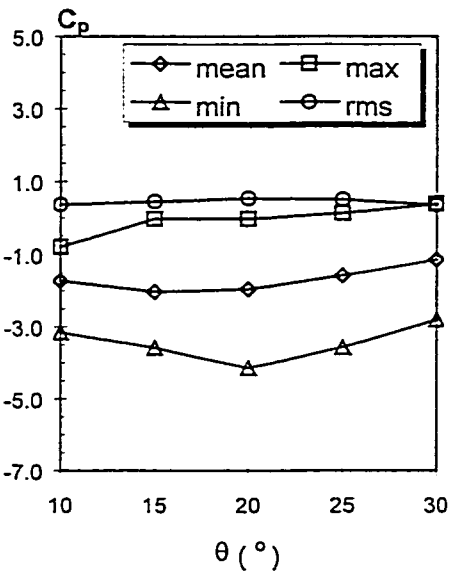

Tap 37

Figure 4.14b) Most critical local pressure coefficients near the roof gable end as functions of roof angle (θ)

The discussion on the most critical local pressure coefficients presented as functions of roof angle may lead to some modifications to be proposed for the current wind provisions in terms of the slope range, particularly related to the classification of both ends of the slope range. The most critical local pressure coefficients, together with their occurrence conditions in terms of roof angle and wind azimuth are presented in Table 4.1. These information and discussion will be addressed in the following chapter.

Table 4.1 Regional most critical local pressure coefficients

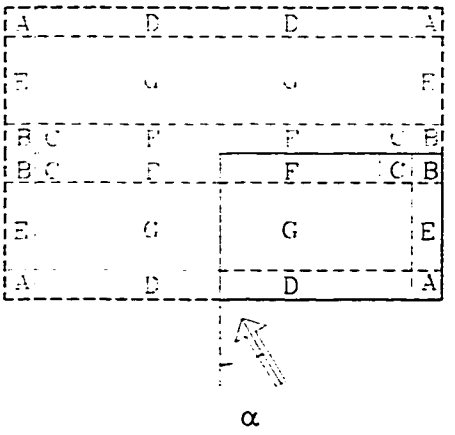

	C_{pmin}	Occurrence location	C_{pmax}	Occurrence location
Region A	-4.9	T01-10-065	1.2	T11-30-030
Region B	-6.6	T39-20-150	0.8	T30-30-000
Region C	-4.5	T41-20-140	0.4	T31-30-030
Region D	-2.9	T06-10-000	0.4	T17-20-000
Region E	-4.5	T28-20-150	0.8	T19-25-030
Region F	-3.8	T42-20-140	0.4	T45-25-090
Region G	-2.6	T23-30-090	0.8	T23-30-030

Note: the acronym "T39-20-150" represents Tap39, 20° roof angle and 150° wind azimuth

4.4 AREA-AVERAGED PRESSURE COEFFICIENTS

In addition to local pressure coefficients, area-averaged pressure coefficients are very significant. The wind loads acting on roof members and cladding are generally due to area-averaged pressures. Most critical area-averaged pressure coefficients are important in order to examine the suitability of the current wind provisions. In fact, the design wind loads presented in the current wind provisions are made up of the most critical area-averaged pressure coefficients specified as functions of tributary area. In this section, variations of the most critical area-averaged pressure coefficients obtained in the present study will be discussed as functions of roof angle and wind azimuth. Furthermore, the most critical area-averaged pressure coefficients will be arranged as functions of tributary area, in consistent with the current codal format.

Figures 4.15 through 4.17 display the area-averaged pressure coefficients as functions of wind azimuth for Eaves corner, Ridge corner and Gable edge in their entire areas, respectively. Recall that in the preceding section the local pressure coefficients measured on these three regions are generally larger than those on the other roof regions. The most critical suction coefficient of -3.2 occurs when wind azimuth α=90° and roof angle θ=25° for Eaves corner. The most critical pressure coefficient of 1.1 occurs on the 30°-roof under 30° wind azimuth. For Ridge corner, the most critical suction coefficient equals to -4.7 on the 20°-roof at 140° wind direction; the most critical pressure coefficient equals to 0.3 on the 30°-roof under 30° wind azimuth. For Gable edge, the minimum pressure coefficient of -2.9 occurs when α is130° on the 15°-roof, whereas the peak positive pressure coefficient equals 0.8 occurring when α is 30° on the 30°-roof.

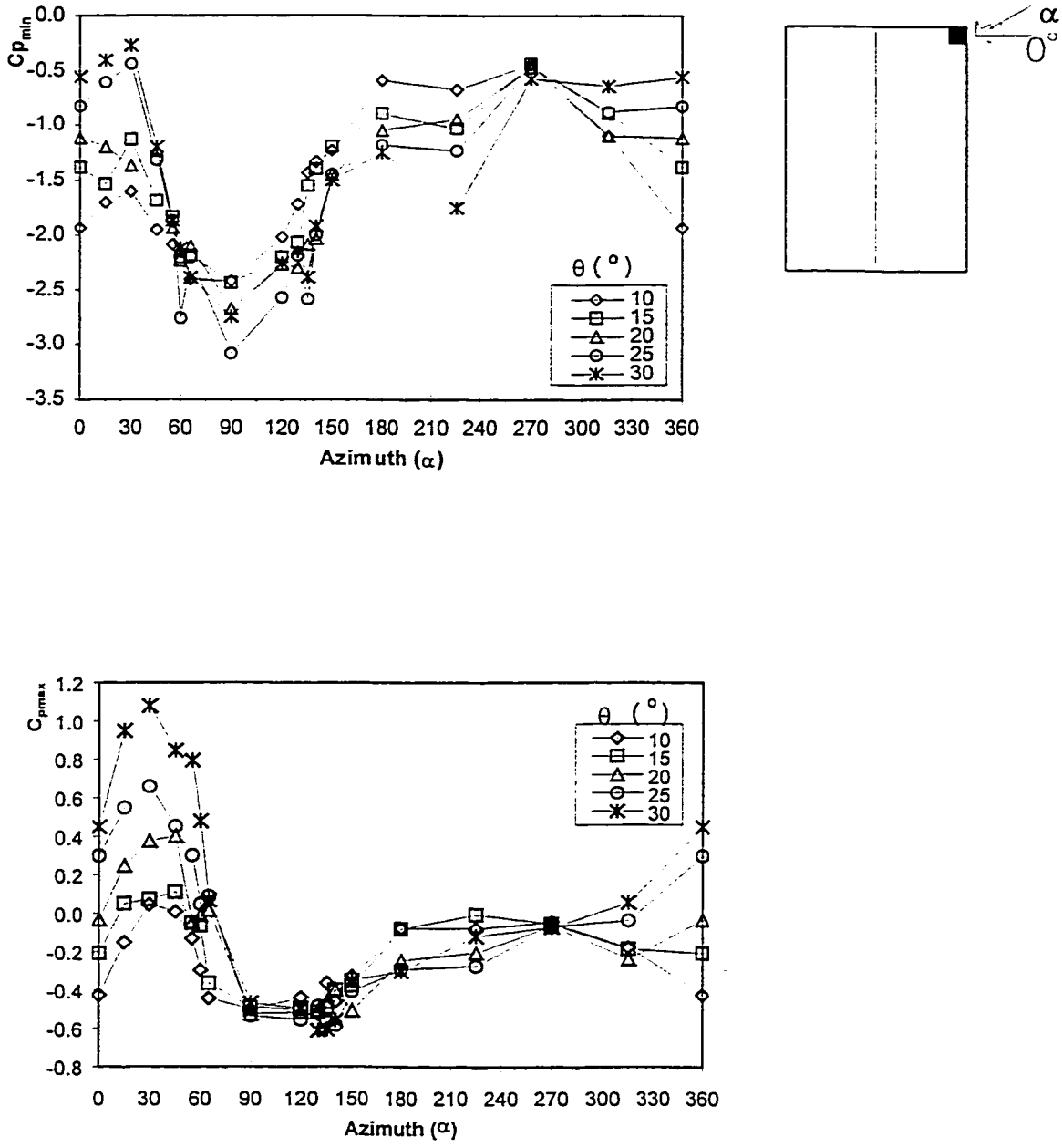

Figure 4.15 Area-averaged pressure coefficients as functions of wind azimuth for the entire area of region A (Eaves corner)

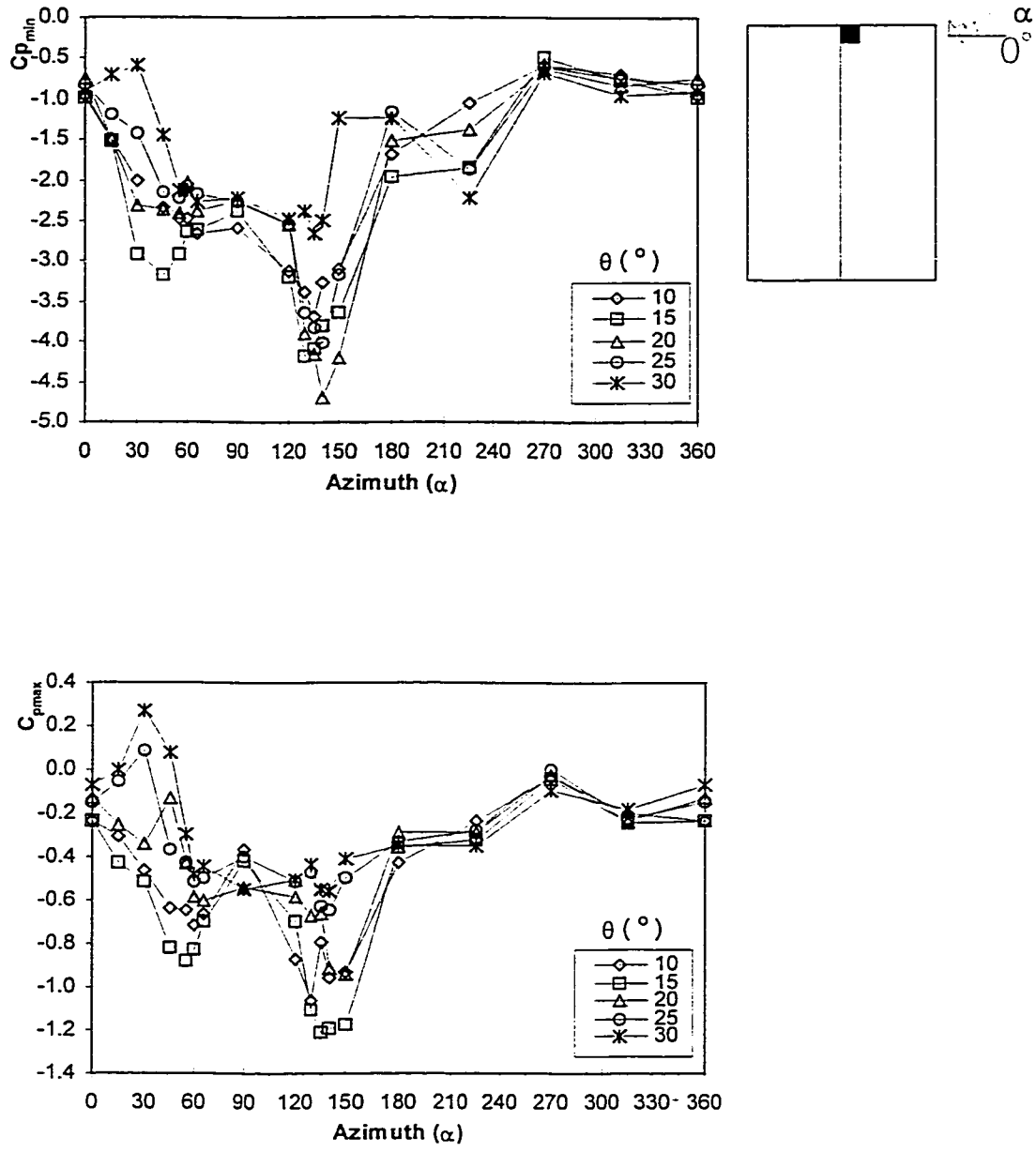

Figure 4.16 Area-averaged pressure coefficients as functions of wind azimuth for the entire area of region B (Ridge corner)

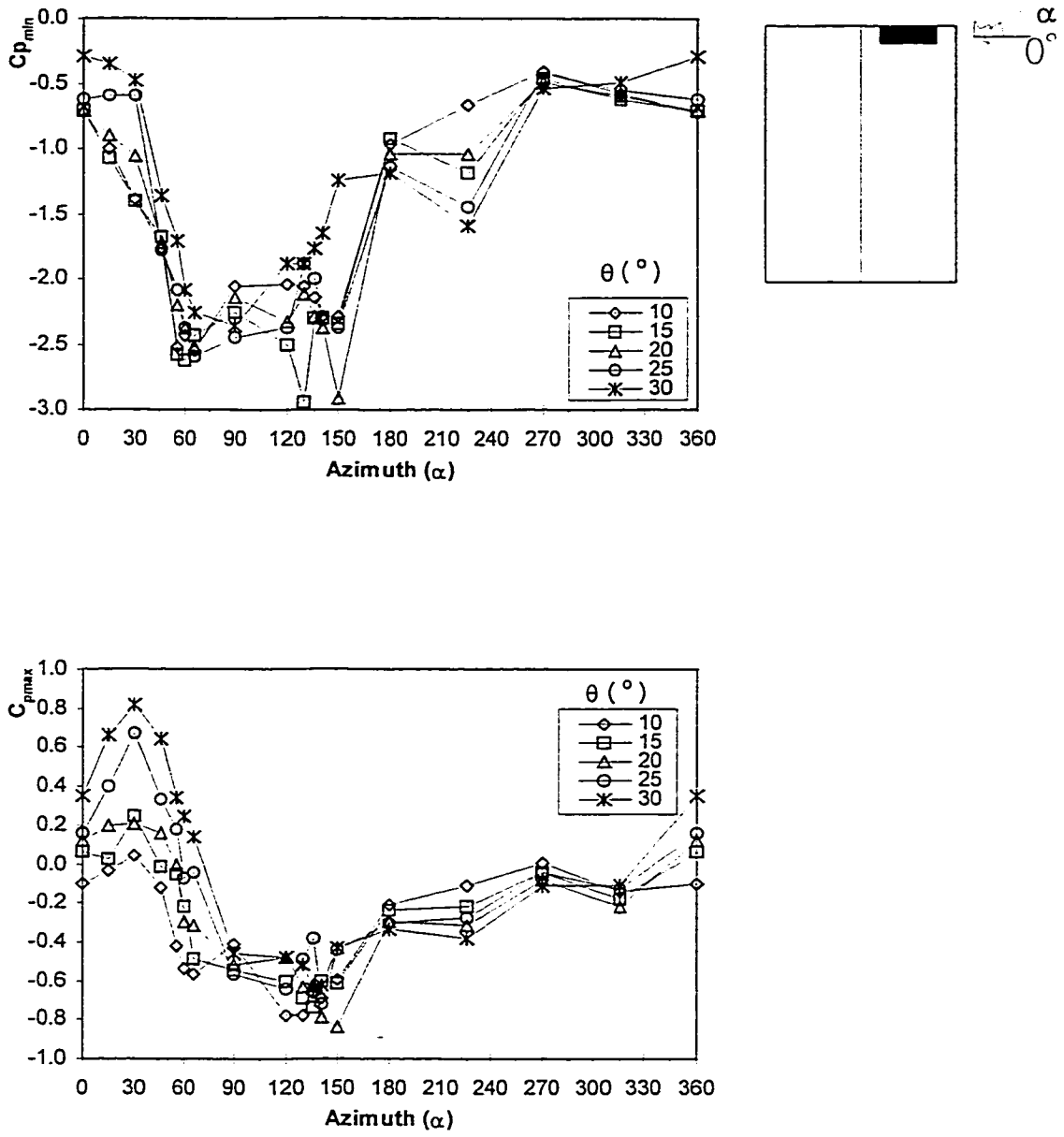

Figure 4.17 Area-averaged pressure coefficients as functions of wind azimuth for region E (Gable edge)

As shown in Figures 4.15 through 4.17, the behaviours of these positive most critical area-averaged pressure coefficients generally appear to be dominated by a quasi-cosine law. They generally increase with roof angle, so that it has to be more considered for design of the roofs of higher roof angles, particularly those near the high-pitched roof range, which might be the 25° and 30° roofs. However, the full treatment will not be carried out until the following chapter.

Also as shown in these figures, the behaviour of the most critical area-averaged suction coefficients is more complicated; however, for those most critical area-averaged suction The difficulty has been found to distinguish the pressure coefficients measured on each of these roofs from the others, although the behaviour of those measured on the 30°-roof can be distinguished out easier. Generally speaking, it appears hard to categorize these pressure coefficients into more groups. It is an alternative way to say that the intermediate slope range can not be split into more subsets in terms of area-averaged suction coefficients.

The area-averaged mean, min, max and rms pressure coefficients as functions of roof angle are shown in Figures 4.18a and 4.18b, for the seven roof regions in their entire regional areas. Both minimum and maximum pressure coefficients are obtained as their most critical values. The wind loading effect of roof angle on the most critical pressure coefficients appears weak, with the exception of the suction on Ridge corner, which appear higher on the 20°-roof than on the other roofs.

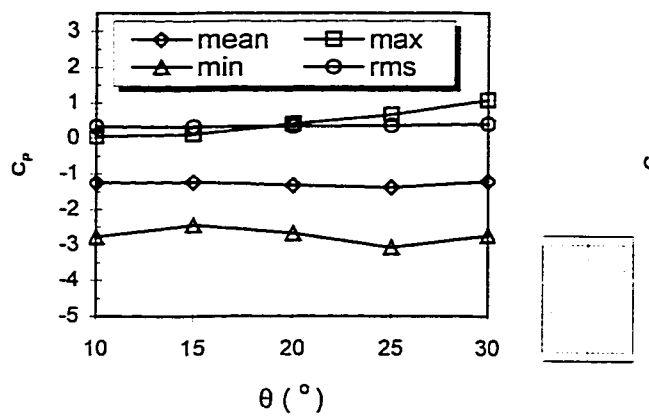

Eaves corner

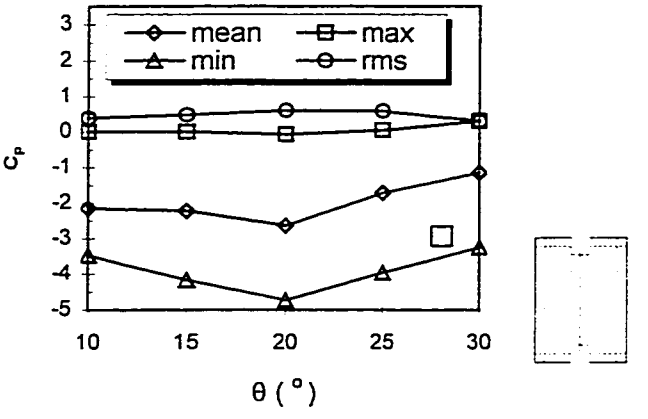

Ridge corner

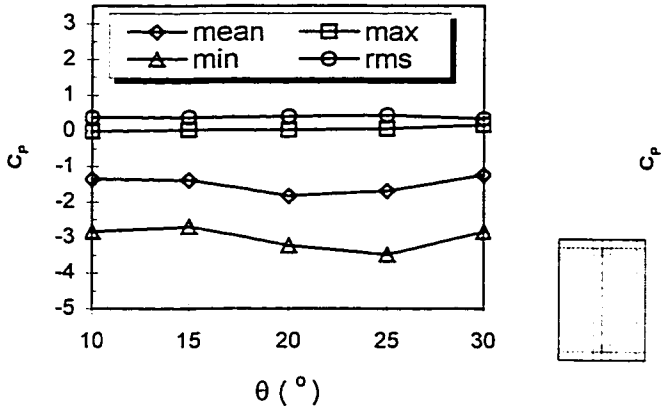

Apex edge

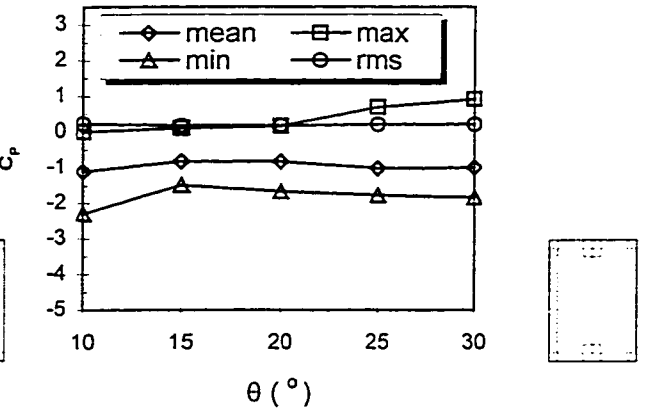

Eaves edge

Figure 4.18a) Most critical area-averaged pressure coefficients as functions of roof angle for Eaves Corner, Ridge corner, Apex edge and Eaves edge

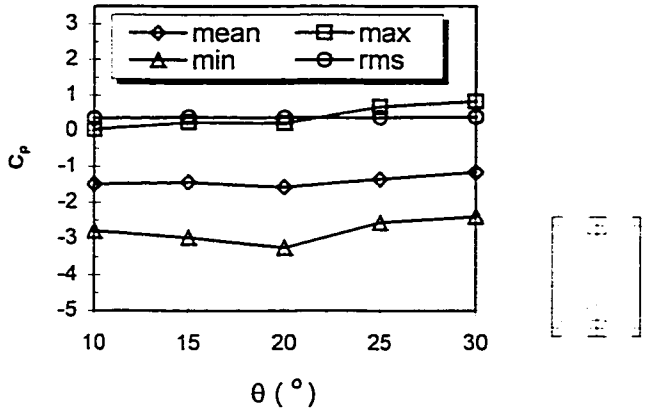

Gable edge

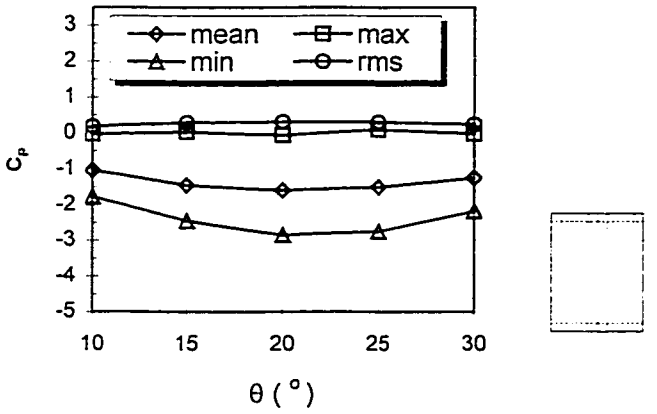

Ridge

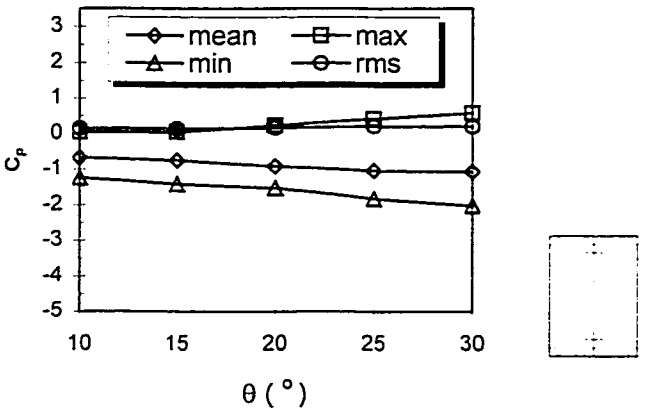

Interior

Figure 4.18b) Most critical area-averaged pressure coefficients as a function of roof angle for Gable edge, Ridge and Interior

The most critical area-averaged pressure coefficients that are associated with their respective roof angles and wind azimuths for each of the seven roof regions are presented in Table 4.2. These results, accompanied with those already shown in Table 4.1, may have distinctive usage in the codification process.

The most critical area-averaged pressure coefficients for each of the seven regions as functions of the tributary area are presented in Figures 4.19 and 4.20, in the same format as that used by the current wind provisions. Figure 4.19 shows that the negative pressure coefficients on Ridge corner are significantly higher than those in the other roof regions. At the same time, it is also distinctive that the difference between the pressure coefficients of the 10°-roof and those of the other roofs is relatively small. Finally, positive pressure coefficients are low with the exception of those for the 30°-roof. All these information will be discussed in the following chapter.

Table 4.2 Minima of the area-averaged most critical pressure coefficients for the seven regions in their entire sizes, respectively

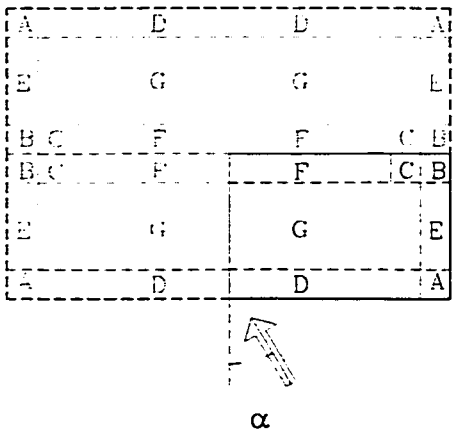

	C_{pmin}	Occurrence condition	C_{pmax}	Occurrence condition
region A	-3.1	25-090	1.1	30-030
region B	-4.7	20-140	0.3	30-030
region C	-3.2	20-120	-0.1	30-030
region D	-2.3	10-000	-0.4	20-000
region E	-2.9	15-130	0.8	30-030
region F	-2.8	20-140	-0.1	25-090
region G	-2.0	30-090	0.5	30-000

Note: the acronym 25-090 represents: 25° roof angle and 90° wind azimuth

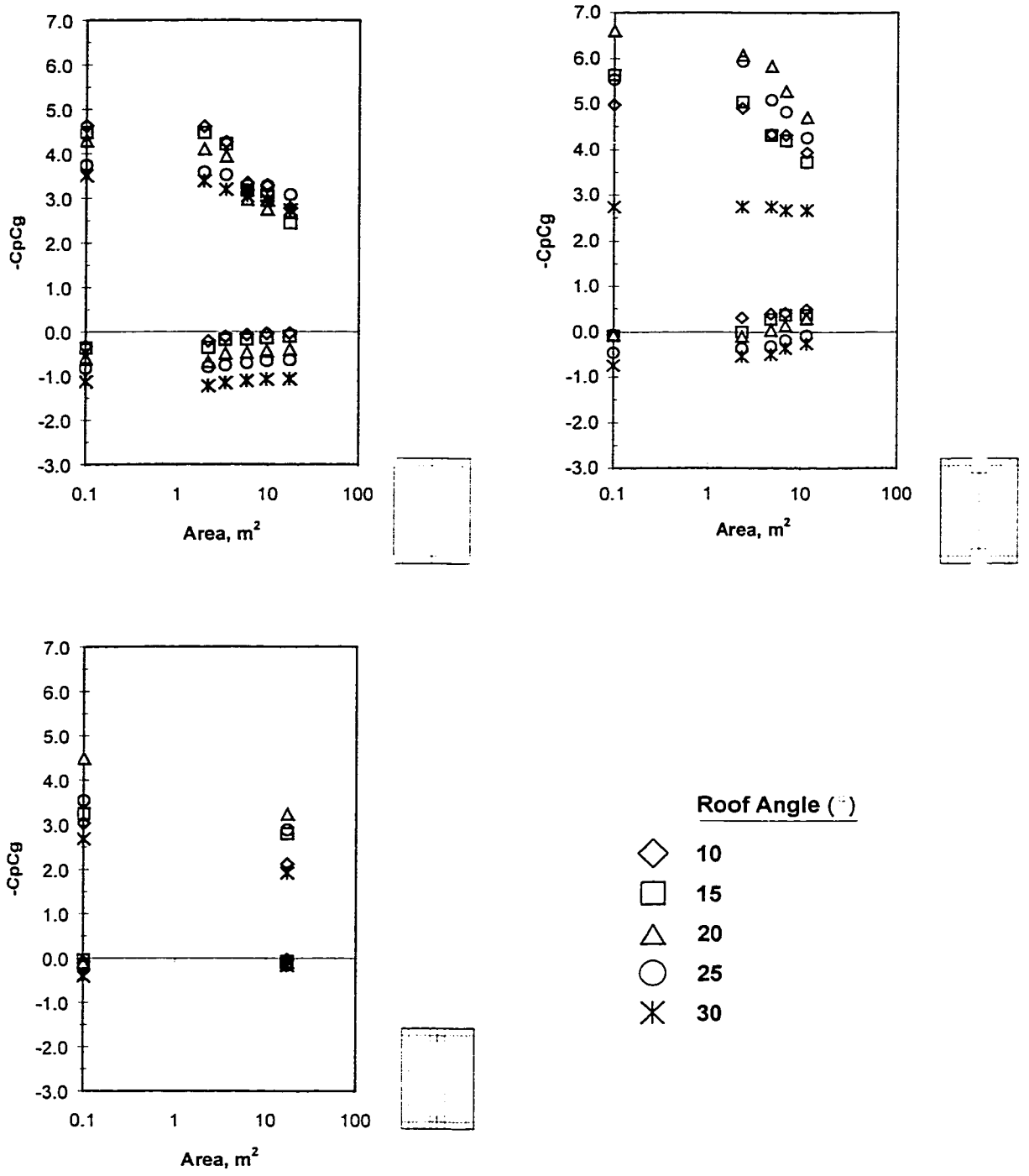

Figure 4.19 Area-averaged pressure coefficients for the regions of Eaves corner, Ridge corner and Apex edge as functions of their tributary area, respectively

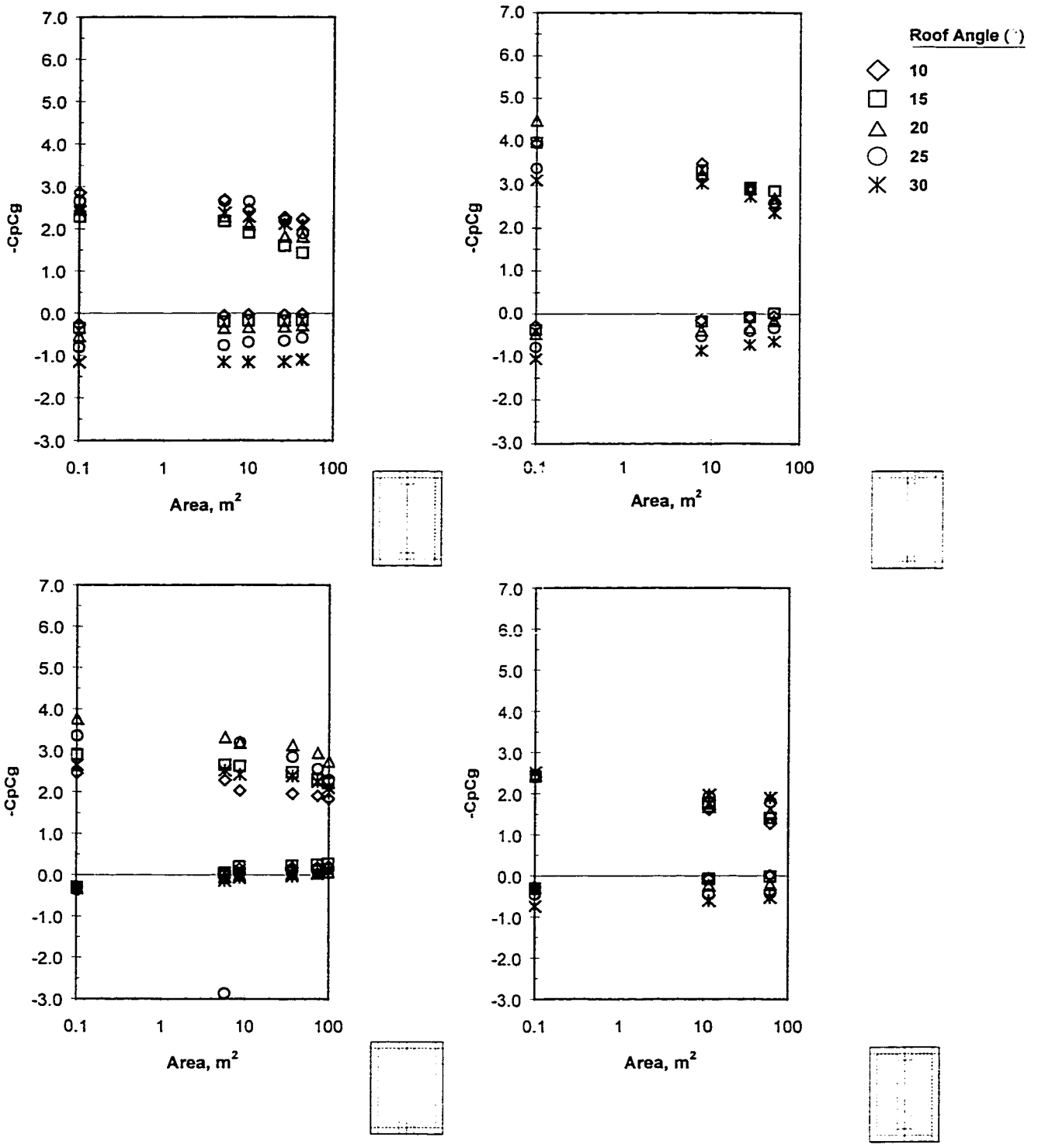

Figure 4.20 Area-averaged pressure coefficients for the regions of Eaves edge, Gable edge, Ridge and Interior as functions of their tributary area

CHAPTER 5

APPLICATION FOR STANDARDS AND CODES OF PRACTICE

5.1 DETAILED DESCRIPTION OF THE CURRENT WIND PROVISIONS

The current wind provisions of NBCC (1995) have already been referred in this thesis. The codification process arriving at the current codal format is briefly described as follows. It is to be noted that the principle of simplicity goes throughout this process.

As indicated in the previous chapters, the codal definition of roof region depends on the distribution of the experimental most critical local and area-averaged pressure coefficients. The roof areas where the local most critical pressure coefficients show similar magnitudes are grouped into a set of regions respectively, namely Region A (Eaves corner), Region B (Ridge corner), Region C (Apex ridge), Region D (Eaves edge), Region E (Gable edge), Region F (Ridge) and Region G (Interior). The roof regions where the regional most critical pressure coefficients show similar magnitudes

are grouped into a set of pressure zones respectively, namely, Eaves and Ridge Corners, Edges near Apex, Edges and Interior. Furthermore, roofs of different roof angles can be grouped together, provided that the corresponding zones of these roofs show similarity in terms of most critical pressure coefficients. The slope ranges are defined in the current wind provisions as: the quasi-flat roof ($0^{\circ}<\theta\leq10^{\circ}$), the intermediate roof ($10^{\circ}<\theta\leq30^{\circ}$) and the high-pitched roof ($30^{\circ}<\theta\leq45^{\circ}$). The format of the current wind provisions for gable roofs of intermediate slopes and those for other roof ranges is illustrated in Figure 5.1.

It has to be noted that the design pressure coefficients in the current codal format are arranged as functions of tributary area denoted as C_pC_g in accordance with the current codal format for the design pressure coefficients of high-rise buildings. More explanation on the notation has been provided by Davenport (1983).

In the current wind provisions, the most critical pressure coefficients measured in the wind tunnel have been multiplied by a reduction factor of 0.8 to account for directionality. This is based on the consideration of the unlikeliness of the extreme wind speed coming from the most critical wind direction for each point on the roof (Stathopoulos, 1979). In this chapter, the measured most critical pressure coefficients that will be employed into the comparison with the codal values are multiplied by this 0.8 reduction factor. Further codal information on design wind loads of low-rise buildings can be found in various standards and codes of practice.

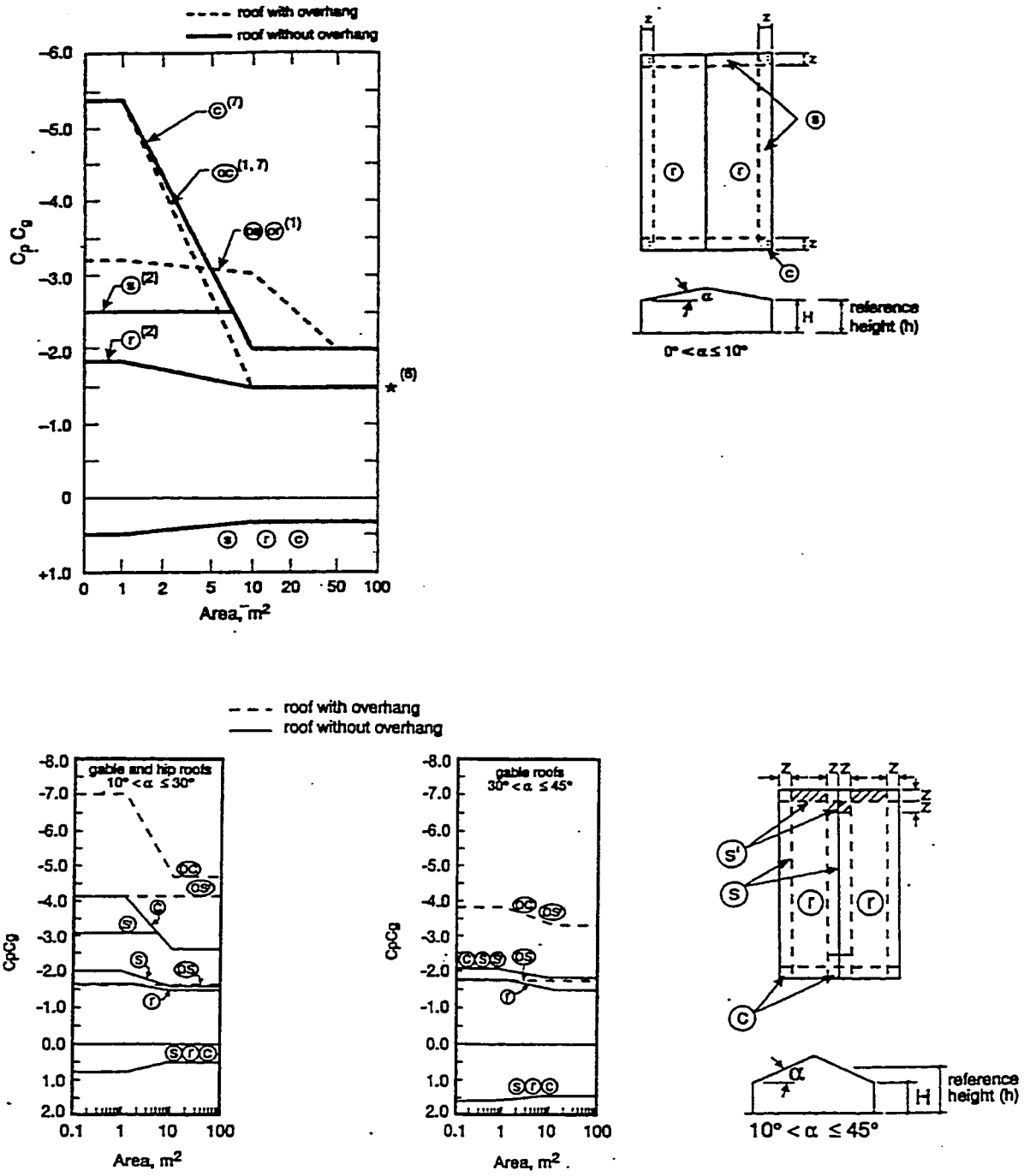

Note: z =10% of least horizontal dimension or 40% of height, H, which is less. Also z ≥1m, z ≥4% of least horizontal dimension.

Figure 5.1 Wind provisions for the low-building gable roofs, after NBCC (1995)

5.2 COMPARISONS WITH THE CURRENT WIND PROVISIONS

Local most critical pressure coefficients measured in this study are compared with design wind pressure coefficients in Figure 5.2. The seven diagrams in this figure apply to the seven code-defined regions. The top straight lines in these diagrams represent the design suction coefficients for the smallest tributary area, while the bottom straight lines indicate the design pressure coefficients.

As shown in this figure, the current wind provisions appear to have underestimated the local peak suction on the regions of Ridge corner, Gable edge and Ridge. Also shown in this figure, the wind loading effect of roof angle on the most critical local pressure coefficients appears less pronounced.

The distributions of the most critical pressure coefficients in the positive domain are almost uniform, though the most critical local pressure coefficients of the 30°-roof are larger than those on the other roofs.

The most critical suction coefficients vary from region to region and reach their peaks on the 20°-roof. These suction coefficient values decrease gradually towards both ends of the intermediate slope range and reach their minima at either end. This shows the difficulty to divide the intermediate slope range into, say, two subsets. Any attempted division would require three or more intervals and this would not be appropriate from the simplicity viewpoint.

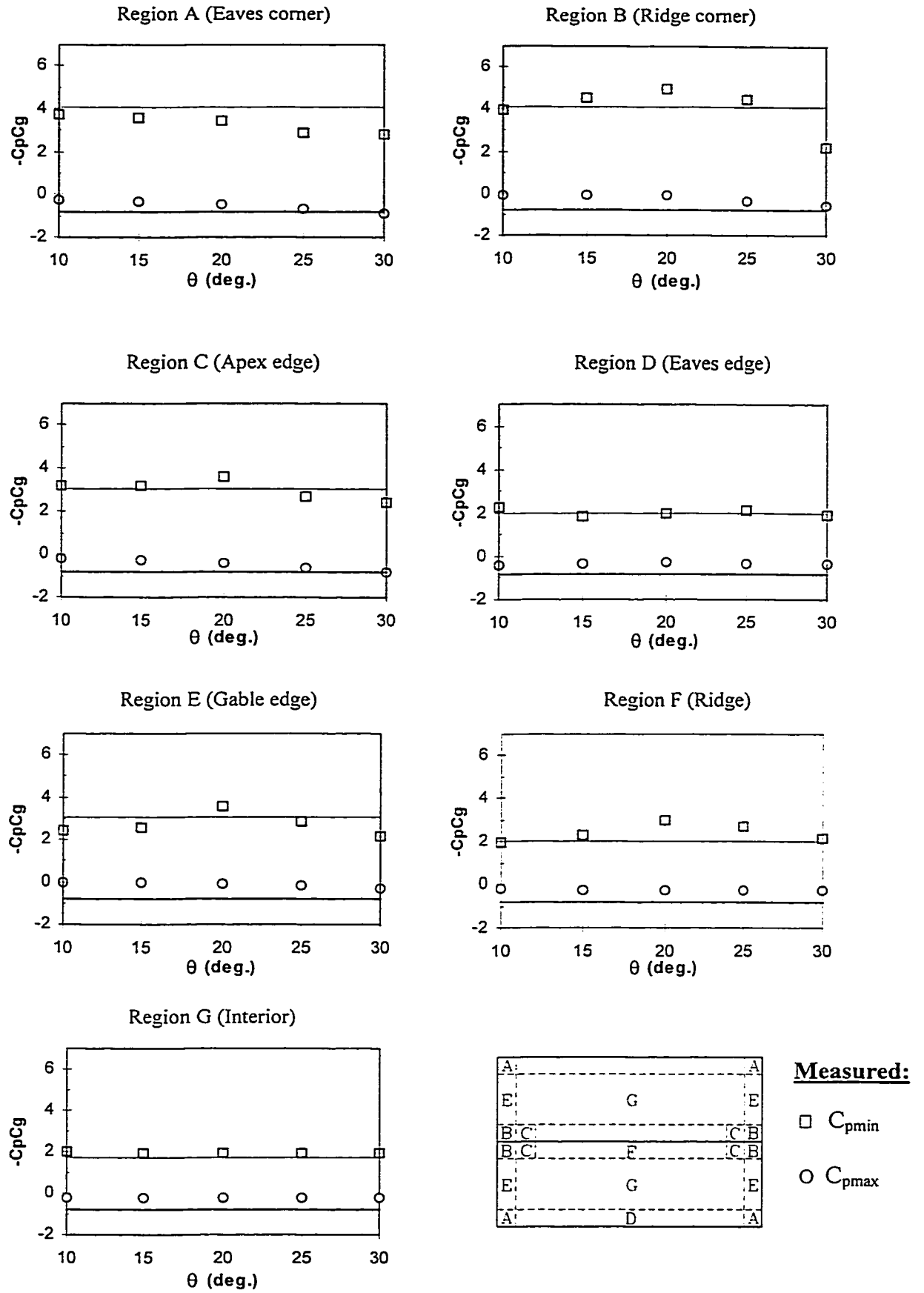

Figure 5.2 Comparison of peak pressure coefficients between the present results (presented in points) and NBCC codal values(in lines) for each of the 7 roof regions, respectively

The most critical pressure coefficients, both local and area-averaged obtained in the present study, have been arranged into the same format of the current wind provisions and compared with the current design wind pressure coefficients. The results are shown in Figure 5.3. Four diagrams of this figure correspond to the four current defined pressure zones, respectively. This figure is used to examine the agreement of the present experimental results with those specified in the current wind provisions. Furthermore, Figures A-3.1 through A-3.5 in Appendix-3 provide the same comparisons, although separately for each individual roof angle tested in the present study in order to provide a clearer view of the comparison results.

The differences between the present results and those from the current wind provisions appear apparent, as shown in Figure 5.3. The most critical suction coefficients measured in the present study of Zone 1(Eaves and Ridge Corners) and Zone 2 (Edge near Apex) have exceeded the current design suction coefficients to certain extents, although for the other two zones (Edge and Ridge, and Interior), the agreement of the present results and the current wind provisions appears well.

A further examination of this figure indicates that the pressure coefficients obtained on the 10°-roof show similarity with those for the other three roofs of 15°, 20° and 25° in magnitude. On the other hand, the pressure coefficients measured on the 30°-roof show seem out of order of those measured on the other four roofs.

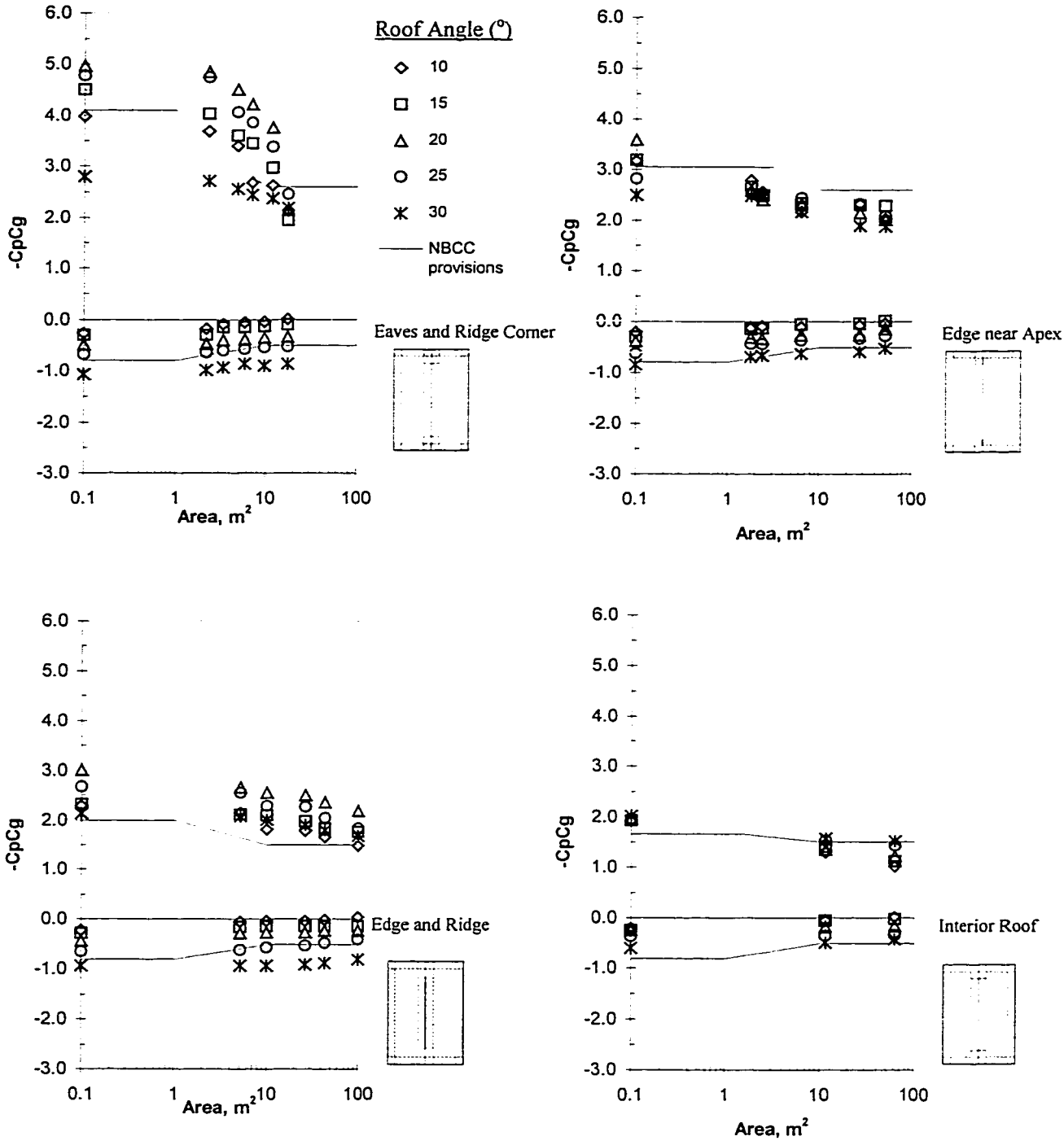

Figure 5.3 Comparison of test values (considering 0.8 factor) and the Canadian code provisions for the 4 zones on the gable roofs

Generally speaking, there is underestimation of peak suctions for the roof corner and ridge regions in the current wind provisions, and the roof range definition seems not suitable. As a result, some updating work needs to be done for the current wind provisions; and some ideas have been invoked by the previous discussions. For instance, the 10°-roof may be taken into the intermediate roof range. On the other hand, the 30°-roof may be taken out of the intermediate roof range, and put into the high-pitched range, if it is more appropriate. In addition, the 25°-roof should be examined to see whether its loading definition would also be suitable for classification in the higher-pitched roof range. Figures 5.4 through 5.6 will be used to examine whether these ideas are suitable or not.

In Figure 5.4, the experimental results obtained on the 10°-roof for each of the seven roof regions are combined into the three pressure zones defined in the current wind provisions for the quasi-flat roof range ($0° < \theta \leq 10°$). The current codal definition on pressure zoning for the quasi-flat roof range can also be referred to Figure 5.1. The comparison in this figure shows that it may not be suitable to place the 10°-roof in the quasi-flat range. In fact, by comparing Figure 5.4 with Figure 5.3, the 10°-roof appears quite clearly to belong to the intermediate roof range.

In Figures 5.5 and 5.6, the experimental results obtained on the 25°- and 30°-roofs for each of the seven roof regions are combined into four pressure zones in conformity with the respective codal pressure zoning definition for the high slope range ($30° < \theta \leq 45°$). The definitions for these pressure zones have also been provided in Figure 5.1.

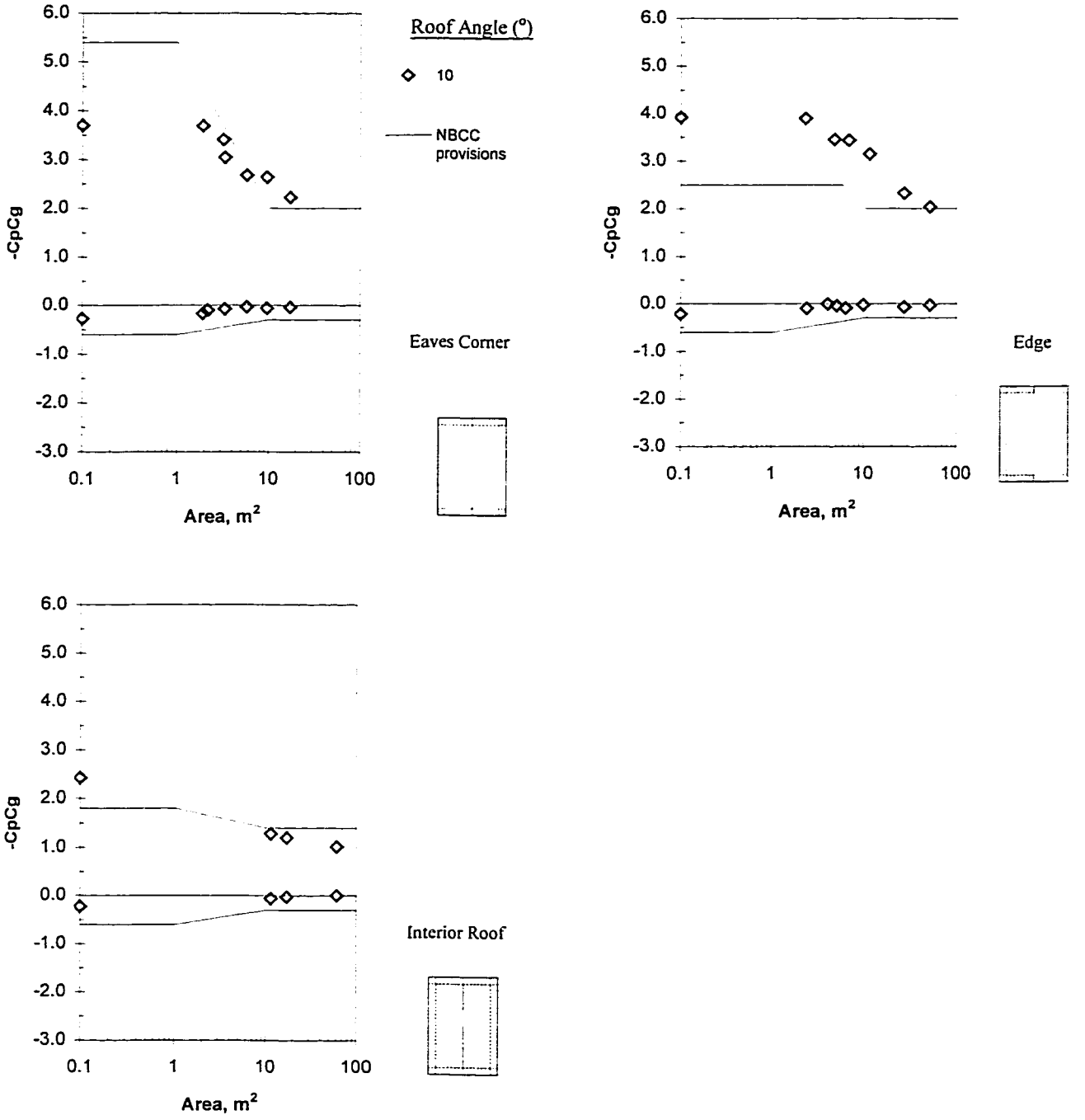

Figure 5.4 Comparison of experimental values measured on 10° roof with the code values specified for gable roofs in slope range ($0° < \theta \leq 10°$)

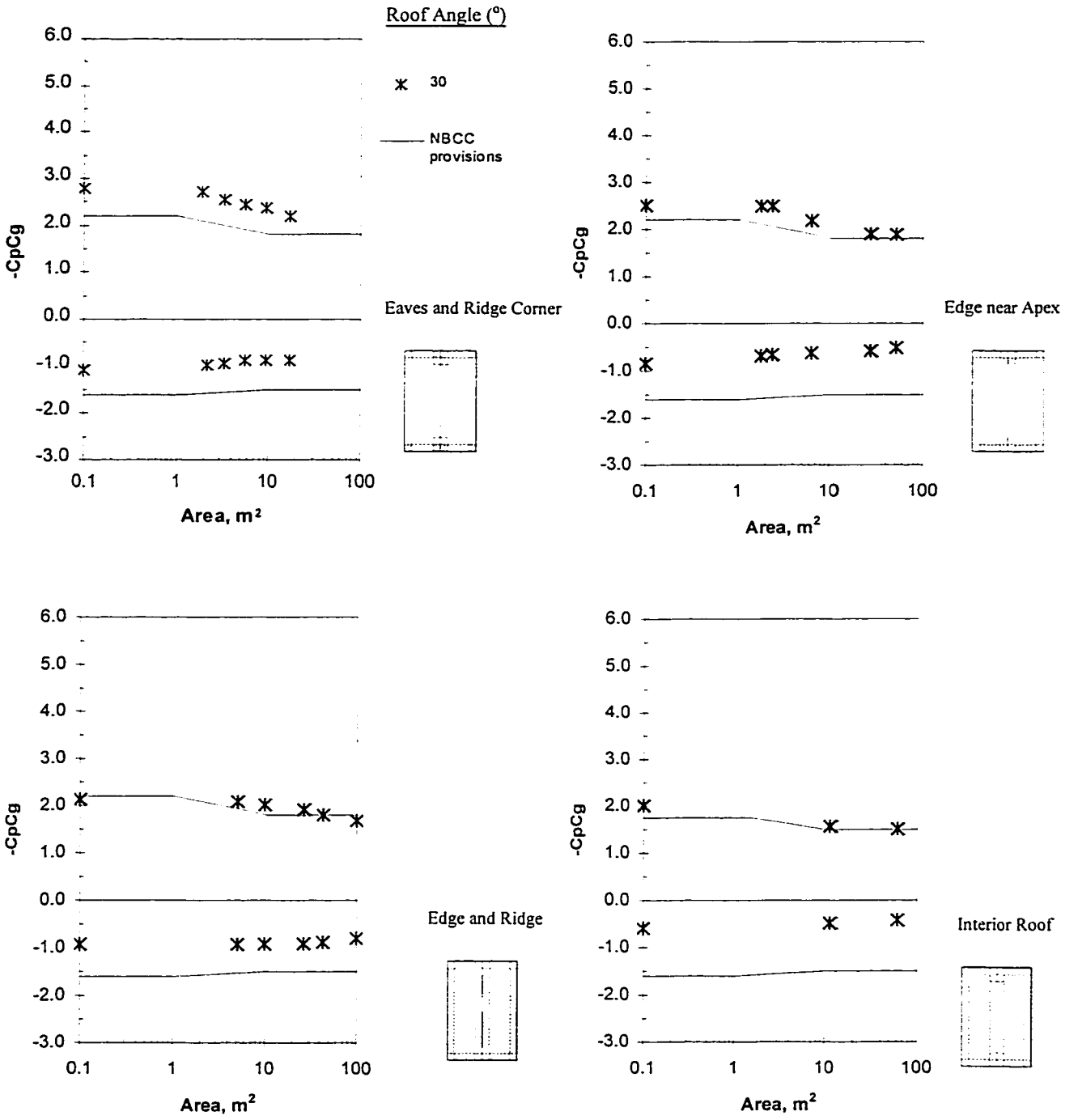

Figure 5.5 Comparison of experimental values measured on 30° roof with the code values specified for gable roofs in slope range ($30° < \theta \leq 45°$)

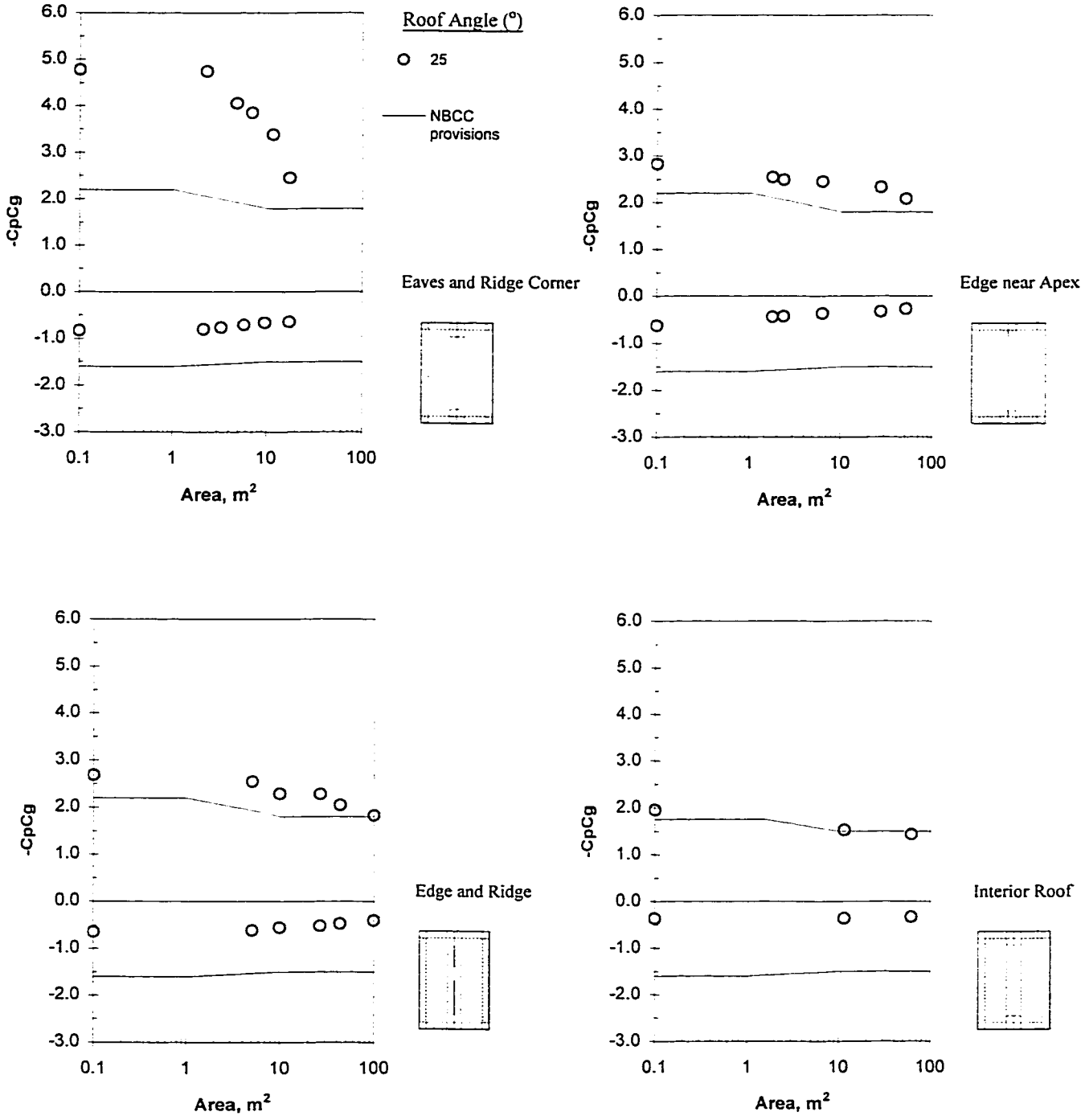

Figure 5.6 Comparison of experimental values measured on 25° roof with the code values specified for gable roofs in slope range ($30° < \theta \leq 45°$)

Figure 5.5 shows that the distributions of the pressure coefficients on the 30°-roof agree well with the definition of the current wind provisions on the high-pitched roof range. In fact, the agreement is much better than that shown in Figure 5.3 for the intermediate slope range. Therefore, it is better to take the 30°-roof out of the intermediate slope range and classify it into the high-pitched roof range. However, this is not the case for the 25°-roof as Figure 5.6 indicates. Clearly, it would have been desirable to examine this issue for additional roof angles between 25° and 30°. However, in the interim and with respect to the codal definition of the slope range, some modification in the slope definitions may be proposed, namely, quasi-flat range ($0° < \theta < 10°$), intermediate range ($10° \leq \theta < 30°$) and high-pitched range ($30° \leq \theta \leq 45°$).

5.3 ALTERNATIVE CODE AND STANDARD PROVISIONS

The examination of the current wind provisions has been completed. The current codal definition on slope range has been modified so that the 10°-roof be taken out of the quasi-flat roof range and put into the intermediate slope range. In the meantime, the 30°-roof would be taken out of the intermediate slope range and relocated into the high-pitched roof range. The attempted and current codal definition on slope range is shown in Table 5.1. From the attempted intermediate roof range, the current pressure zoning definition is modified. The attempted zoning definition is shown in Table 5.2, in association with the current definition. The attempted pressure zones can be called as Corner, Ridge and Gable Edge-Zone 1, Ridge Corner -Zone 2, and Interior and Eaves Edge-Zone 3.

Table 5.1 Comparison of proposed and current codal definition on slope range

Category	Current definition	Proposed definition
quasi-flat roof	$0°<\theta \leq 10°$	$0°<\theta < 10°$
intermediate roof	$10°<\theta \leq 30°$	$10°\leq\theta < 30°$
high-pitched roof	$30°<\theta \leq 45°$	$30°\leq\theta \leq 45°$

Table 5.2 Comparison of the proposed and current codal definition on pressure zoning

Proposed zoning	Regions	Current zoning	Regions
Zone 1	Region B	Zone 1	Regions A, B
Zone 2	Regions A, C, E, F	Zone 2	Regions C, E
Zone 3	Regions D, G	Zone 3	Regions D, F
		Zone 4	Region G

A new set of design wind pressure coefficients has been formulated with the principle of simplification taken into account. The proposed design wind pressure coefficients are presented in Figure 5.7 along with the current provisions corresponding to the most critical areas of the new zones (Wu et al, 1998). The proposed curves quasi-envelope the most critical local and area-averaged pressure coefficients obtained in the present experimental study. There are several reasons for that, merely related to economics and the acceptance of any new specifications for codes and standards not to fully envelope the measured pressure coefficients. For instance, the variability of measured peak values is such that it would be adequately claimed that small convenient reductions could be tolerated for simplicity and economy.

Furthermore, the new set of local design wind pressure coefficients have been compared with respect to available experimental data and the current wind provisions. The comparison shows that the proposed provisions are generally compatible with the data from previous studies, although they may be overall somewhat more expensive in their implementation.

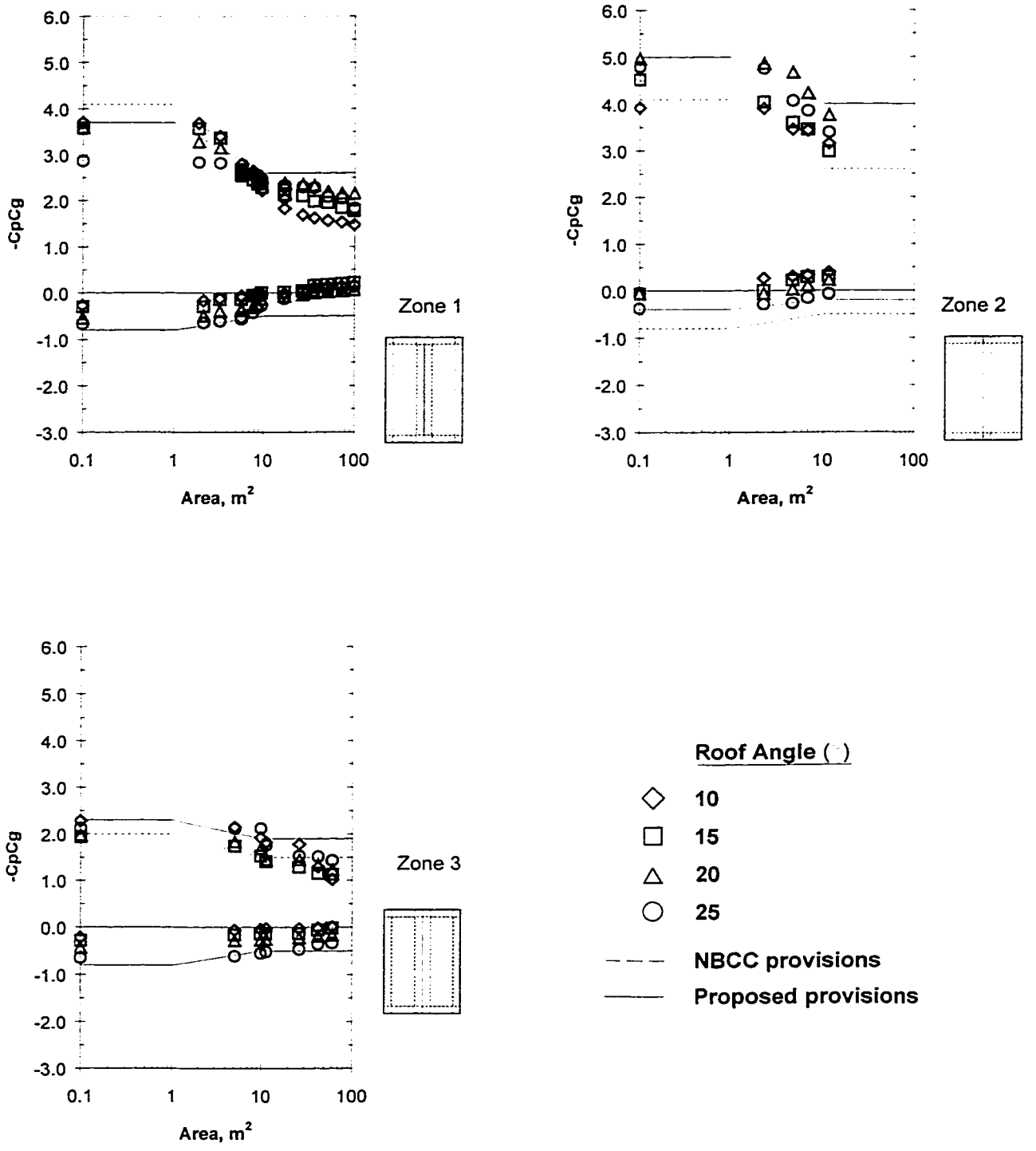

Figure 5.7 Experimental most critical pressure coefficients, current NBCC and proposed new codal provisions

Table 5.3 Comparison of the proposed wind design pressure coefficients with those from the current wind provisions and those from previous experimental findings

	Most-critical local suction coefficients for each region						
	A	B	C	D	E	F	G
Current wind provisions	-4.1	-4.1	-3.1	-2.0	-3.1	-2.0	-1.6
Meecham et al (1991)	-4.4	-5.3	-3.8	-2.6	-5.3	-3.4	-2.6
Holmes (1981)	-3.1	-5.2	-3.3	-1.8	-3.8	-3.4	-2.7
Proposed wind provisions	-3.7	-5.0	-3.7	-2.3	-3.7	-3.7	-2.3

5.4 ASSESSMENT OF THE INCREASE OF DESIGN WIND LOADS BROUGHT BY THE PROPOSED PROVISIONS

From the economics point of view, updating of the current wind provisions may have large-scale effects on the cost of roof construction, since safety and economy always fight against each other in engineering. Thus it is necessary to assess the feasibility of the proposed provisions in terms of the increases of design wind loads in comparison to the current ones.

A number of assumptions have been made for the comparison. Typical roof cases have been selected. The roof gable wall length would be equal to or longer than 10m. The ratios of roof length over roof width of these roofs have been considered as 1:1, 2:1 and 3:1. The notations of L and B, which have been applied for long wall length and gable wall length, are now used for roof length and width, implying that the difference between roof width with its horizontal projection is neglected. Moreover, for simplicity, only local pressure coefficients, which can be applied for roof cladding with tributary area $\leq 1m^2$, have been considered since only a "feeling" of the potential increase is to be provided in the present study. Furthermore, positive pressure coefficients have not been considered here, albeit their values are smaller as indicated in Figure 5.7, simply because positive wind loads are not generally dominant for the design of a roof.

Under the given assumptions, the weighting factor (F) of each pressure zone, which represents the ratio of the zone's size to the entire roof size, can be obtained for each of

the three roof cases by considering the areas of their respective pressure zones, as specified in Figure 5.7. These factors have been calculated and presented in Table 5.4.

With the weighting factors of Table 5.4, the comparison of the proposed provisions with the current ones in terms of local suction coefficient values can be carried out by using the equation:

$$(C_p C_g)_{roof} = \sum_{i=1}^{3} (C_p C_g)_i F_i \qquad (5.1)$$

where $(\mathbf{C_pC_g})_{\mathbf{roof}}$ is the expected or "average" design local pressure coefficient, **i** denotes the respective zone number and $\mathbf{C_pC_g}$ represent design local suction coefficient for the proposed and current provisions, as specified in Figure 5.7. The results of this comparison are shown in Table 5.5. Please not that this comparison is simplified since the current provisions have applied to the new Zones 1, 2 and 3 in an approximate way. For instance, design pressure coefficients on Zone 1 have considered the most critical roof corner value, whereas respective current provisions for Zone 3 have adopted the predominant interior roof suction coefficient.

Clearly, the proposed wind provisions appear to increase the design pressure coefficients by approximately 15%, at least as far as local roof suction are concerned. This is not excessive and may be well justified by considering the results of the present study and previous findings as well.

Table 5.4 Zone weighting factors (F) of three different roofs

	Zoning Areas			Weighting factors (F)		
Roof geometry (L:B)	1:1	2:1	3:1	1:1	2:1	3:1
Zone1	0.32 B^2	0.52 B^2	0.72 B^2	0.32	0.26	0.24
Zone2	0.04 B^2	0.04 B^2	0.04 B^2	0.04	0.02	0.01
Zone3	0.64 B^2	0.64 B^2	2.24 B^2	0.64	0.72	0.73
Total roof area	1 B^2	2 B^2	3 B^2			

Table 5.5 Comparison of the proposed and current provisions in terms of expected values of design local suction coefficients for three roof configurations

(1) Roof 1 (L:B=1:1)

		Proposed provisions		Current provisions	
Zone	F_i	$(C_pC_g)_i$	$(C_pC_g)_iF_i$	$(C_pC_g)_i$	$(C_pC_g)_iF_i$
1	0.32	3.7	1.18	4.1	1.31
2	0.04	5.0	0.20	4.1	0.16
3	0.64	2.3	1.47	1.7	1.09
$(C_pC_g)_{roof}$			2.85		2.56
Proposed/Current	1.11				

(2) Roof 2 (L:B=2:1)

		Proposed provisions		Current provisions	
Zone	F_i	$(C_pC_g)_i$	$(C_pC_g)_iF_i$	$(C_pC_g)_i$	$(C_pC_g)_iF_i$
1	0.26	3.7	0.96	4.1	1.07
2	0.02	5.0	0.10	4.1	0.08
3	0.72	2.3	1.66	1.7	1.22
$(C_pC_g)_{roof}$			2.72		2.37
Proposed/Current	1.15				

(3) Roof 3 (L:B=3:1)

		Proposed provisions		Current provisions	
Zone	F_i	$(C_pC_g)_i$	$(C_pC_g)_iF_i$	$(C_pC_g)_i$	$(C_pC_g)_iF_i$
1	0.24	3.7	0.89	4.1	0.98
2	0.013	5.0	0.067	4.1	0.06
3	0.73	2.3	1.69	1.7	1.24
$(C_pC_g)_{roof}$			2.65		2.28
Proposed/Current	1.16				

CHAPTER 6

CONCLUSIONS AND RECOMMENDATIONS

6.1 SUMMARY AND CONCLUSIONS OF THE PRESENT STUDY

A series of wind tunnel model tests have been carried out to examine the suitability of the current wind provisions of NBCC (1995) for low buildings in the intermediate roof slope range ($10^{\circ}<\theta\leq30^{\circ}$). Five gable roof models with roof angles of 10°, 15°, 20°, 25° and 30° have been investigated in wind tunnel. These roof models were assumed to be representative for gable roofs of intermediate slopes. This addresses the criticisms on the current approach that low building roofs within the intermediate slope range are designed by testing models with only one roof slope (18.4°). In order to provide an accurate wind tunnel simulation, the experimental settings are designed to follow the respective criteria requested in the ASCE wind loading test standard (ASCE Draft, 1997). An intensive set of experimental results has been obtained and applied for codification process.

Prior to the application of the experimental results obtained, the present data were compared with data from previous studies. Although there are some differences among

these experimental studies, the comparisons seem satisfactory. This and the adequacy of wind tunnel simulation confirm the suitability of the present experimental results for codification purposes.

A series of comparisons have been carried out to examine the adequacy of the current wind provisions in the National Building Code of Canada for the design of gable roofs with angles lower or higher than 18.4°. The codal definitions of slope range, roof region category, pressure zoning category and design wind pressure coefficients have been discussed, respectively. Although the experimental results generally agree with the current wind provisions, the latter clearly underestimate the peak suctions on corner and edge regions. Moreover, the roof angles involved within the current slope category definition may be somewhat changed.

An alternative set of provisions has been derived from these comparisons and discussions. The current codal definition on the roof regions has been maintained but the pressue zoning definition has been modified. For the proposed pressure zones, a new set of design wind pressure coefficients has been formulated. Furthermore, the slope range definition has also been somewhat modified.

For the proposed wind provisions, a preliminary assessment of the increase of the design wind loads has been conducted. It appears that the proposed wind provisions may increase the design local wind loads for gable roofs of intermediate slopes by an amount, typically varying between 6 and 16 percent depending on the building's geometry.

6.2 RECOMMENDATIONS FOR FUTURE STUDY ON THIS TOPIC

A set of five gable roof models with roof angles in the intermediate slope range has been tested and various interesting results have been found. The interval between these roof angles was set at 5°, in order to sufficiently model the wind pressure distributions for the entire intermediate slope range. This assumption was justified by comparison with the experiments conducted in previous studies. However, the results obtained show that the pressure distributions on the intermediate slope roof could be very sensitive to the roof slope. Therefore, it would be of interest in a future study to model roofs with adjustable roof angle to detect differences in the pressure distributions corresponding to a very small variation of roof slope.

In the present study, several factors affecting the wind loads on low-building gable roofs of intermediate slopes have not been taken into account, because only the suitability of the current wind provisions is the major concern of the present study. For instance, the variation of the upstream terrain exposure and the actual building configuration have not been included in the scope of the present study. In order to better understand the behaviour of wind pressures on roofs, these factors should be considered.

In fact, low-rise buildings with gable roofs may be located either in open country or in suburban exposure. Besides the isolated case of the present study, such buildings could also be in grouping or surrounded by other obstacles such as fences, trees. Moreover, gable roofs often have overhangs and other decorative components. The roofs may be

exposed not only to the boundary layer wind but also to other storm systems, for instance, tornadoes. In order to protect low building gable roofs from wind damage, the wind loading effects of the above-mentioned factors need further studies for future update of the codes and standards of practice.

REFERENCES

ASCE 7-95 (1995) Minimum Design Loads for Building and Other Stuctures, American Society of Civil Engineers, New York, N.Y.

ASCE Standard (1997) Wind Tunnel Testing for Building and Other Structures (Draft), American Society of Civil Engineers, New York, N.Y.

Davenport, A. G. (1983) On the Assessment of the Reliability of Wind Loading on Low Buildings, J. Wind Eng. Ind. Aerodyn., 11, 21-37.

Ginger, J. D. and Letchford, C. W. (1992) Peak Wind Loads under Delta Wing Vortices on Canopy Roofs, J. Wind Eng. Ind. Aerodyn., 41-44, 1739-1750.

Gumbel, E. J. (1958) Statistics of Extremes, Columbia University Press.

Hensen, S. O and Sorensen, E. G. (1986) The Aylesbury Experiment. Comparison of Model and Full-scale Tests, J. Wind Eng. Ind. Aerodyn., 22, 1-22.

Holmes, J. D. (1981) Wind Pressures and Forces on Tropical Houses, Technical Report, Australian House Research Council.

Holmes, J. D. (1983) Wind Loads on Low Rise Buildings - A Review, Commonwealth Scientific and Industrial Research Organization (CSIRO)-Division of Building Research.

Holmes, J. D. (1984) Effects of Frequency Response on Peak Pressure Measurements, J. Wind Eng. Ind. Aerodyn., 17, 1-9.

Holmes, J. D. (1994) Wind Pressures on Tropical Housing, J. Wind Eng. Ind. Aerodyn., 53, 105-123.

Hoxey, R. P. and Moran, P. (1983) A Full-scale Study of the Geometric Parameters that Influence Wind Loads on Low Rise Buildings, J. Wind Eng. Ind. Aerodyn., 13, 277-288.

Kanda, M. and Maruta, E. (1993) Characteristics of Fluctuating Wind Pressure on Long Low-Rise Buildings with Gable Roofs, J. Wind Eng. Ind. Aerodyn., 50, 173-182.

Kawai, H. and Nishimura, G. (1996) Characteristics of Fluctuating Suction and Conical Vortices on a Flat Roof in Oblique Flow, J. Wind Eng. Ind. Aerodyn., 60, 211-225.

Kramer, C. and Gerhardt, H. J. (1991) Wind Pressure on Roofs of Very Low and Very Large Industrial Buildings, J. Wind Eng. Ind. Aerodyn., 38, 285-295.

Levitan, M. L. Mehta, K. C., Vann, W. P. and Holmes, J. D. (1991) Field Measurements of Pressures on the Texas Tech Building, J. Wind Eng. Ind. Aerodyn., 38, 235-247.

Mayne, J. R. and Cook, N. J. (1980) Proceedings of the Fifth International Conference on Wind Engineering, Pengamon Press, 1339-1355.

Meecham, D., Surry, D. and Davenport, A. G. (1991) The Magnitude and Distribution of Wind-Induced Pressures on Hip and Gable Roofs, J. Wind Eng. Ind. Aerodyn., 38, 257-272.

Mousset, S. (1986) The International Aylesbury Collaborative Experiment in C. S. T. B., J. Wind Eng. Ind. Aerodyn., 23, 19-36.

NBCC, (1995) Supplement to the National Building Code of Canada, Associate Committee on the National Building Code, National Research Council of Canada, Ottawa.

Richardson, G. M., Robertson, A. P., Hoxey, R. P. And Surry, D. (1990) Full-scale and Model Investigation of Pressures on an Industrial/Agricultural Building, J. Wind Eng. Ind. Aerodyn., 36, 1053-1062.

Richardson, G. M. and Surry, D. (1991) Comparisons of Wind-Tunnel and Full-scale Surface Pressure Measurements on Low-Rise Pitched Roof Buildings, J. Wind Eng. Ind. Aerodyn., 38, 249-256.

Richardson, G. M. and Surry, D. (1992) The Silsoe Buildings: A Comparison of Pressure Coefficients and Spectra at Model and Full-scale, J. Wind Eng. Ind. Aerodyn., 41-44, 1653-1664.

Saathoff, P. J. and Melbourne, W. H. (1989) The Generation of Peak Pressures in Separated/Reattaching Flows, J. Wind Eng. Ind. Aerodyn., 32, 121-134.

Saathoff, P. J. and Stathopoulos, T. (1992) Wind Loads on Buildings with Sawtooth Roofs, J. Struct. Eng., 118,429-446.

Savory, E., Dalley, S. and Toy, N. (1992), The Effects of Eaves Geometry, Model Scale and Approach Flow Conditions on Portal Frame Building Wind Loads, J. Wind Eng. Ind. Aerodyn., 41-44, 1665-1676.

Sill, B. L., Cook, N. J. and Blackmore, P. A. (1989) IAWE Aylesbury Comparative Experiment – Preliminary Results of Wind Tunnel Comparisons, J. Wind Eng. Ind. Aerodyn., 32, 285-302.

Sill, B. L. and Cook, N. J. (1990) The Aylesbury Comparative Experiment: A Status Report, J. Wind Eng. Ind. Aerodyn., 36, 1047-1052.

Sill, B. L., Cook, N. J. and Fang, C. (1992) The Aylesbury Comparative Experiment: A Final Report, J. Wind Eng. Ind. Aerodyn., 41-44, 1553-1564.

Simiu, E. and Scanlan, R. H., Wind Effects on Structures: An Introduction to Wind Engineering. John Wiley & Sons, New York, 1986.

Surry, D. and Stathopoulos, T. (1978) An Experimental Approach to the Economical Measurement of Spatially-Averaged Wind Loads. J Wind Eng. Ind. Aerodyn.,2, 385-397.

Stathopoulos, T. (1979) Turbulent Wind Action on Low Rise Buildings, Ph. D. Thesis, The University of Western Ontario.

Stathopoulos, T. (1984a) Wind Loads on Low-Rise Buildings: A Review of the State of the Art, Engng. Strct., Vol. 6, April.

Stathopoulos, T. (1984b) Design and Fabrication of a Wind Tunnel for Building Aerodynamics, J. Wind Eng. Ind. Aerodyn., 16, 361-376.

Stathopoulos, T., Surry, D. and Davenport, A. G. (1985) A Simplified Model of Wind Pressure Coefficients for Low-Rise Buildings, In Proc. ICOSSAR'85.

Stathopoulos, T. and Saathoff, P. J. (1991) Wind Pressure on Roofs of Various Geometries, J. Wind Eng. Ind. Aerodyn., 38, 273-284.

Surry, D. and Lin, J. X. (1995) The Effect of Surroundings and Roof Corner Geometric Modifications on Roof Pressures on Low-Rise Buildings, J. Wind Eng. Ind. Aerodyn., 58, 113-138.

Tieleman, H. W., Surry, D. and Lin, J. X. (1994) Characteristics of Mean and Fluctuating Pressure Coefficients under Corner (Delta Wing) Vortices, J. Wind Eng. Ind. Aerodyn., 52, 263-275.

Uematsu, Y. and Isyumov, N. (1996) Wind Pressure Acting on the Leading Edge and Corner Regions of a Low-Rise Building - A Study of the CWC Low-Rise Building Data Base, Technical Paper of University of Western Ontario.

Wu, H., Wang, K. and Stathopoulos, T. (1998) Pressure Coefficients for Gable Roofs of Intermediate Slopes, Presented for the Eastern European Wind Engineering Conference, Prague, September 7-11.

Appendix-1

Roof Pressure Coefficient Contours for Typical Wind Azimuths

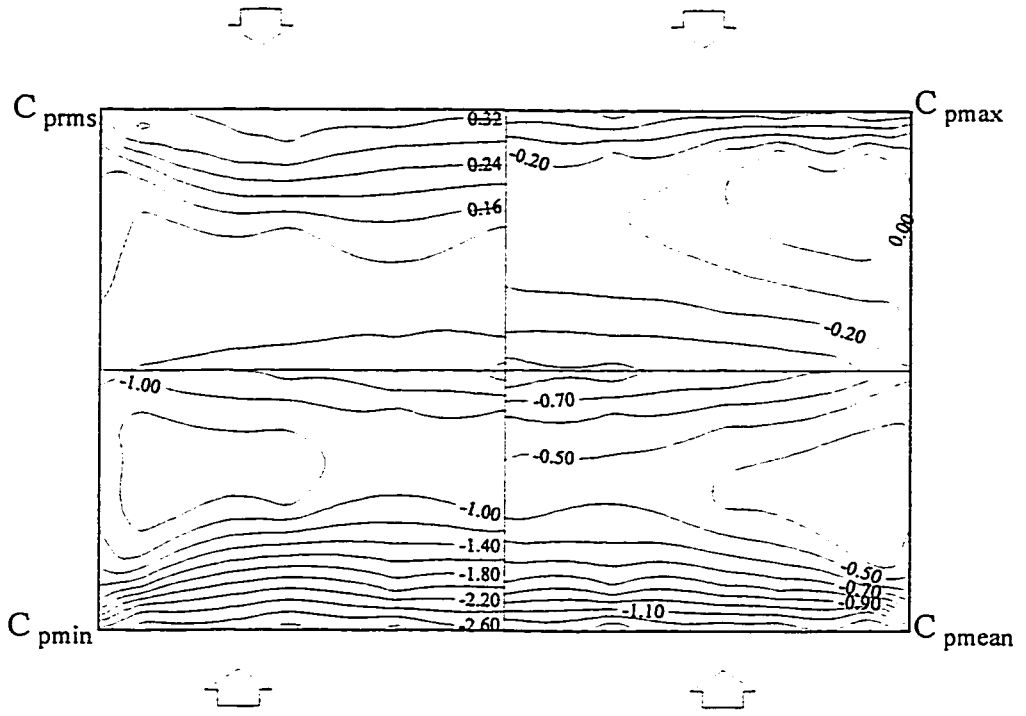

Figure A-1.1 Pressure field on the quartering roof of 10° slope at 0° wind azimuth

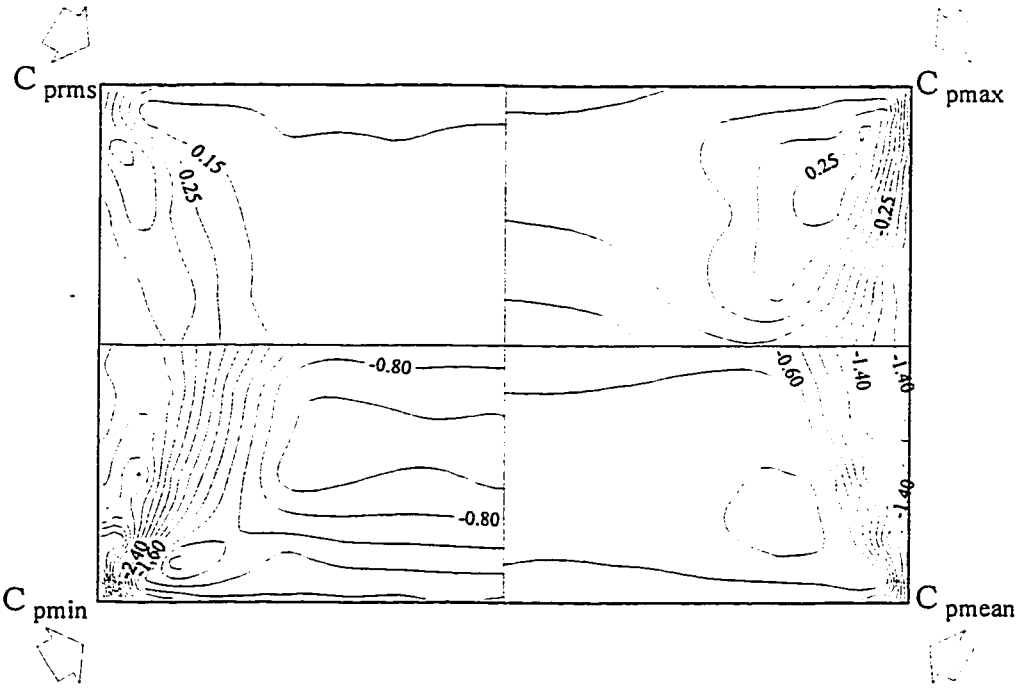

Figure A-1.2 Pressure field on the quartering roof of 10° slope at 60° wind azimuth

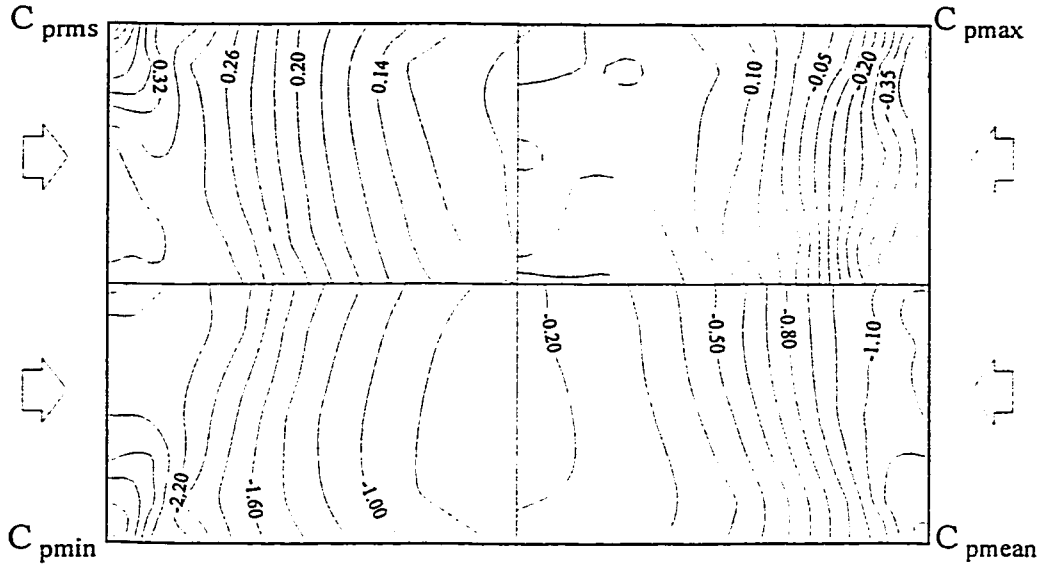

Figure A-1.3 Pressure field on the quartering roof of 10° slope at 90° wind azimuth

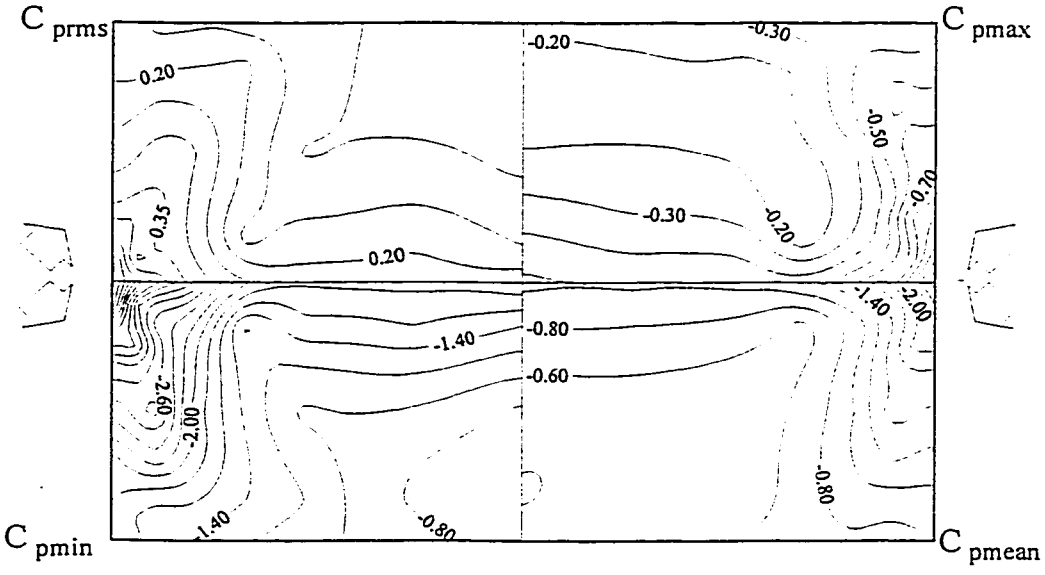

Figure A-1.4 Pressure field on the quartering roof of 10° slope at 135° wind azimuth

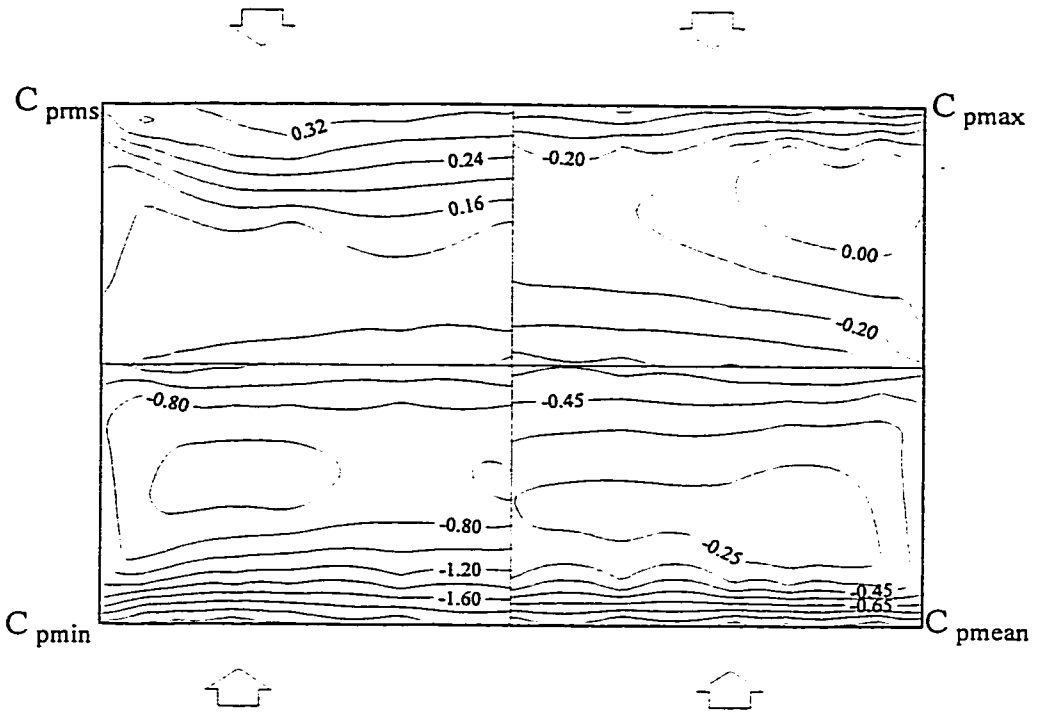

Figure A-1.5 Pressure field on the quartering roof of 15° slope at 0° wind azimuth

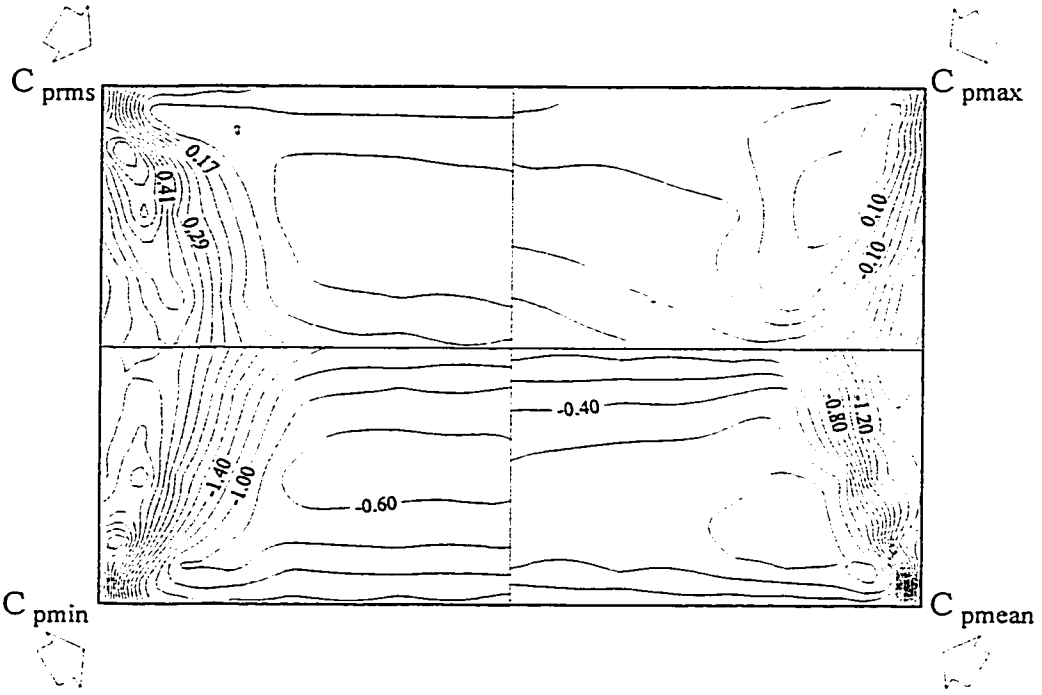

Figure A-1.6 Pressure field on the quartering roof of 15° slope at 60° wind azimuth

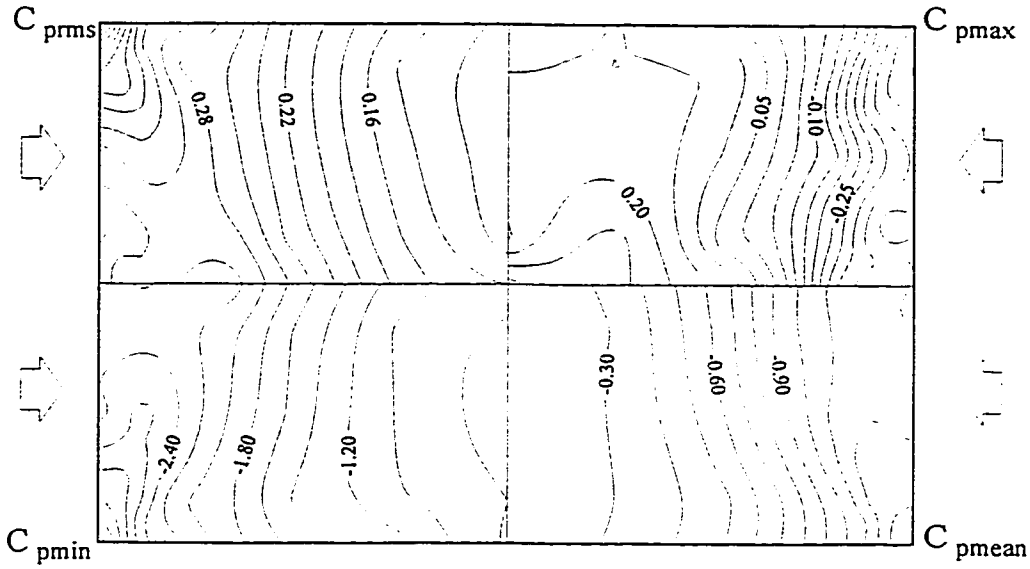

Figure A-1.7 Pressure field on the quartering roof of 15° slope at 90° wind azimuth

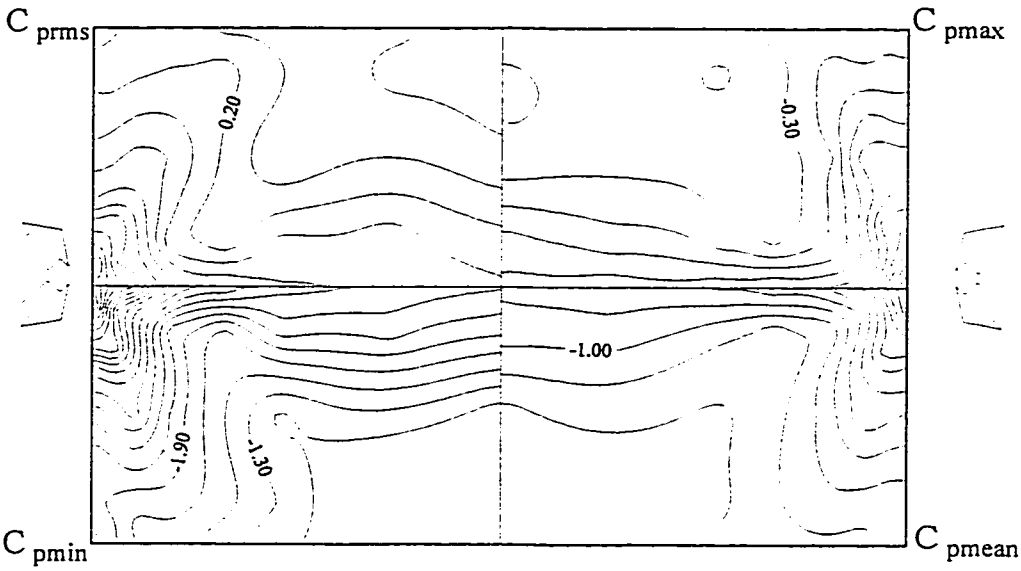

Figure A-1.8 Pressure field on the quartering roof of 15° slope at 135° wind azimuth

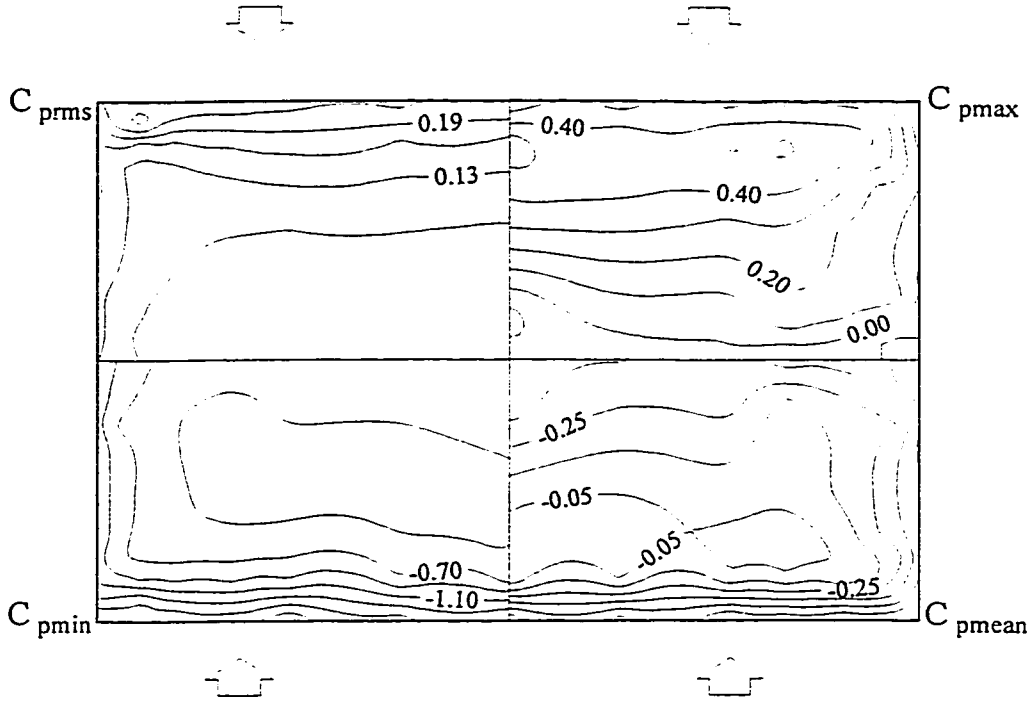

Figure A-1.9 Pressure field on the quartering roof of 20° slope at 0° wind azimuth

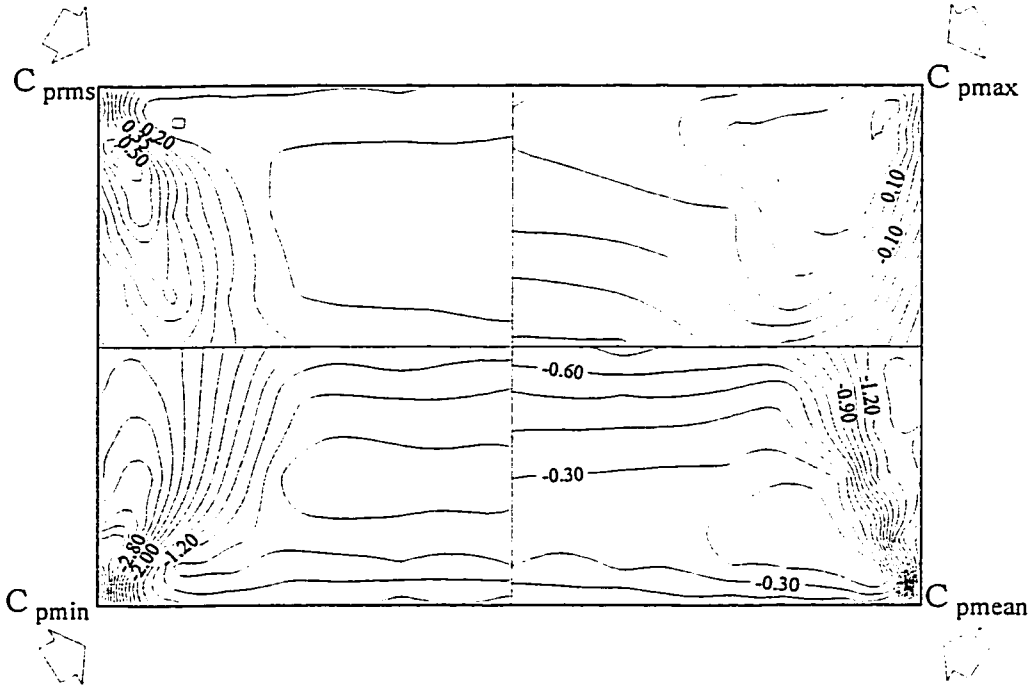

Figure A-1.10 Pressure field on the quartering roof of 20° slope at 60° wind azimuth

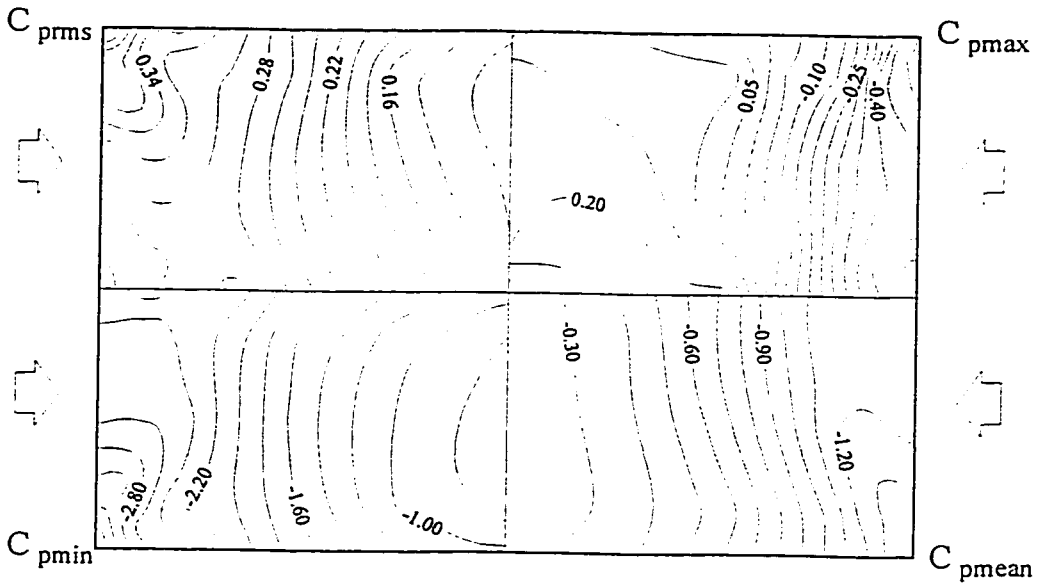

Figure A-1.11 Pressure field on the quartering roof of 20° slope at 90° wind azimuth

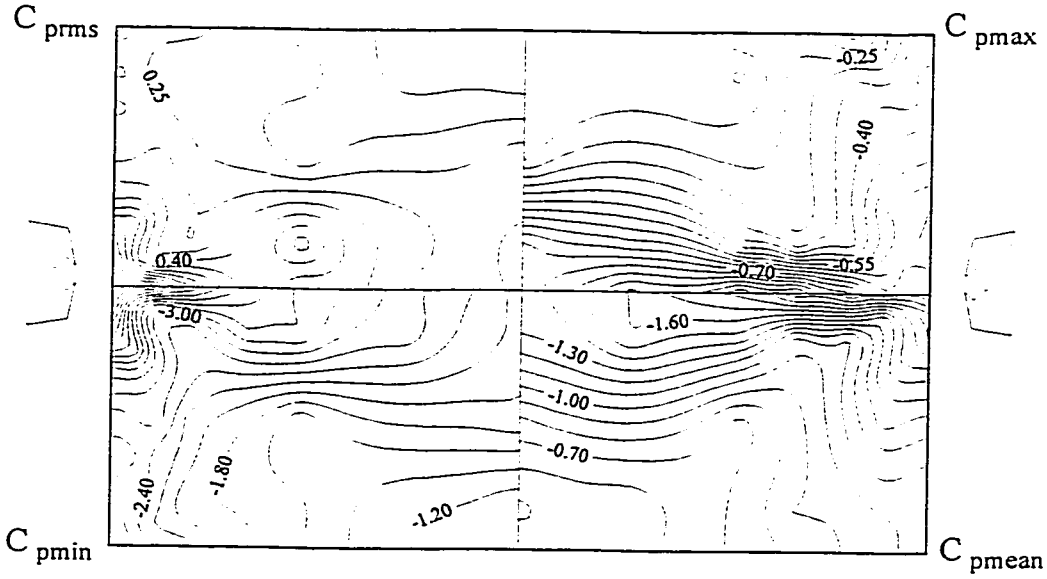

Figure A-1.12 Pressure field on the quartering roof of 20° slope at 135° wind azimuth

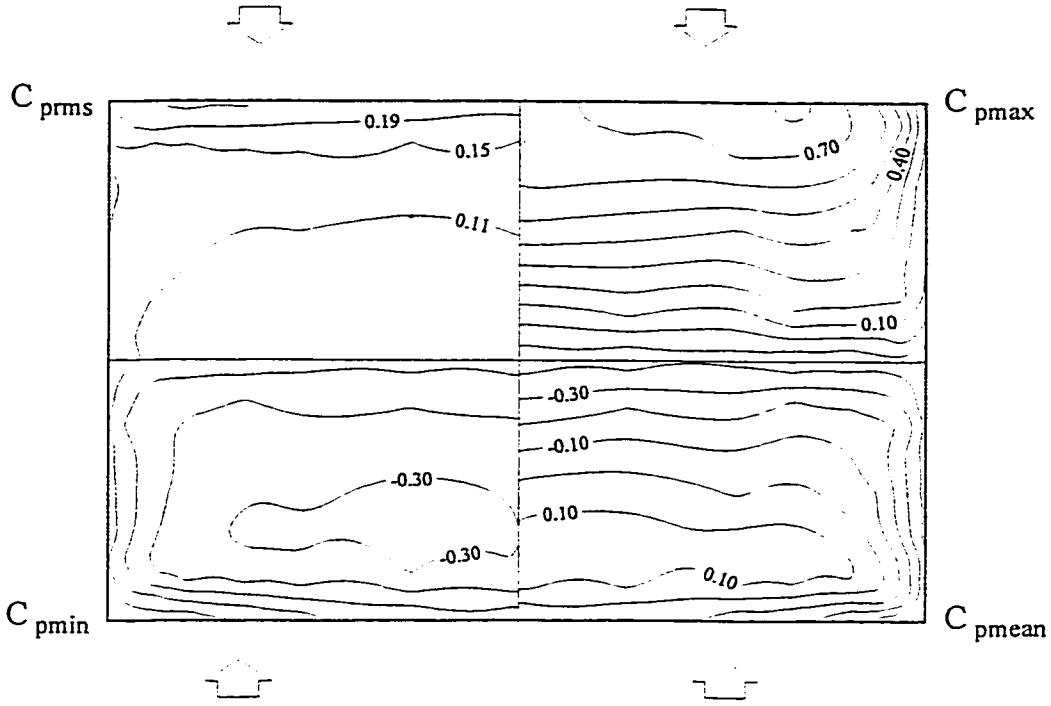

Figure A-1.13 Pressure field on the quartering roof of 25° slope at 0° wind azimuth

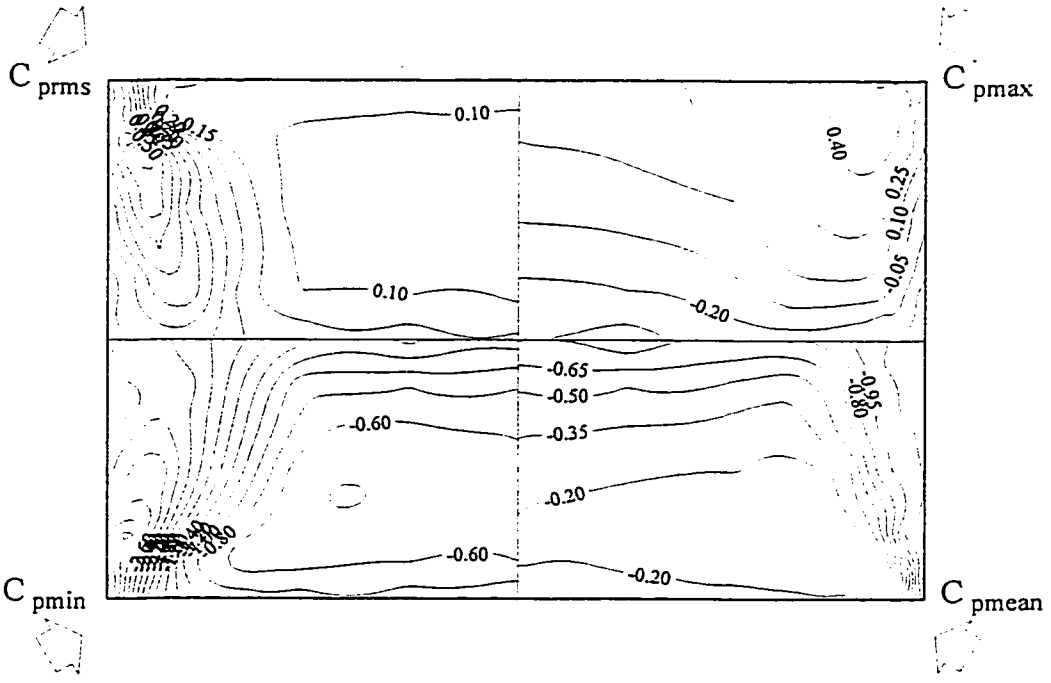

Figure A-1.14 Pressure field on the quartering roof of 25° slope at 60° wind azimuth

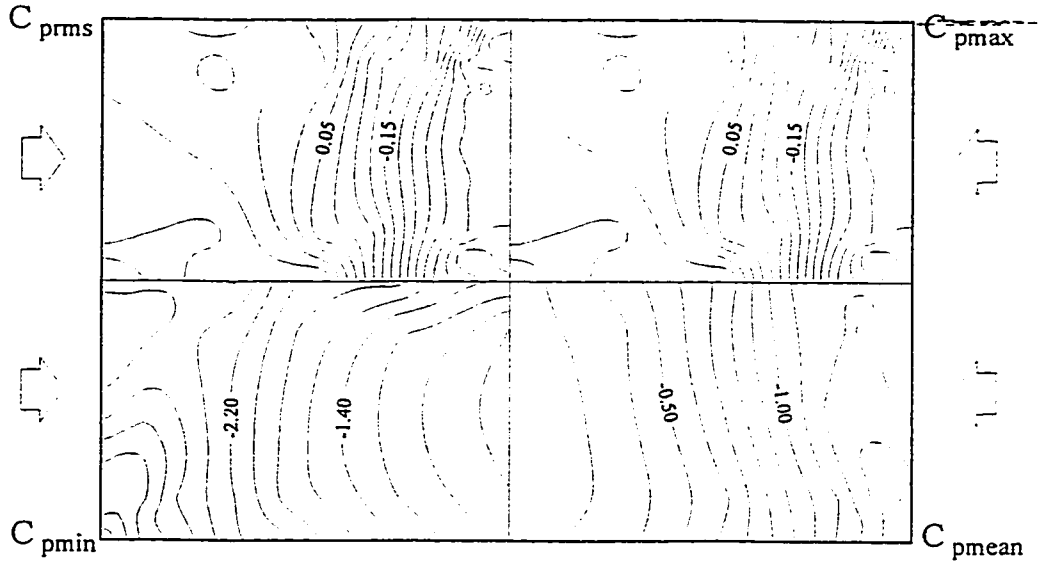

Figure A-1.15 Pressure field on the quartering roof of 25° slope at 90° wind azimuth

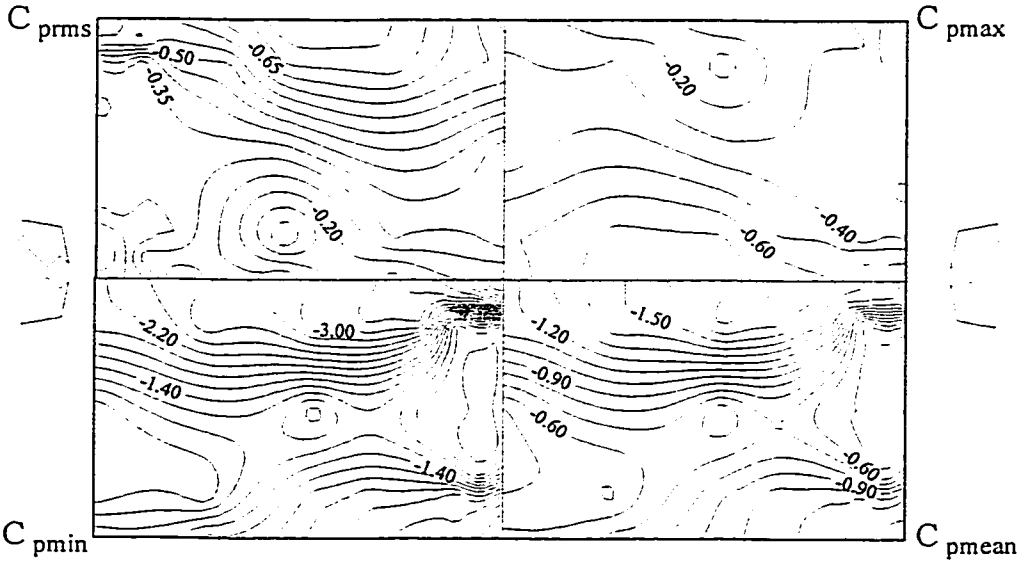

Figure A-1.16 Pressure field on the quartering roof of 25° slope at 135° wind azimuth

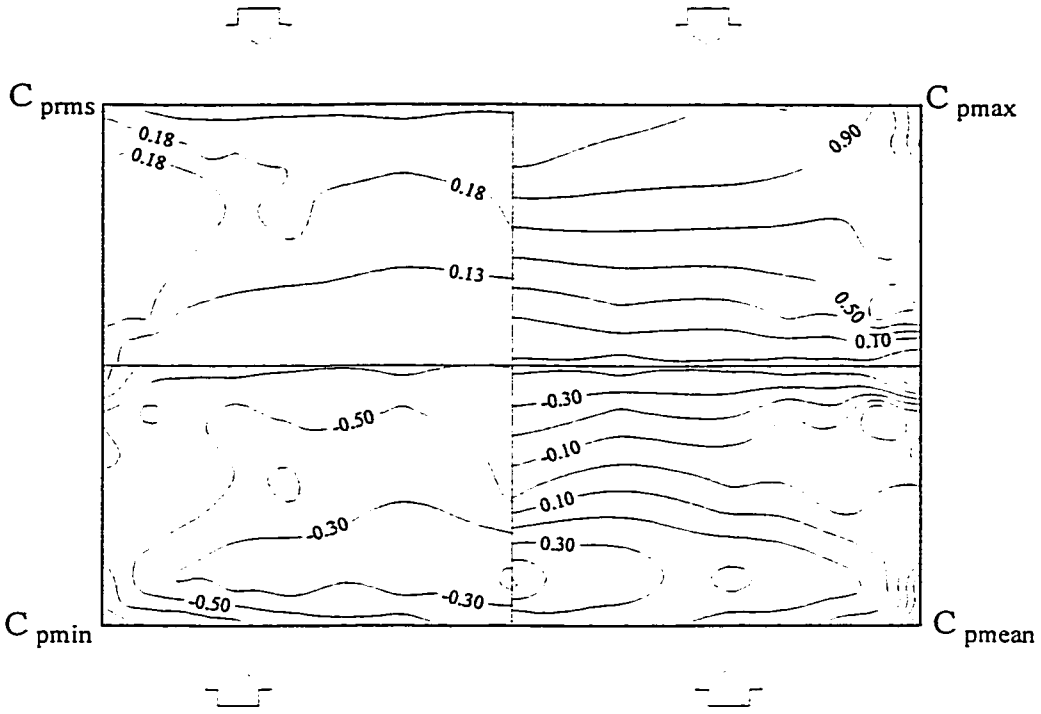

Figure A-1.17 Pressure field on the quartering roof of 30° slope at 0° wind azimuth

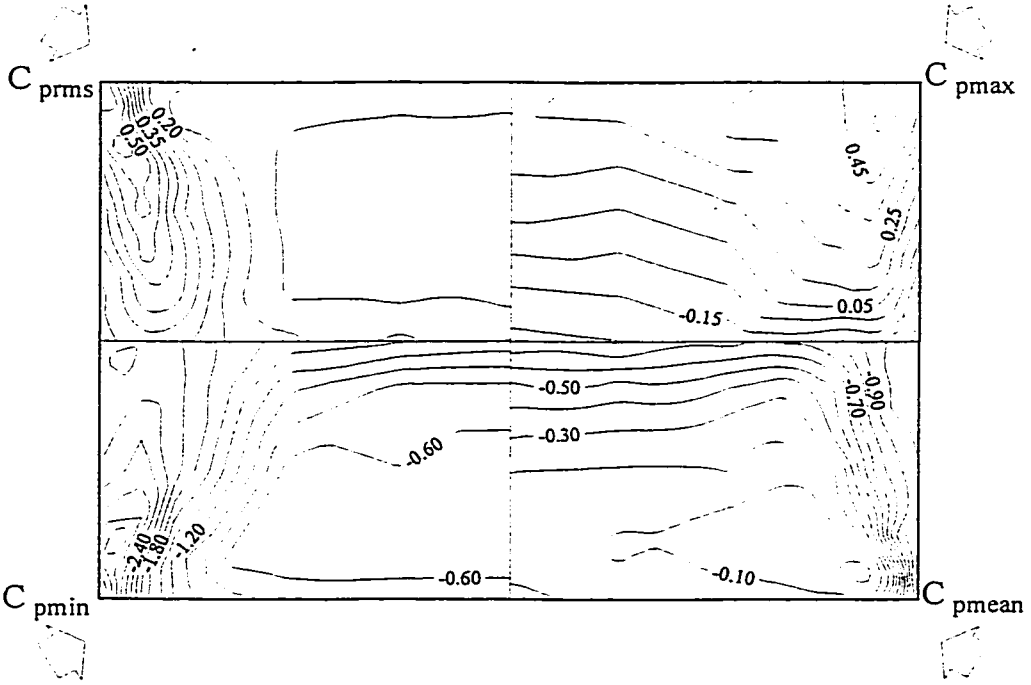

Figure A-1.18 Pressure field on the quartering roof of 30° slope at 60° wind azimuth

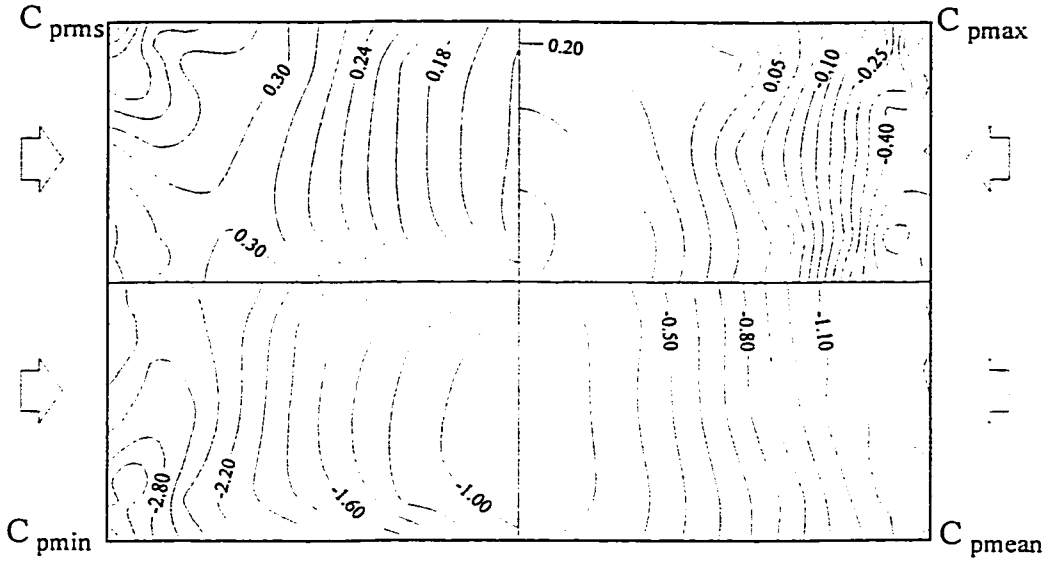

Figure A-1.19 Pressure field on the quartering roof of 30° slope at 90° wind azimuth

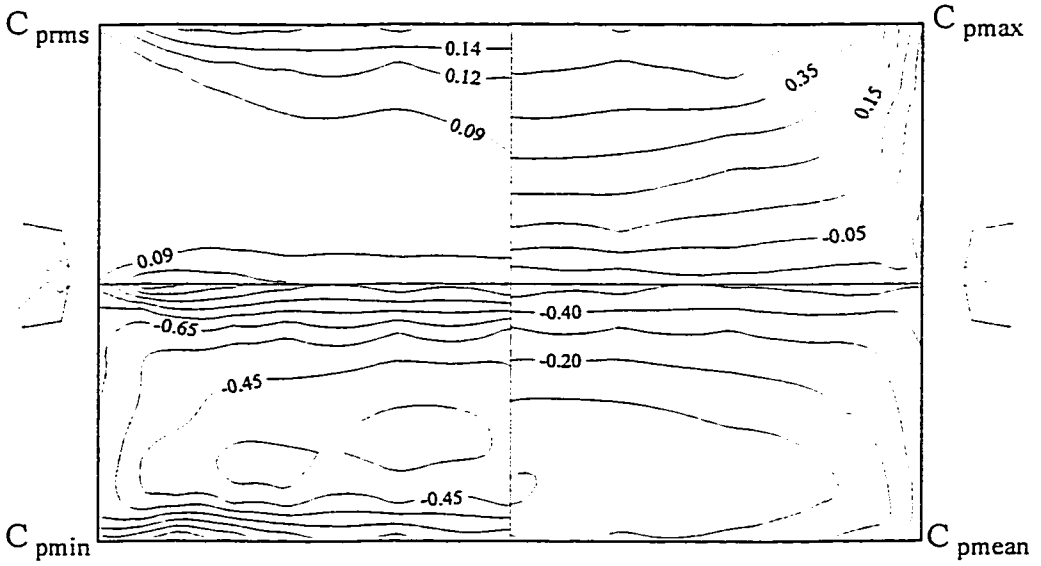

Figure A-1.20 Pressure field on the quartering roof of 30° slope at 135° wind azimuth

Appendix-2

Corner Wind Pressure Coefficients as Functions of Wind Azimuth

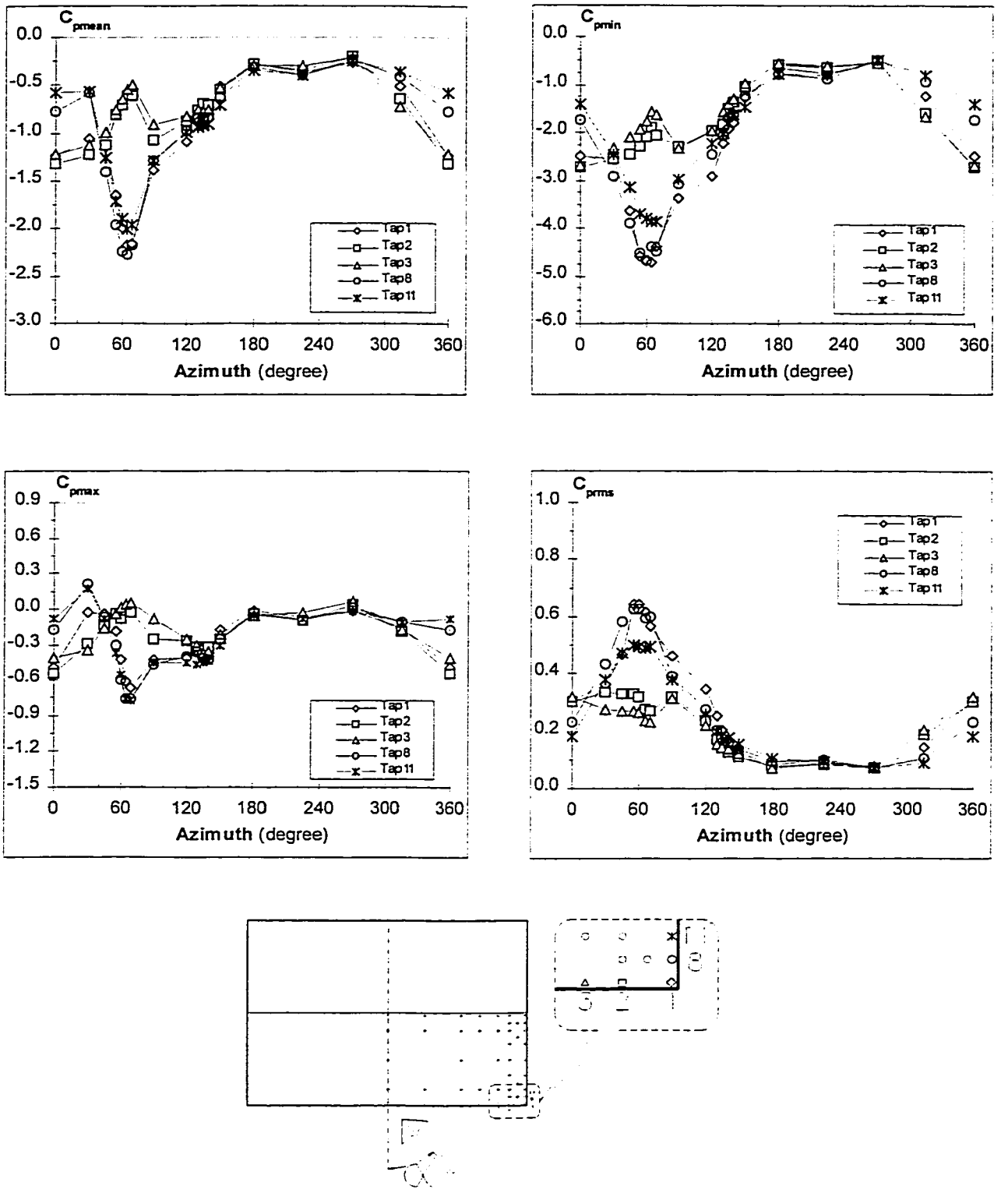

Figure A-2.1 Local pressure distribution on Eaves corner for 10° roof, all azimuths

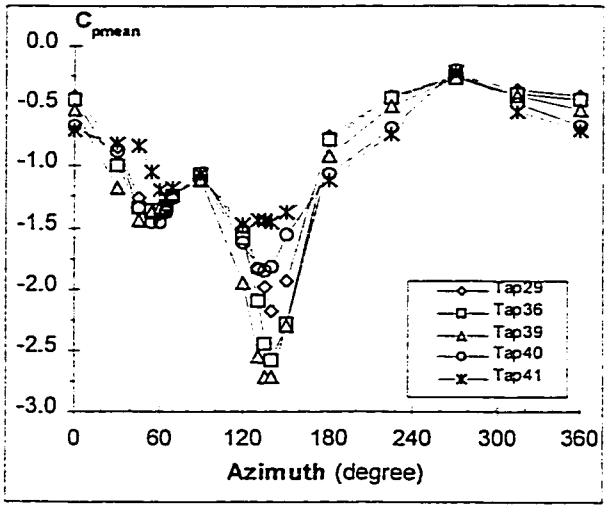

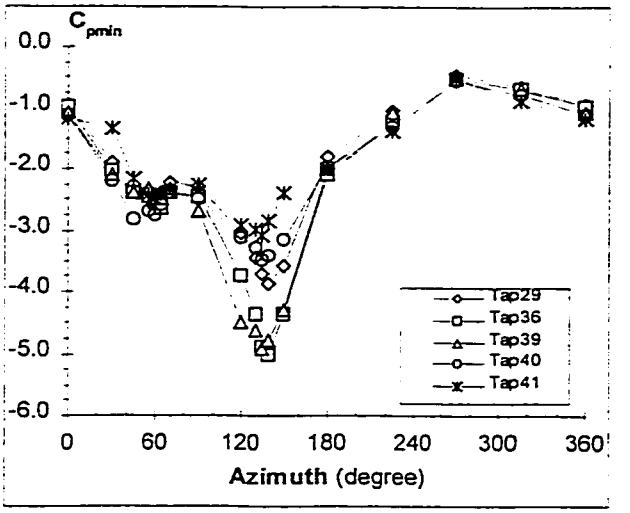

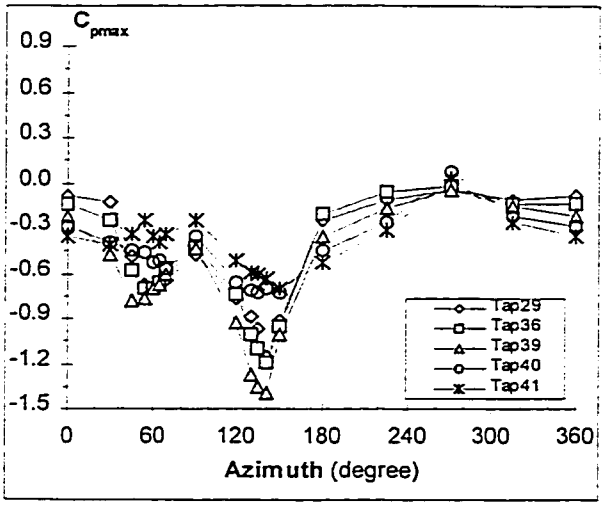

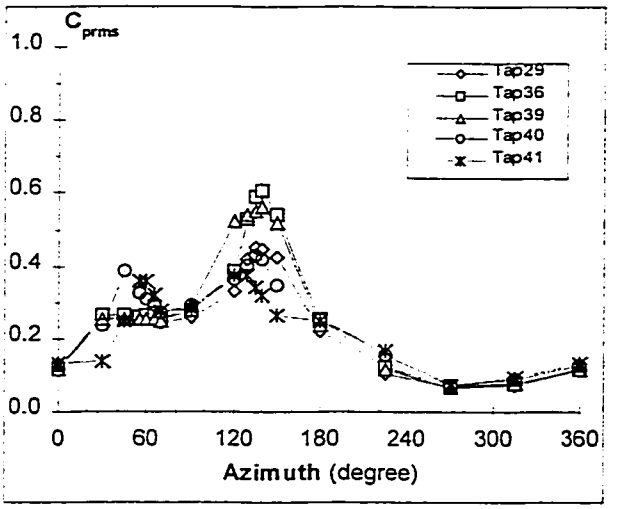

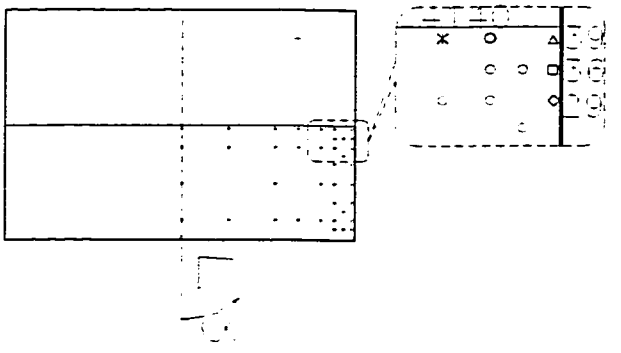

Figure A-2.2 Local pressure distribution on Ridge corner for 10° roof, all azimuths

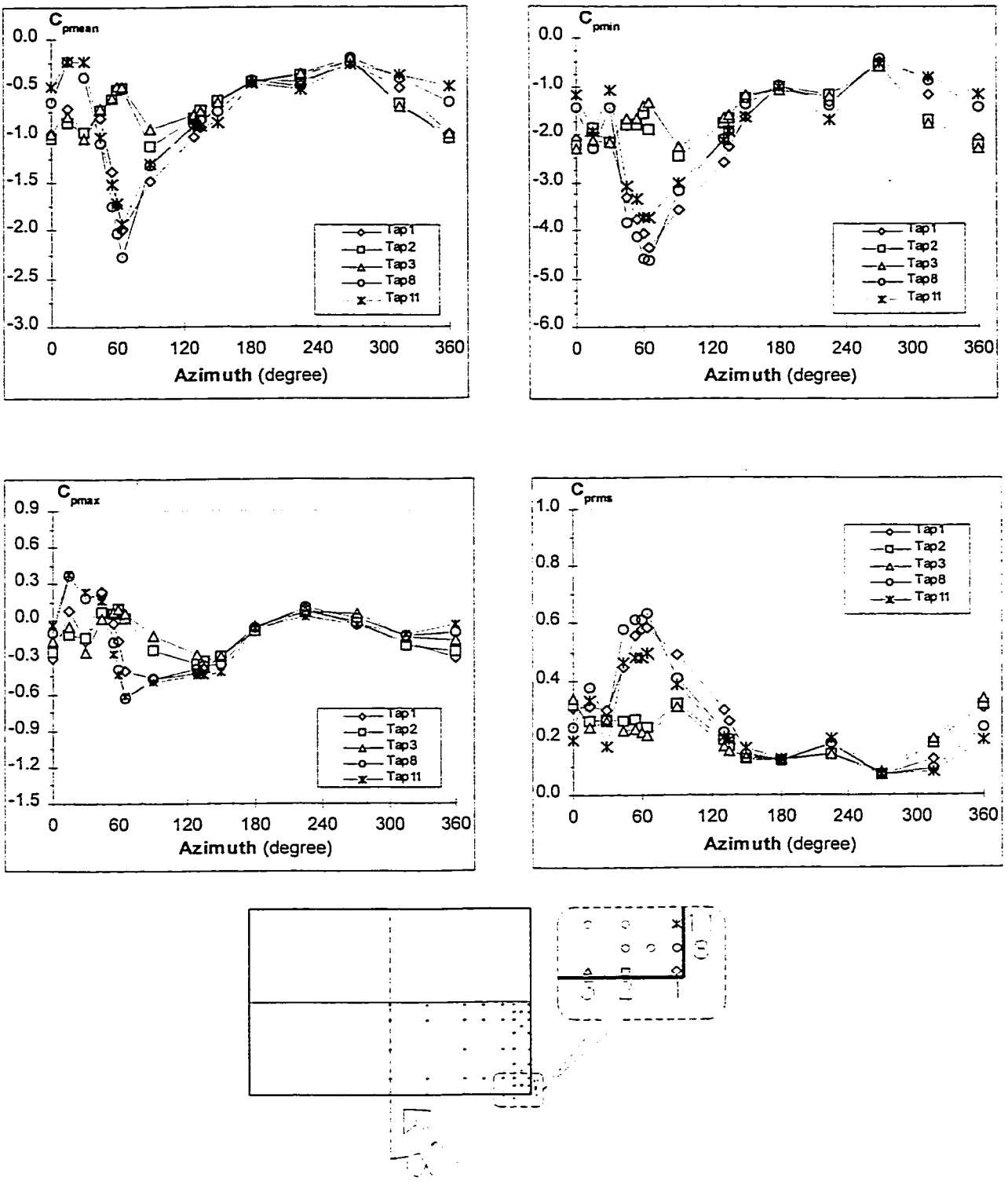

Figure A-2.3 Local pressure distribution on Eaves corner for 15° roof, all azimuths

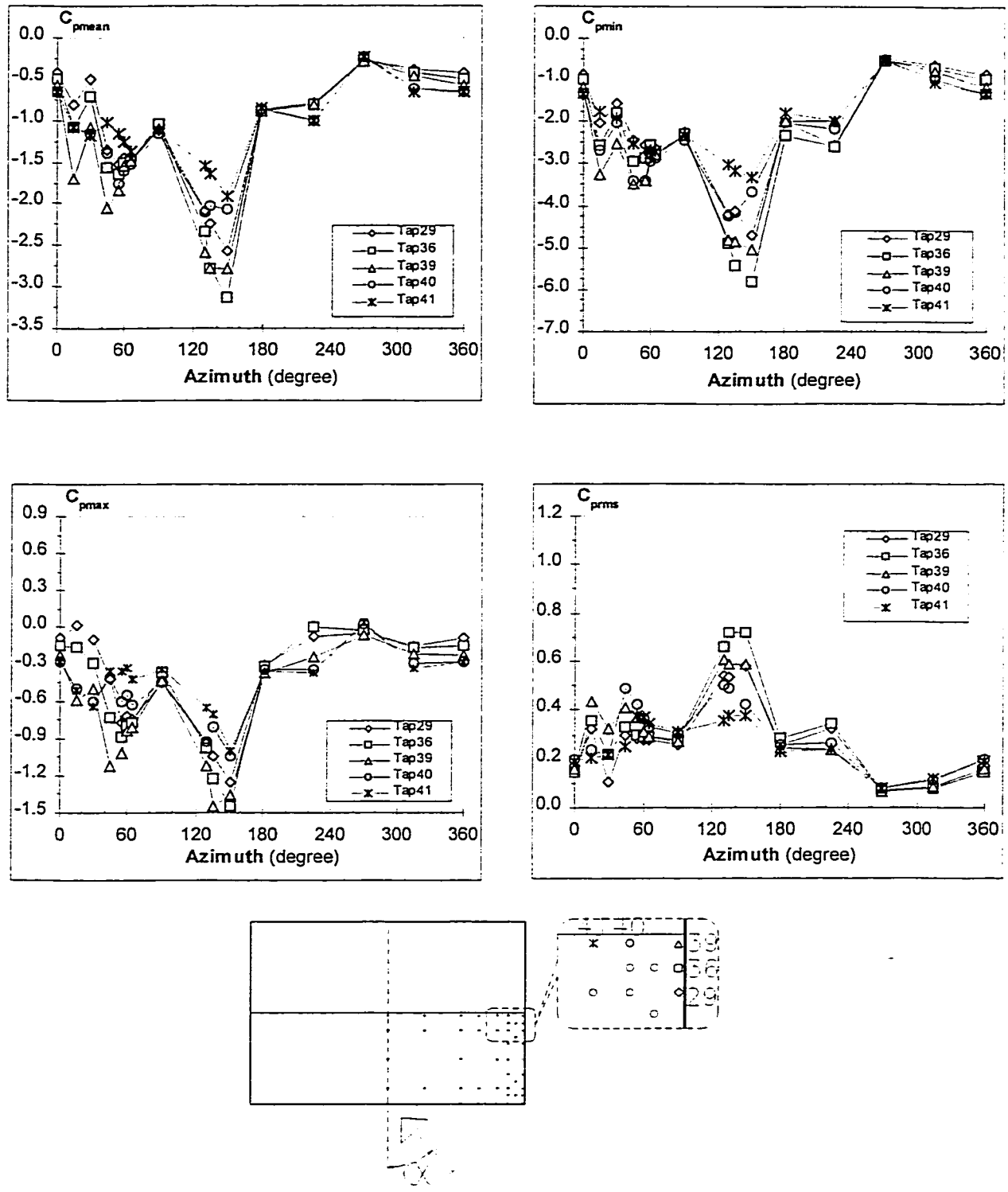

Figure A-2.4 Local pressure distribution on Ridge corner for 15° roof, all azimuths

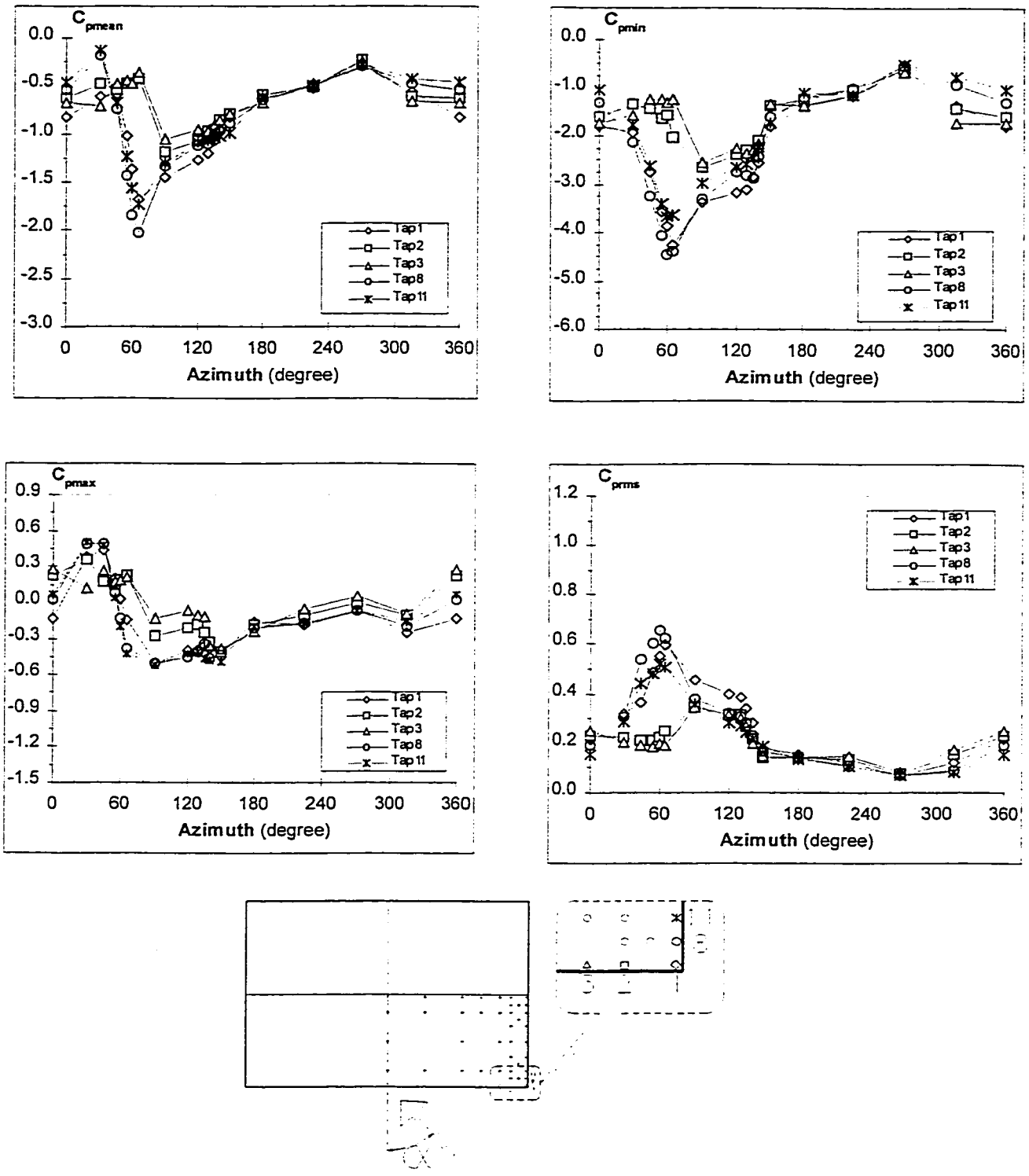

Figure A-2.5 Local pressure distribution on Eaves corner for 20° roof, all azimuths

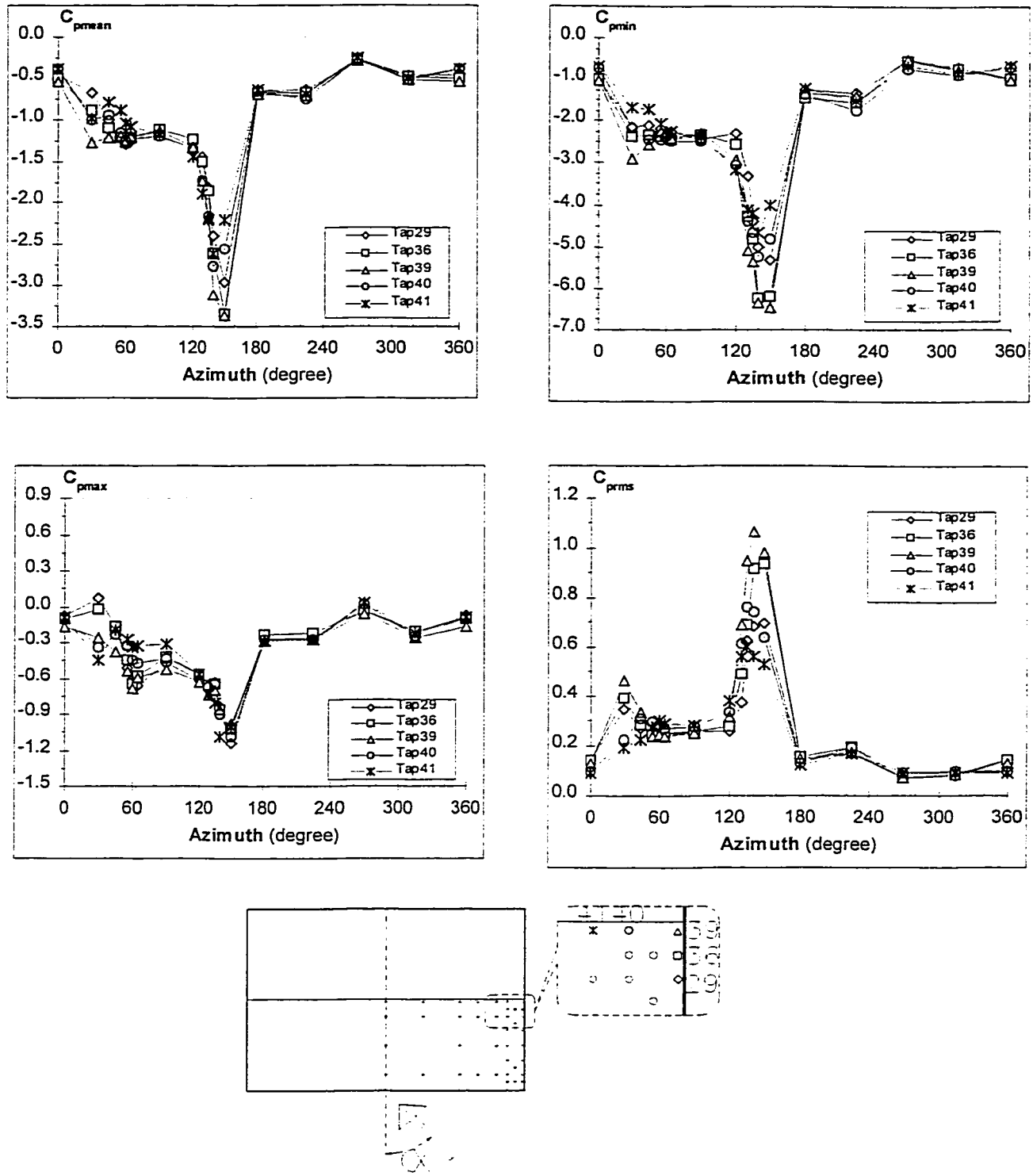

Figure A-2.6 Local pressure distribution on Ridge corner for 20° roof, all azimuths

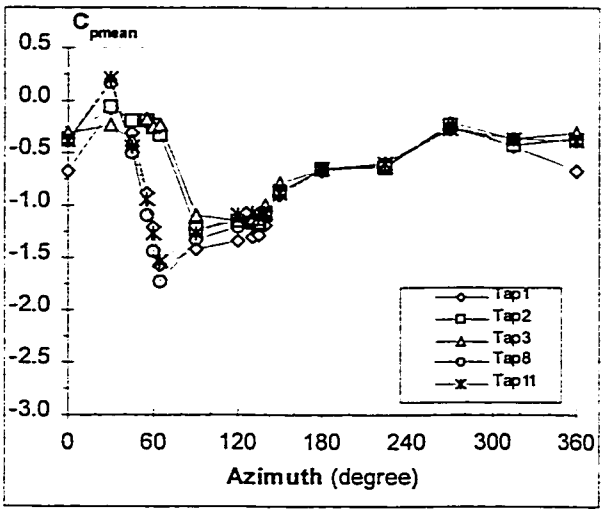

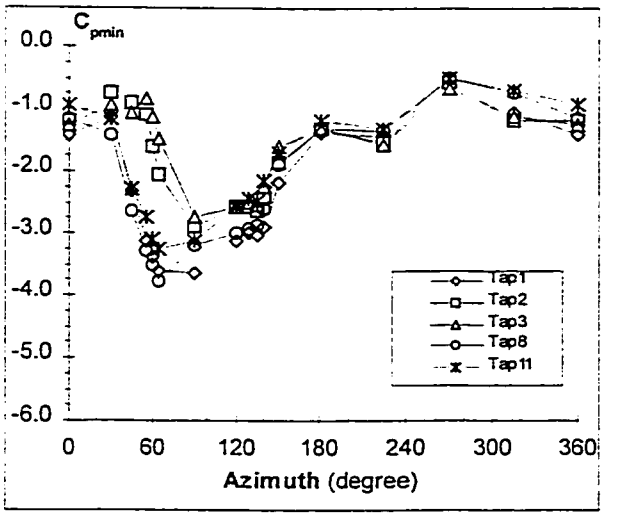

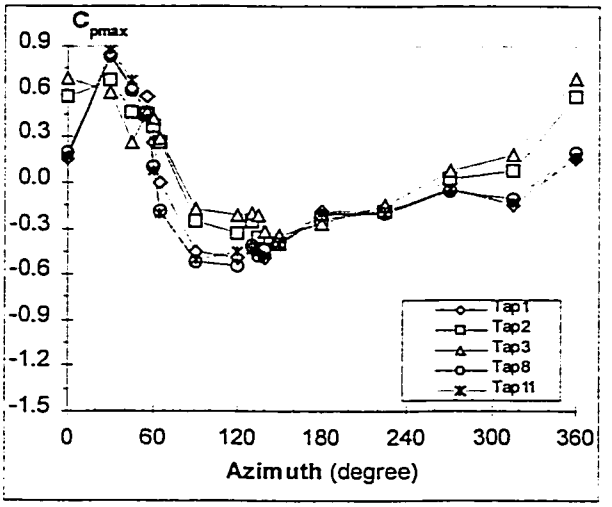

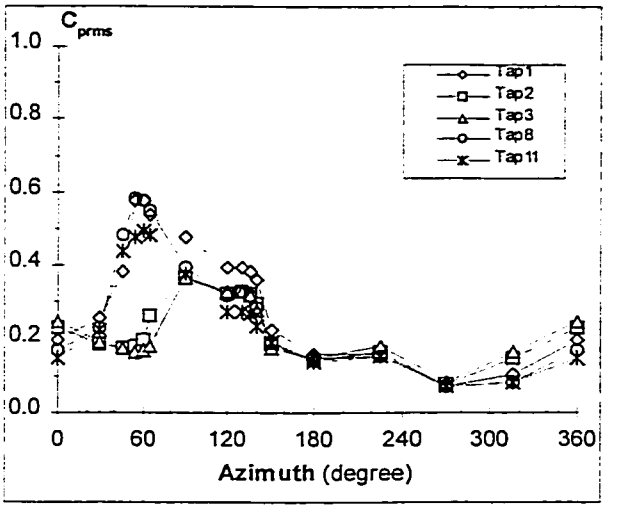

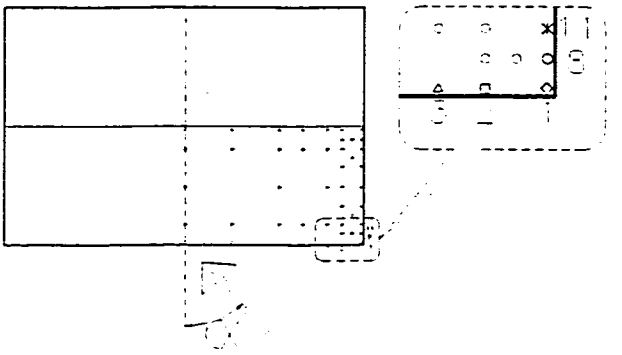

Figure A-2.7 Local pressure distribution on Eaves corner for 25° roof, all azimuths

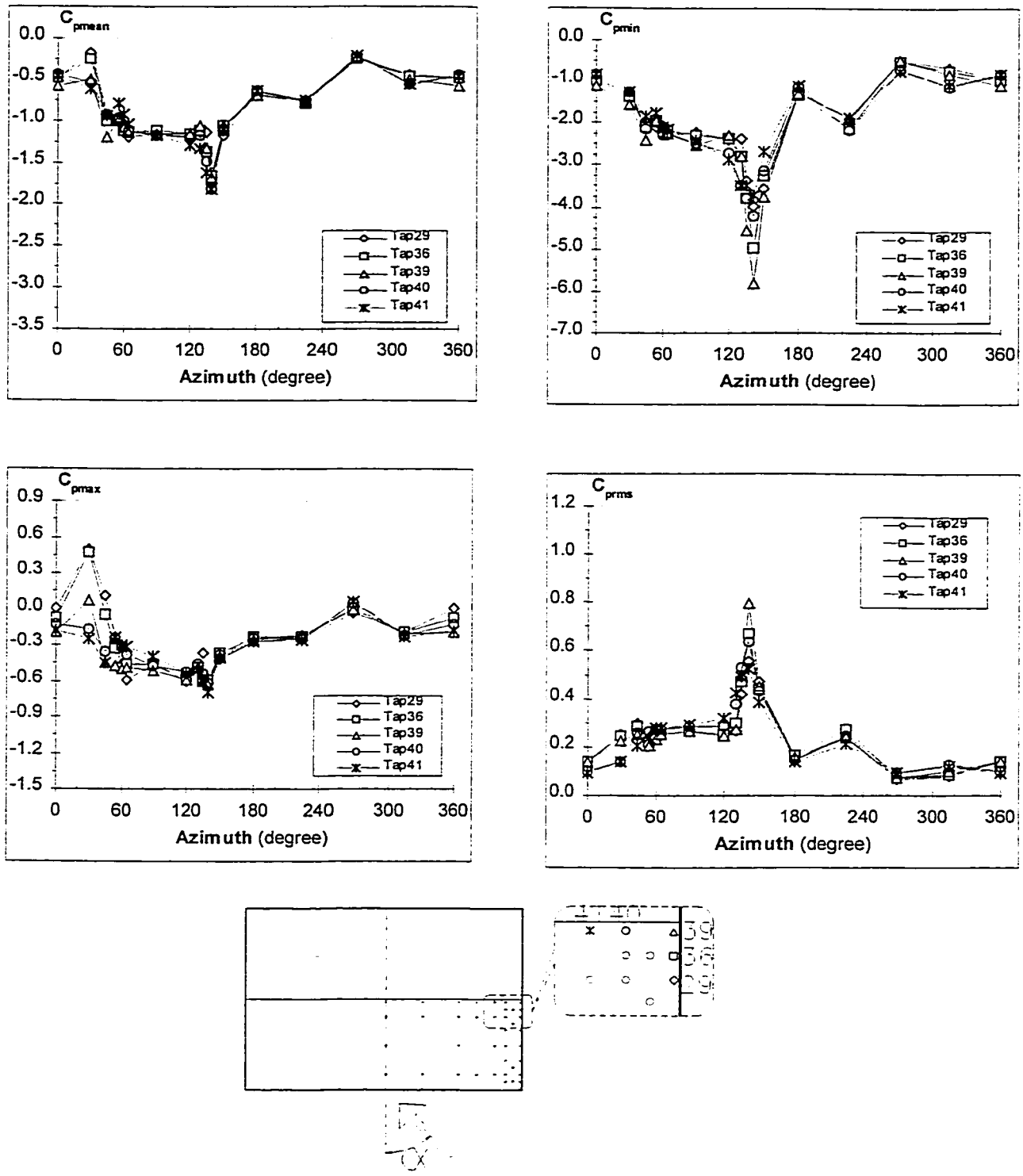

Figure A-2.8 Local pressure distribution on Ridge corner for 25° roof, all azimuths

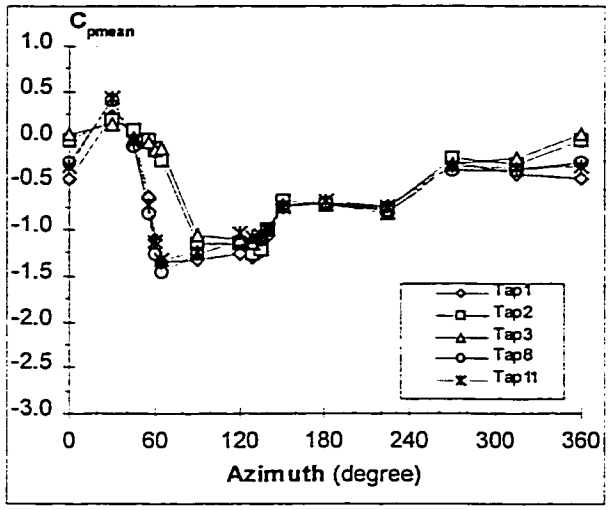

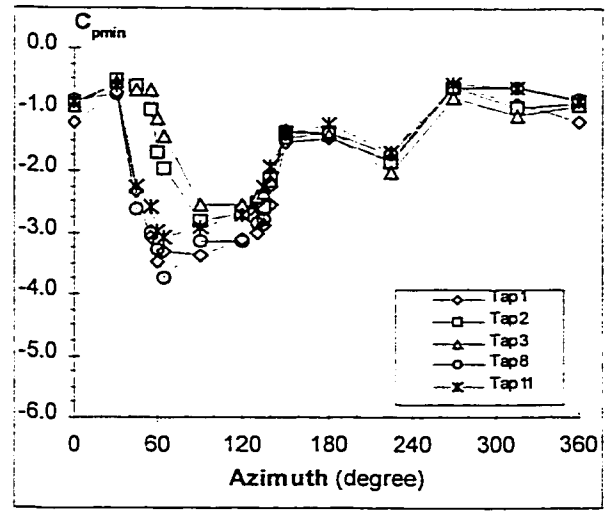

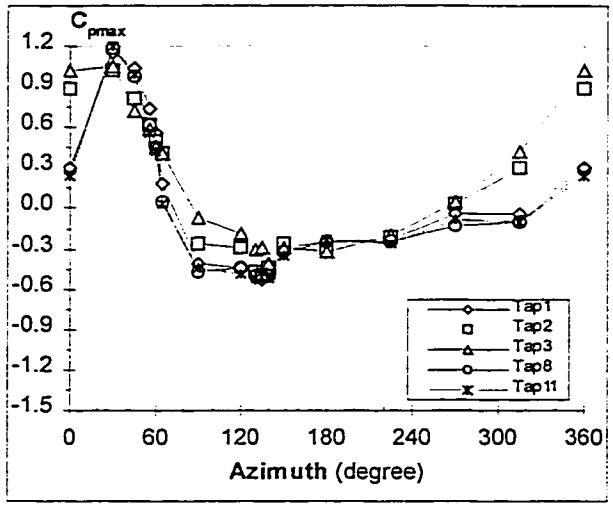

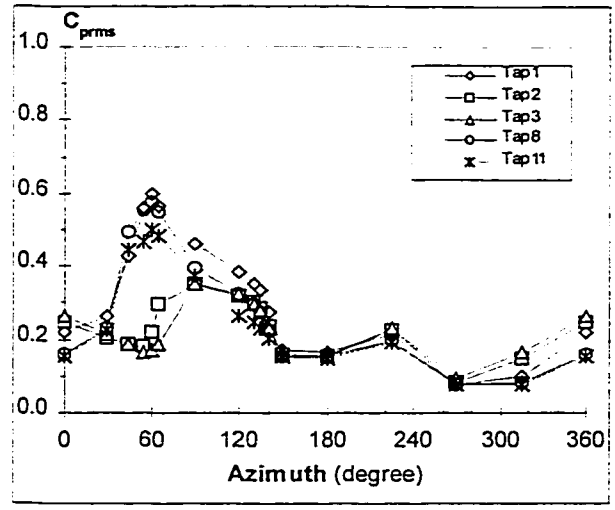

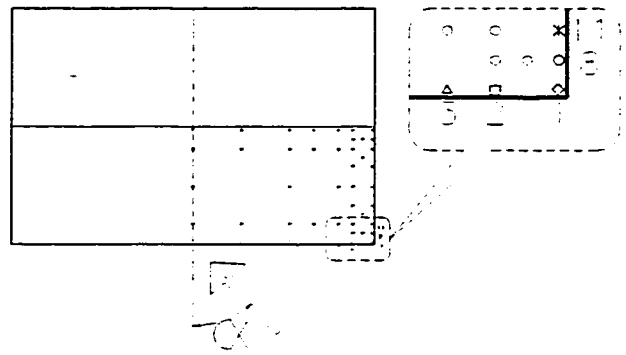

Figure A-2.9 Local pressure distribution on Eaves corner for 30° roof, all azimuths

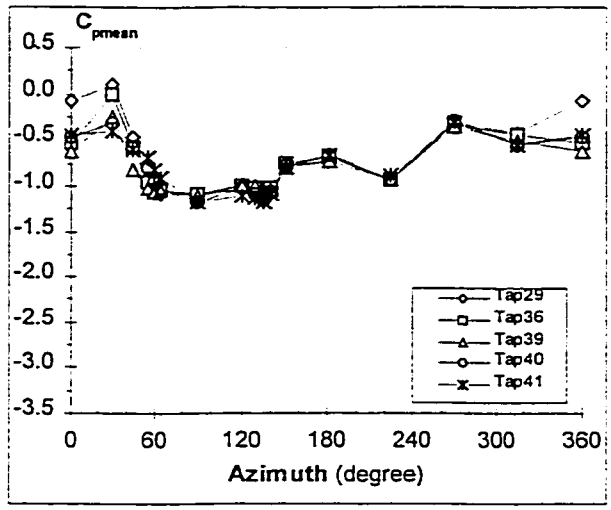

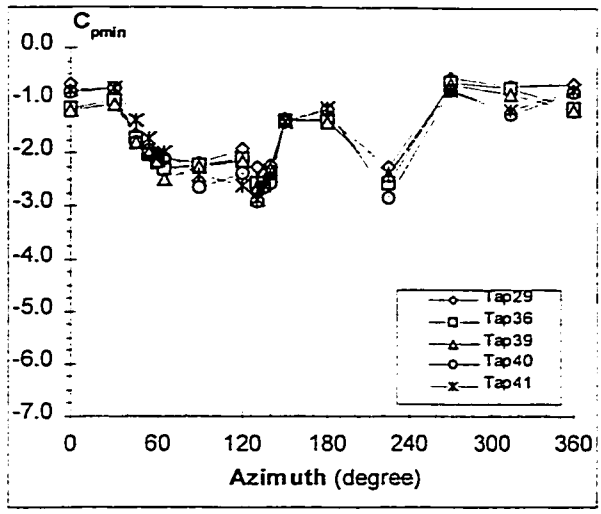

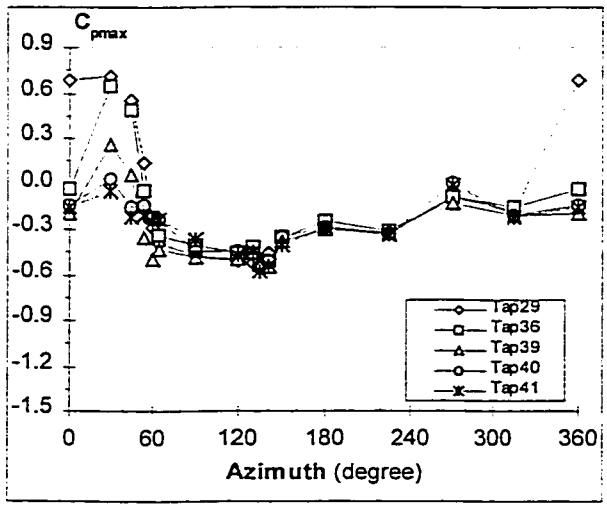

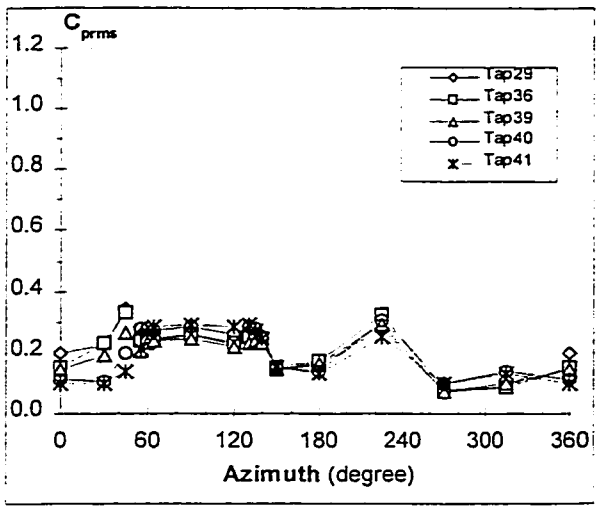

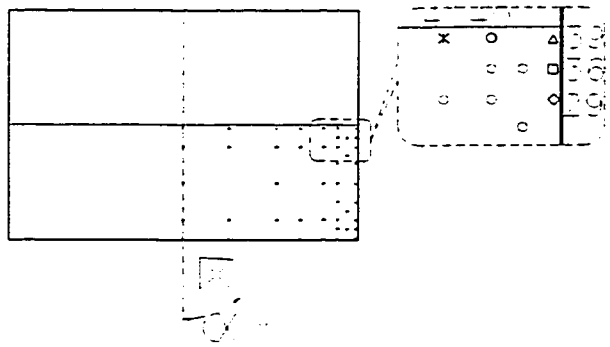

Figure A-2.10 Local pressure distribution on Ridge corner for 30° roof, all azimuths

Appendix-3

Comparison of the Experimental Data Tested on each Slope with the Current Design Wind Pressure Coefficients

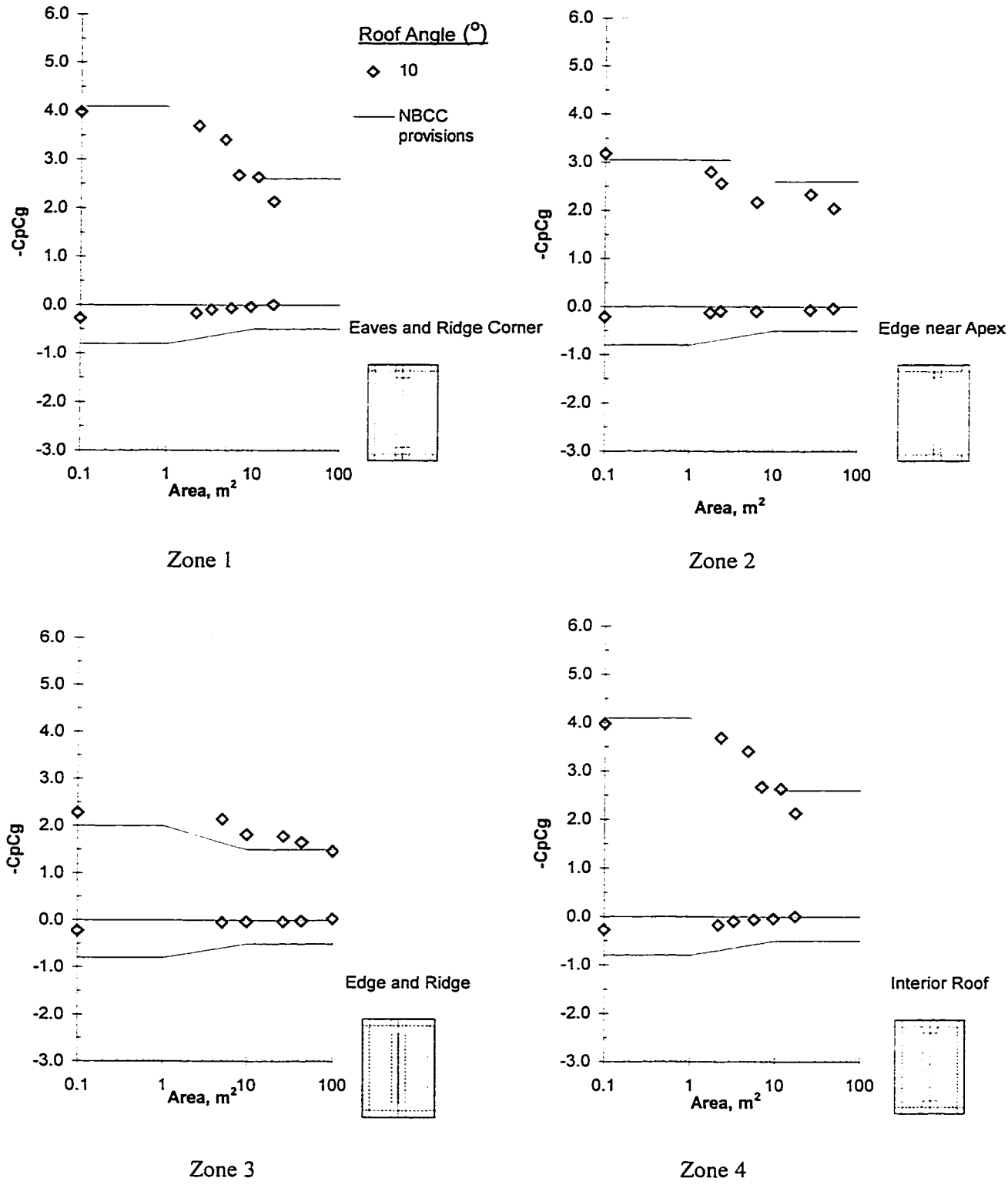

Figure A-3.1 Comparison of the experimental results obtained for the 10°-roof with the current wind provisions specified for the whole10°-30° slope range

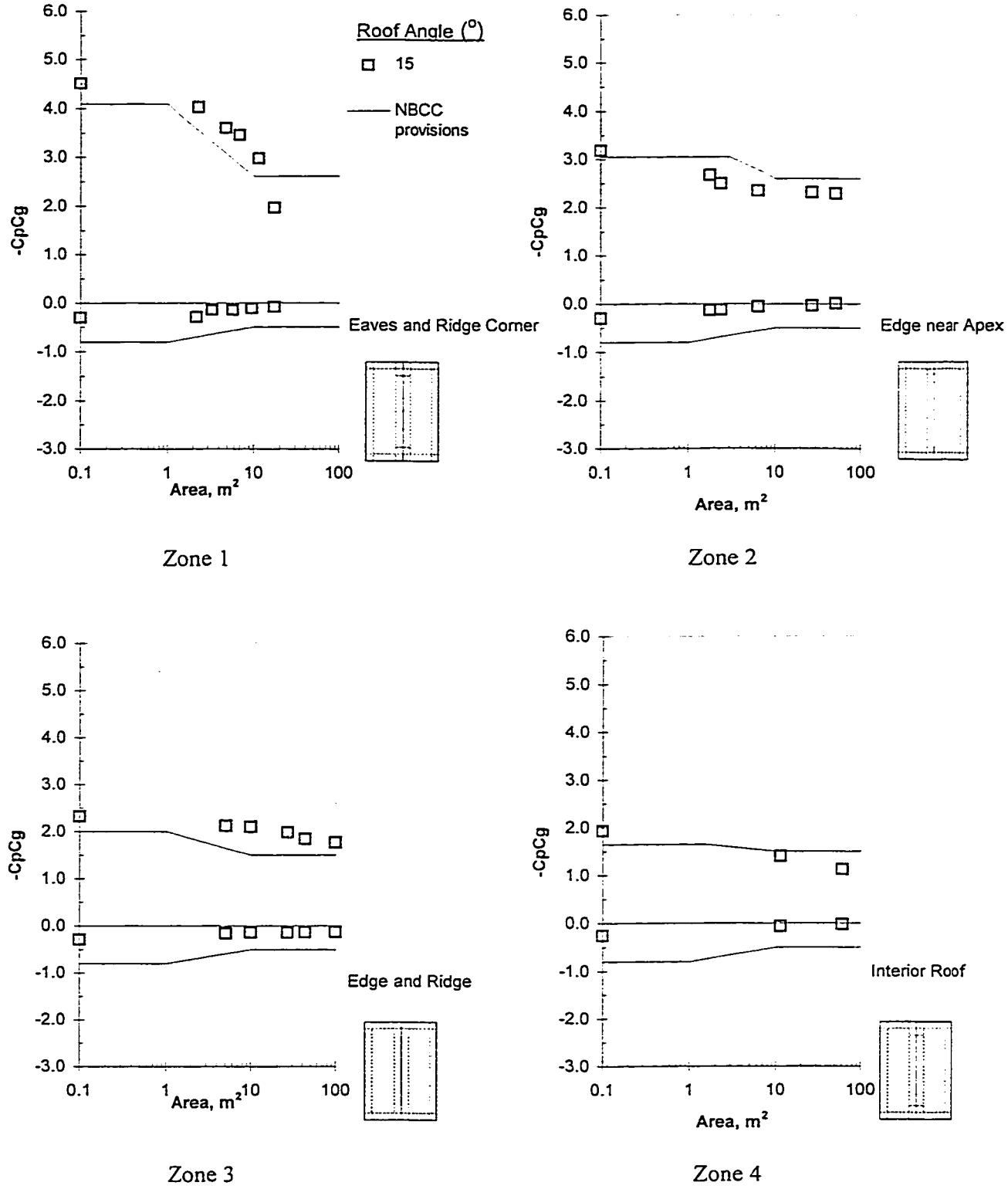

Figure A-3.2 Comparison of the experimental results obtained for the 15°-roof with the current wind provisions specified for the whole10°-30° slope range

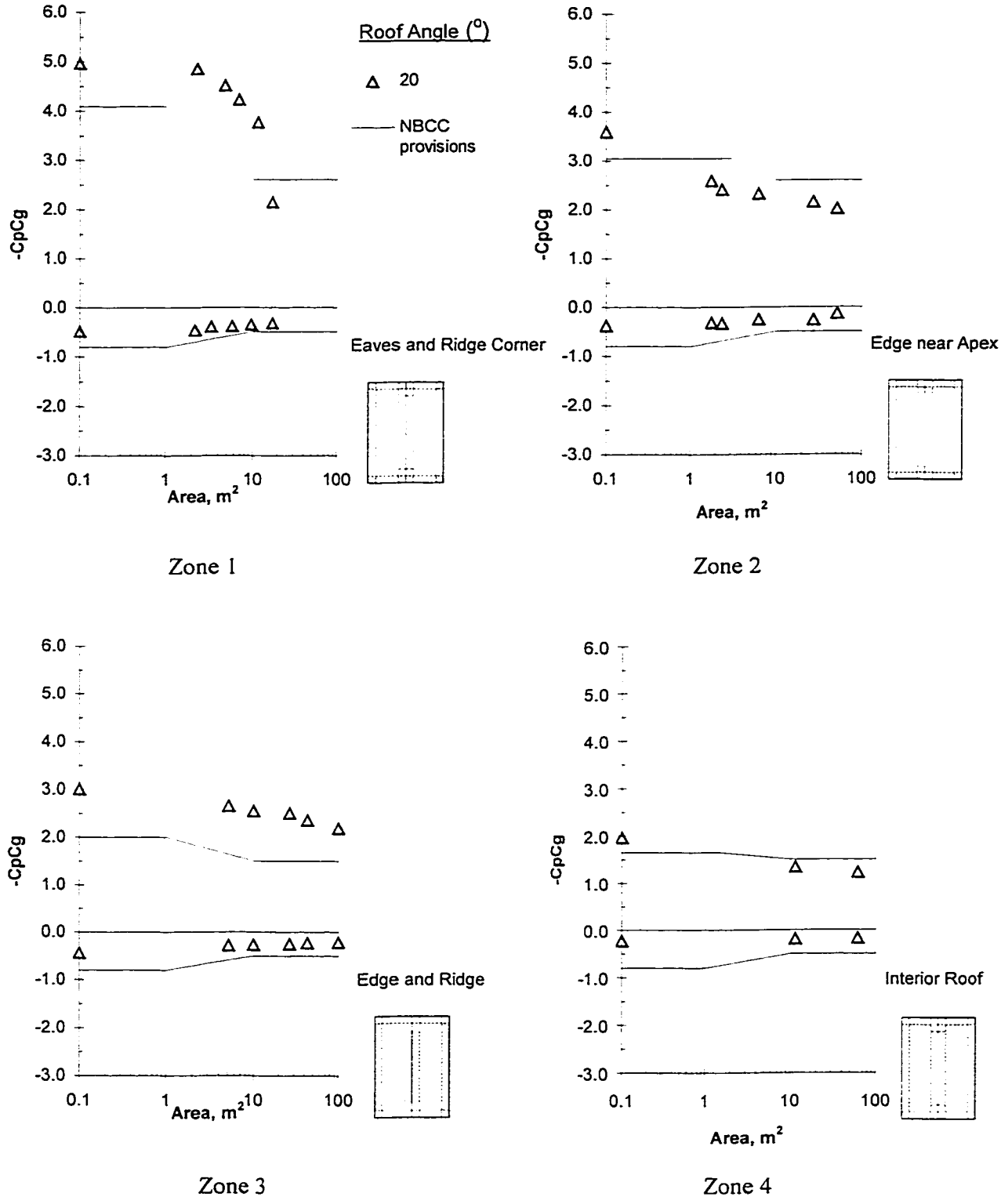

Figure A-3.3 Comparison of the experimental results obtained for the 20°-roof with the current wind provisions specified for the whole10°-30° slope range

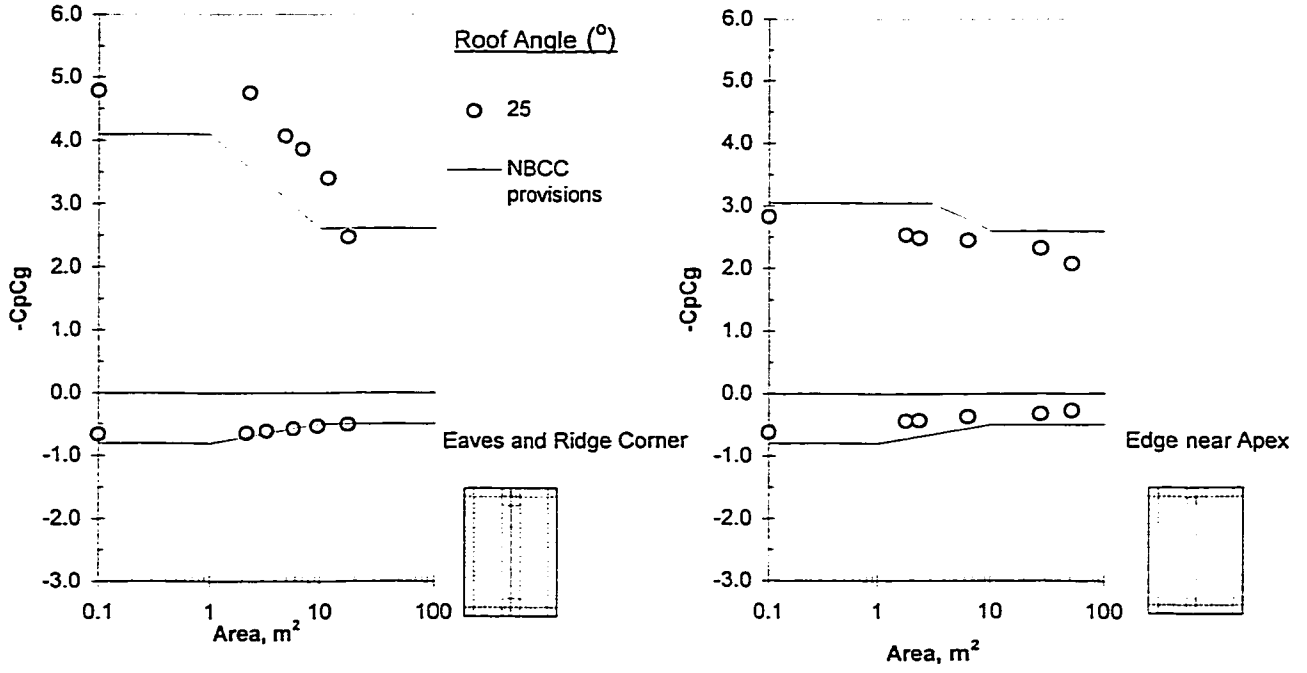

Zone 1 Zone 2

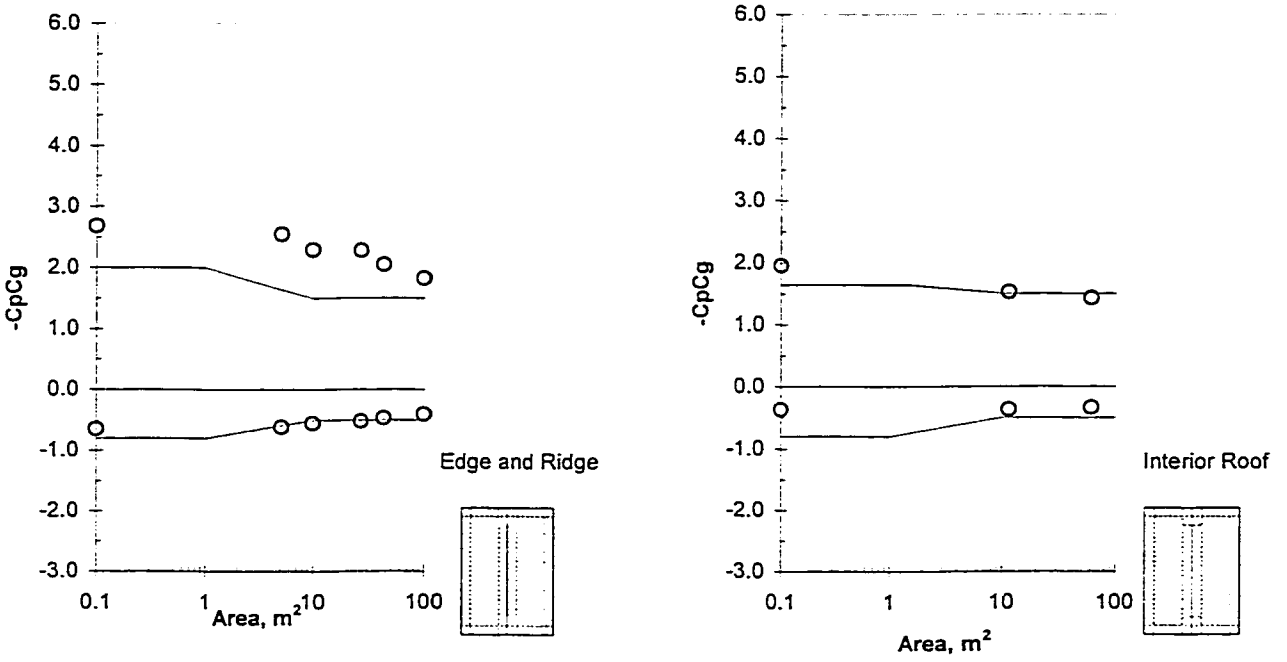

Zone 3 Zone 4

Figure A-3.4 Comparison of the experimental results obtained for the 25°-roof with the current wind provisions specified for the whole10°-30° slope range

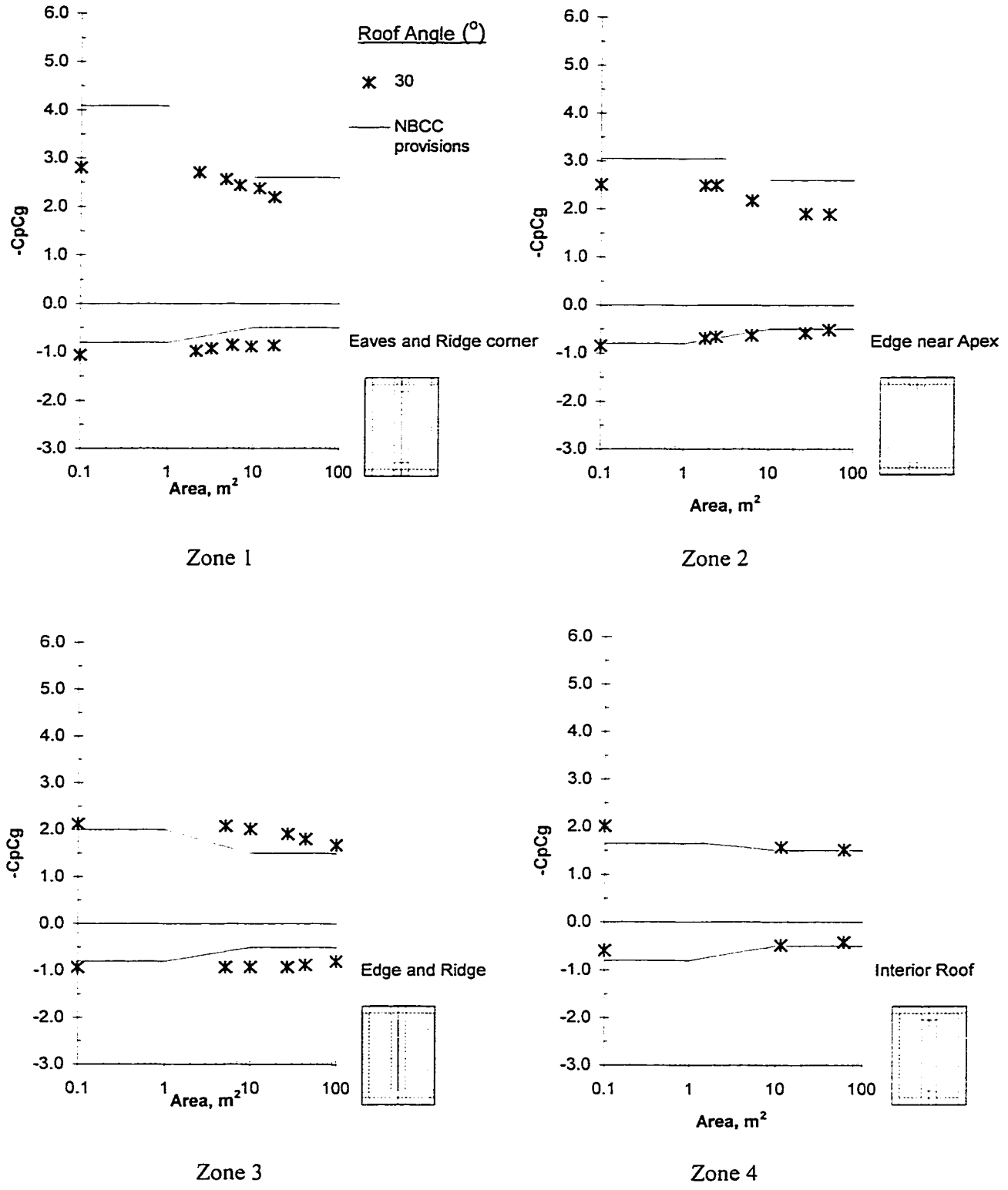

Figure A-3.5 Comparison of the experimental results obtained for the 30°-roof with the current wind provisions specified for the whole10°-30° slope range